GEOPHYSICAL STUDIES IN TASMANIA

Part A

Interpretation of the Gravity Potential Field Using the Frequency Domain

by

C.N.G. Dampney, B.Sc. (Hons.) (Sydney)

submitted in fulfillment of the
requirements for the Degree of

Master of Science

UNIVERSITY OF TASMANIA

HOBART

November, 1966

Candidate's Declaration

I hereby declare that except as stated herein, this thesis contains no material which has been accepted for the award of any other degree or diploma in any university, and that, to the best of my knowledge and belief, this thesis contains no copy or paraphrase of material previously published or written by another person, except when due reference is made in the text of the thesis.

C.N.G. Dampney.

(C.N.G. Dampney)

GEOPHYSICAL STUDIES IN TASMANIA

Part A

Interpretation of the Gravity Potential Field Using the Frequency Domain

Supporting paper: "Three Criteria for the Judgements of Vertical Continuation and Derivative Methods of Geophysical Interpretation". (inside front cover)

ABSTRACT

The frequency domain assembles gravity potential field information into a more meaningful form then the spacial domain. The gravity potential field becomes mathematically well behaved, allowing, ideally, an exact expression for the interpretation procedures of vertical continuation and derivatives; and the formulation of criteria to examine previously proposed interpretation methods of this class.

Moreover, approximations, which are an inevitable component of interpretation, can be more clearly examined. Using the frequency domain it is shown that a discrete system of point masses, judiciously chosen, adequately synthesize any gravity field. The proposed "Equivalent Source Technique" results in the projection of irregularly spaced data on rough topography, onto a regularly gridded horizontal plane. It also allows vertical continuation of the potential field and the effective removal of the regional from the Bouguer Anomaly.

ACKNOWLEDGEMENTS

The author gratefully acknowledges the assistance and helpful discussion he received from his supervisor, Dr. R. Green.

Advice from Messrs. J.T. Boothroyd and W. Warne, Computing Centre, University of Tasmania has also been much appreciated.

FRONTISPIECE

The Derby Winnaleah Area

Plateau looking south

and

Valley looking north-east.

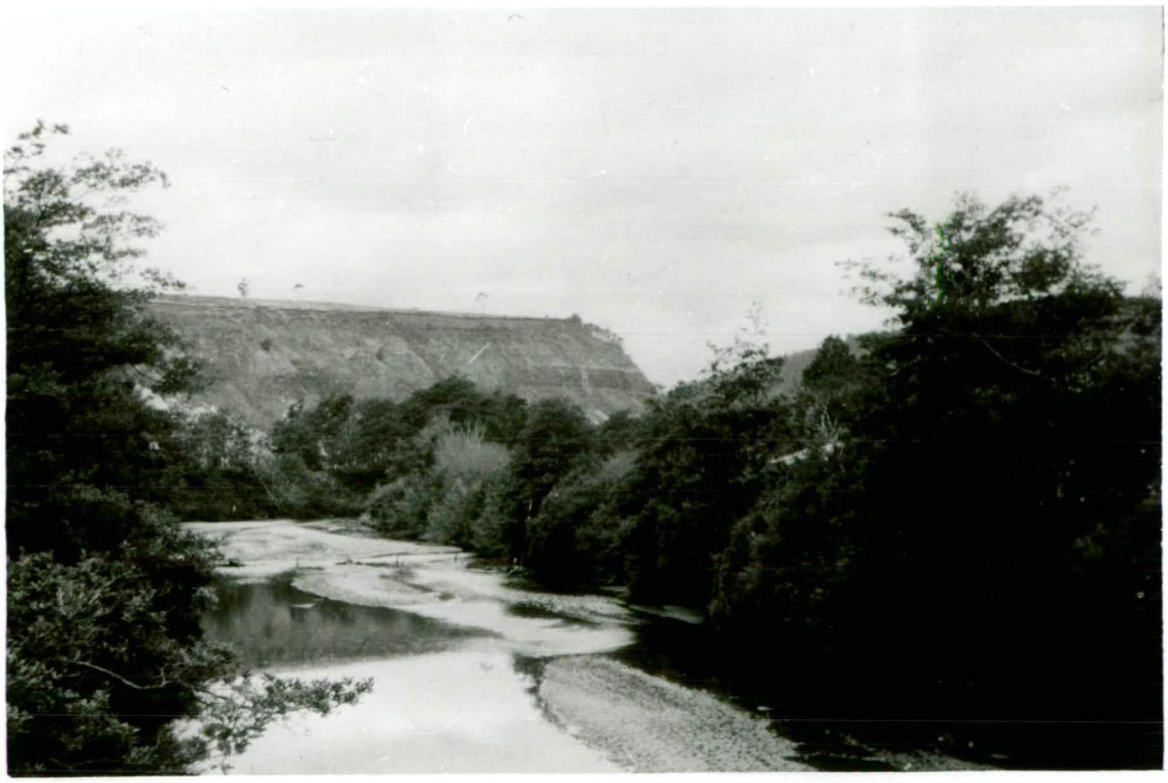

1. INTRODUCTION

The determination of an area's geology is an intriguing and often difficult process. Only the upper surface can be directly observed without expensive drilling; so that in some way the surface information must be extrapolated downwards to discover what lies beneath. Geophysical measurements can be made to help carry out this process as they provide additional information on the physical relationships between the geological structures forming the area.

In fact all these measurements are linked in some way to the characteristics of the surrounding geology. Such parameters as the elasticity, conductivity, density and magnetism vary significantly between structures setting them apart as individual entities capable of being interpreted.

Every geophysical measurement must always contain information related to each geological body in its locality. To interpret the geology from the measurements, however, is not a simple process. The measurements are so much data that has to be manipulated, corrected and filtered in a variety of ways to strain off the useful information.

Yet while it is important to know what information can be extracted from the data it is also important to present the data in a final form in which the information is most readily accessible. Information gains clarity as it becomes more directly related to its source in the eyes of the observer. In this sense we say information gains order and coherence. The gravity potential field was thus examined theoretically to find how data could be assembled into a more meaningful form. It was found that the frequency domain we will denote by F more clearly expressed gravity data than the spacial domain (denoted by S).

The concept that information should be translated into a domain producing greater coherence than the domain of measurement is not new. The frequency domain F has been commonly used in seismic interpretation, while in geomagnetism the global coverage of magnetic variations has forced the use of the spherical harmonic domain to express the otherwise complex variations.

Usually transformations between domains are ideally made by an integral transformation involving every point in the old domain to define one point in the frequency domain. A further condition is also imposed that a one-to-one relationship can be established between the points of the two domains.

The purpose of this thesis is to examine the behaviour of the gravity potential field in F and in that way carry out interpretation of gravity data. The transformation is carried out ideally by the Fourier integral transform which does involve every point in S to define one point in F while maintaining the one-to-one relationship. The importance of this last condition is that, if obeyed, information content is neither suppressed nor over extended.

In practice, however, there are only a finite number of measurements and the value of every point in S is not known. To overcome this problem transformation is carried out using an orthogonal series

$$g_k(x) = \sum_{i=0}^{N-1} G_i(\phi) f_i(\phi) \qquad (1.1)$$

which defines a new set of N values $G_i(\phi)$ in F from the set of N values

$g_k(x)$ in S by means of the orthogonal functions $f_i(\phi)$. The orthogonal series, in general, sufficiently closely approximates the integral transform to the extent that the new domain defined on the basis of the orthogonal series can be considered to have the desirable properties of the domain defined by the integral transform. However, this is not always the case, and limitations have to be realised.

The Fourier series is therefore used to transform points from S into F.

The potential field, in this instance, the gravity potential field, is shown in chapter 2 to become mathematically well-behaved in F as the intensity varies smoothly independent of the disturbing body's shape. This feature allows trends indicating orientation and depth of disturbing bodies in the data to show up.

More importantly gravity field intensity in the frequency domain is found to rapidly diminish as frequency increases. This allows the vertical continuation and derivative processes on potential fields to be more accurately expressed in F as a filter with a particular frequency response. Thus various methods of vertical continuation such as Bullard and Cooper's (1948), Elkins (1952), Peters (1948) and Henderson's (1960) are compared on the basis of their filter responses in chapter 2.

If the data is assumed perfect, to contain all information related to gravity field variations and known on a regular horizontal grid, then a matrix of coefficients can be found which carry out exactly the vertical continuation and derivative processes. These matrices are found in chapter 3 from theoretical relationships in the frequency domain. They may then be used to

show up the limitations of these processes.

Gravity field measurements, however, are not generally made on a regular horizontal grid. In order to project data onto this grid, a new method, called "the equivalent source technique" is developed in chapter 4. The equivalent source technique simply substitutes disturbing bodies at depth which synthesize the field intensity measurements taken at irregular points on rough topography. The intensity at the grid points is then found directly by calculating the attraction of these bodies.

Similarly, methods are available to interpolate irregularly spaced data (restricted to flat topography) onto a grid (Jones, 1965; Brown, 1955; Saltzer, 1948) but as polynomials are used they are found to be unsatisfactory for reasons discussed in chapter 4. The equivalent source technique is found to have many useful applications.

Practical computer programs to carry out the new technique are discussed in chapter 5. Fortunately, a new iterative approach to solving matrices made the program development straight forward.

The analysis of gravity field intensity data from Derby-Winnaleah is carried out in chapter 6. As the area was extremely varied in height due to a valley being cut out in a basalt plateau by the Ringarooma river, the data had to be projected onto a flat plane in order to be analysed correctly. A "regional" variation was removed from the data using a further application of the equivalent source technique. The object of the analysis was to find the general structure of the area, particularly the old path of the Ringarooma river before it was buried by Tertiary basalt flows.

2. THE FREQUENCY DOMAIN

2.1 Fundamentals

The frequency domain is convenient for examining potential fields, which by definition satisfy Laplace's Equation

$$\nabla^2 V = 0 \tag{2.1}$$

for the potential V at points where there are no sources to the field. From the identity

$$\nabla^2\left(\frac{1}{r}\right) = 0 \tag{2.2}$$

it is seen that V may be proportional to the inverse of the distance from the origin of co-ordinates, as, in fact is the case for the gravitational potential field, $V(x,y,z)$ at (x,y,z).

In three dimensional cartesian co-ordinates V (fig. 1) is given by

$$V(x,y,z) = \frac{G\, m(\alpha,\beta,\gamma)}{r} \tag{2.3}$$

where $r = \{(x-\alpha)^2 + (y-\beta)^2 + (z-\gamma)^2\}^{1/2}$

G = the gravitational constant and the mass $m(\alpha,\beta,\gamma)$ at (α,β,γ) is the source of the field.

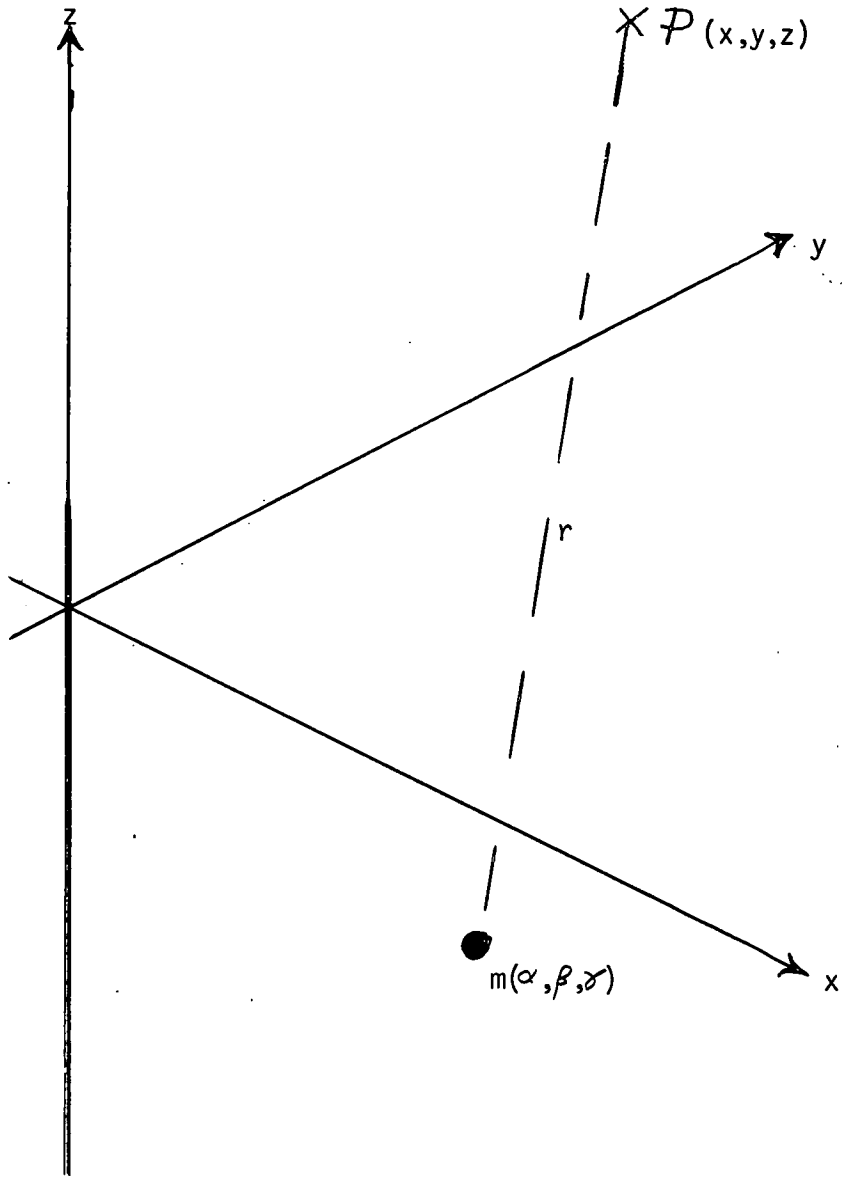

FIGURE 1. The gravitational potential V(x,y,z) at P is related to the mass $m(\alpha,\beta,\gamma)$ at (α,β,γ) by equation (2.3).

Generally speaking, however, the geophysicist measures the gravitational field intensity $\underset{\sim}{g}$, where

$$\underset{\sim}{g} = \underset{\sim}{\nabla} V \tag{2.4}$$

more conveniently as the gravitymeter is designed to measure the vertical component of $\underset{\sim}{g}$ directly. As the gravitational attraction of the real earth is sufficiently great that we may define the horizontal reference plane as being perpendicular to it for practical purposes, the variations in $\underset{\sim}{g_z}$ need only be considered.

Thus from eqns. (2.3) and (2.4)

$$g_z(x,y,h) = \sum_{k=1}^{N} \frac{m_k (z-\gamma_k)}{\{(x-\alpha_k)^2+(y-\beta_k)^2+(z-\gamma_k)^2\}^{3/2}} \tag{2.5}$$

where the N masses m_k at $(\alpha_k, \beta_k, \gamma_k)$ are point masses we now consider as representing approximately the mass deviations of the real earth from the model earth.

In the limit as $N \to \infty$, the approximation disappears as the masses close infinitesimaly together and become a continuum. Thus g_z in eqn. (2.5) may be expressed as

$$g_z(x,y,h) = \iiint_\tau \frac{\rho(\alpha,\beta,\gamma)\, d\tau \quad (z-\gamma)}{\{(x-\alpha)^2+(y-\beta)^2+(z-\gamma)^2\}^{3/2}} \tag{2.6}$$

where $$\lim_{k\to\infty} \sum_{k=1}^{N} m_k = \iiint_\tau \rho(\alpha,\beta,\gamma)\, d\tau \tag{2.7}$$

and $\rho(\alpha,\beta,\gamma)$ is the contrast density of the real from a model earth at (α,β,γ) with integration being carried out over its volume τ .

In practical gravimetric problems of the exploration type the integration is confined to the region underlying the survey area and encompasses all relatively significant mass deviations. Usually it is sufficiently accurate to assume a flat earth.

As there is no pre-determined tendency for the contrast density to vary systematically, except with respect to depth under some assumptions, the field intensity $g_z(x,y,z)$ in the spacial domain will show an unsystematic variation with respect to the horizontal co-ordinates (x,y) on the plane z = h.

2.2 The spectrum of $g_z(x,y,h)$

However, the gravity field becomes mathematically better behaved in the frequency domain as can be seen from its spectrum $G(u,v)$.

$$G(u,v) = \int_{-\infty}^{\infty}\int_{-\infty}^{\infty} g_z(x,y,h)\, e^{-iux-ivy}\,dx\,dy \qquad (2.8)$$

found using the two-dimensional Fourier Transform to map the spacial parameters (x,y) onto the frequency parameters (u,v).

Hence from eqn. (2.5) considering the source of the field to be a series of point masses

$$G(u,v) = \sum \int_{-\infty}^{\infty}\int_{-\infty}^{\infty} \frac{G\, m_k\,(h-\gamma_k)\, e^{-iux-ivy}\,dx\,dy}{\{(x-\alpha_k)^2+(y-\beta_k)^2+(h-\gamma_k)^2\}^{3/2}} \qquad (2.9)$$

$$= \sum_{k=1}^{N} G m_k e^{-i u \alpha_k - i v \beta_k} e^{-(h-\gamma_k)\sqrt{u^2+v^2}}$$

$$= G F e^{-H\sqrt{u^2+v^2}} \qquad (2.10)$$

by the Mean Value Theorem

where $|F| \leq 2 m_k$

$$H \geq 0 \qquad (2.11)$$

In practice the anomalous masses will be some distance below the topography and thus $H \gg 0$.

Therefore, from equation (2.10) the general statement can be made that the gravity field intensity spectrum has a marked tendency to decrease as the frequency parameters increase. Thus the gravity potential field becomes mathematically well behaved no matter what the anomalous mass (or contrast density) distribution is.

As an example consider a mass point, m, at the origin. From eqn. (2.9)

$$G(u,v) = G m e^{-h\sqrt{u^2+v^2}} \qquad (2.12)$$

so that even for this highly irregular potential field, the amplitude $G(u,v)$ of the spectrum smoothly and rapidly approached zero as u and v increase.

These theoretical considerations and the relative ease by which g is transformed into G suggests that we use the frequency domain for examining methods of potential field interpretation. In fact, Danes (1960).

Odeguard and Berg (1965), Bhattacharyya (1965, 1966) have recognized this by using the domain in their interpretative procedures.

2.3 Transformation of $g_z(x,y,z)$ into the frequency domain

As has been stated more generally in the introduction it is necessary to approximate the Fourier Transform by the Fourier Series as $g_z(x,y,z)$ will not be known at every point in the spacial domain $\mathcal{S}$. While ideally in the one-dimensional case

$$G(u) = \int_{-\infty}^{\infty} g_z(x,z)\, e^{-iux}\, dx \tag{2.13}$$

for a profile $g_z(x,z)$ across $g_z(x,y,z)$, gravitational intensity will only be known over a finite area and therefore a finite length $2\pi\lambda$ along its profile. That is

$$-\lambda\pi \leqslant x \leqslant \lambda\pi \tag{2.14}$$

It is then necessary to assume that the function $g_z(x,z)$ repeats itself periodically in the intervals

$$(2n+1)\lambda\pi \leqslant x \leqslant (2n-1)\lambda\pi$$

Hence

$$G(u) = \sum_{p=-\infty}^{\infty} \int_{(2p-1)\pi\lambda}^{(2p+1)\pi\lambda} g(x)\, e^{-iux}\, dx \tag{2.15}$$

as $g(x) = g(x + 2\pi\lambda p)$

$$= \sum_{p=-\infty}^{\infty} e^{-2\pi i u p \lambda} \int_{-\lambda\pi}^{\lambda\pi} g(x + 2\pi\lambda p)\, e^{-iux}\, dx \qquad (2.16)$$

$$= \lim_{N\to\infty} \sum_{p=-N}^{N} e^{-2\pi i u p \lambda} \int_{-\lambda\pi}^{\lambda\pi} g(x)\, e^{-iux}\, dx \qquad (2.17)$$

if $u\lambda$ is non integer

$$\sum_{p=-\infty}^{\infty} e^{-2\pi i u p \lambda} = 0 \qquad (2.18)$$

Suppose $u = n/\lambda$

$$G(u) \times \lim_{N\to\infty} N 2\pi\lambda = C_n \qquad (2.19)$$

$$\therefore C_n = \frac{1}{2\pi\lambda} \int_{-\lambda\pi}^{\lambda\pi} e^{-inx/\lambda} g(x)\, dx \qquad (2.20)$$

Thus our limited spacial knowledge of $g_2(x)$ results in only the amplitude of a finite number of frequencies $\frac{n}{2\pi\lambda}$ for integer n being known

$$\therefore g(x) = \sum_{n=-\infty}^{\infty} C_n\, e^{inx/\lambda} \qquad (2.21)$$

Furthermore, in practice, measurements of $g_x(x)$ are confined to a discrete number so that there will only be N values, say Δx apart, known along a profile. To retain the one-to-one correspondence between domains it is therefore only possible to find N values of C_n. For simplicity we take the smallest values such that if N is odd, then

$$-\left(\frac{N-1}{2}\right) \leqslant n \leqslant \left(\frac{N-1}{2}\right) \tag{2.22}$$

If N is even

$$-\left(\frac{N}{2}-1\right) \leqslant n \leqslant \frac{N}{2} \tag{2.23}$$

therefore $2\pi\lambda = N\Delta x$

$$\lambda = \frac{N\Delta x}{2\pi} \tag{2.24}$$

Hence $g(x) = \sum_{n=-a}^{b} C_n \exp(i n x 2\pi / N\Delta x)$

put $\xi = 2\pi/N$; $g_r = g(r\Delta x)$

$$g_r e^{-irm\xi} = \sum_{n=-a}^{b} C_n e^{ir(m-n)\xi}$$

$$\sum_{r=-a}^{b} g_r e^{-irm\xi} = \sum_{r=-a}^{b}\sum_{n=-a}^{b} C_n e^{ir(m-n)\xi}$$

$$= (a+b+1)C_n$$

Note $a + b + 1 = N$ whether N odd or even.

Therefore $$C_n = \frac{1}{N} \sum_{r=-a}^{b} g_r e^{-irn\xi} \tag{2.25}$$

$$g_r = \sum_{n=-a}^{b} C_n e^{irn\xi} \tag{2.26}$$

$$= \sum_{n=0}^{b} \{(C_n + C_{-n}) \cos(rn\xi) + i(C_n - C_{-n}) \sin(rn\xi)$$

Note $C_{-n} = 0$ for even N when $n = -a$

$$g_r = \sum_{n=0}^{b} \{A_n \cos(rn\xi) + B_n \sin(rn\xi)\} \tag{2.27}$$

where $$\left.\begin{aligned} A_n &= \frac{2}{N} \sum_{r=-a}^{b} g(r\Delta x) \cos(rn\xi) \\ B_n &= \frac{2}{N} \sum_{r=-a}^{b} g(r\Delta x) \sin(rn\xi) \end{aligned}\right\} \tag{2.28}$$

unless $n = 0$ or $n = b$ for even N where the normalising factor = 1/N .

This may be extended to two dimensions.

$$g_{r,s} = g(r\Delta x, s\Delta y) = \sum_{m=-a_x}^{b_x} \sum_{n=-a_y}^{b_y} C_{m,n} e^{irm\xi + isn\zeta} \tag{2.29}$$

where a_x, a_y are defined similarly to a

b_x, b_y " " " " b

Thus
$$g_{r,s} = \sum_{m=-a_x}^{b_x} e^{irm\xi} \sum_{n=-a_y}^{b_y} C_{m,n}\, e^{isn\zeta}$$

$$= \sum_{m=-a_x}^{b_x}{}' e^{irm\xi} \sum_{n=0}^{b_y} \Big\{ \big(C_{m,n} + C_{m,-n}\big)\cos(sn\zeta) + i\big(C_{m,n} - C_{m,-n}\big)\sin(sn\zeta) \Big\}$$

$$= \sum_{m} e^{irm\xi} \sum_{n=0}^{b_y} \Big\{ P_{m,n}\cos(sn\zeta) + Q_{m,n}\sin(sn\zeta) \Big\}$$

$$= \sum_{m=0}^{b_x} \sum_{n=0}^{b_y} \Big\{ \big(P_{m,n} + P_{-m,n}\big)\cos(rm\xi)\cos(sn\zeta) \qquad (2.30)$$

$$+ \big(Q_{m,n} + Q_{-m,n}\big)\cos(rm\xi)\sin(sn\zeta)$$

$$+ i\big(P_{m,n} - P_{-m,n}\big)\sin(rm\xi)\cos(sn\zeta)$$

$$+ i\big(Q_{m,n} - Q_{-m,n}\big)\sin(rm\xi)\sin(sn\zeta) \Big\}$$

This gives in Bhattacharyya's (1966) notation,

$$g_{r,s} = \sum_{m} \sum_{n} \left\{ \begin{array}{l} A_{m,n}\cos(rm\xi)\cos(sn\zeta) \\ + B_{m,n}\cos(rm\xi)\sin(sn\zeta) \\ + E_{m,n}\sin(rm\xi)\cos(sn\zeta) \\ + F_{m,n}\sin(rm\xi)\sin(sn\zeta) \end{array} \right\} \qquad (2.31)$$

where $A_{m,n}$; $B_{m,n}$; $C_{m,n}$ and $F_{m,n}$ correspond to the amplitudes of the various "waves" shown in fig 2.

CONTOURS OF 2 DIMENSIONAL WAVES

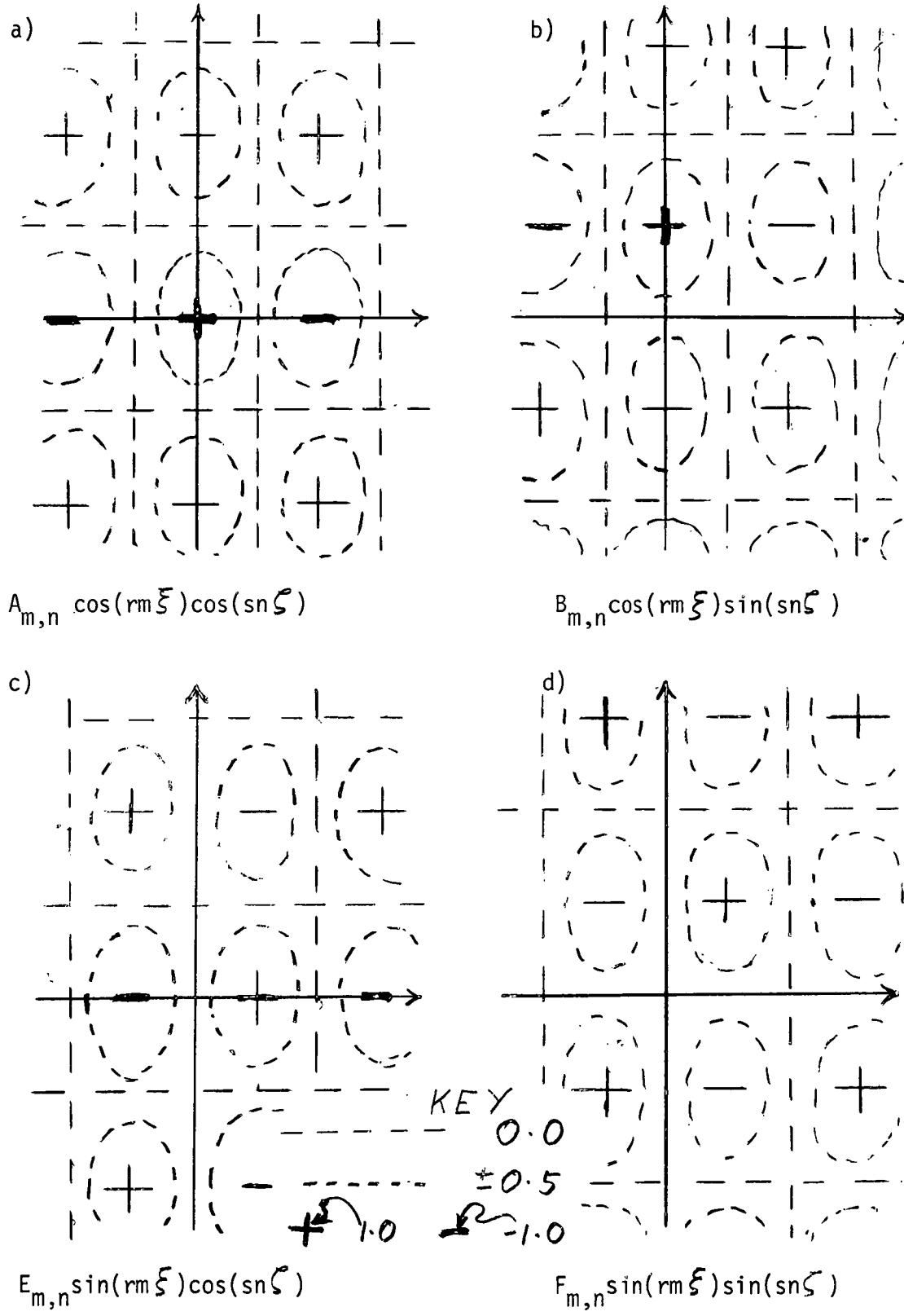

FIGURE 2.

Thus $C_{m,n}$ is the complex amplitude of the wave with frequency $m/M\Delta x$, $n/N\Delta y$.

and substituting from eqn. (2.29) into (2.30) we find

$$\begin{aligned} C_{m,n} &= \frac{1}{4}\left\{(A_{m,n} - F_{m,n}) - i(B_{m,n} + E_{m,n})\right\} \\ C_{m,-n} &= \frac{1}{4}\left\{(A_{m,n} + F_{m,n}) + i(B_{m,n} - E_{m,n})\right\} \\ C_{-m,n} &= \frac{1}{4}\left\{(A_{m,n} + F_{m,n}) - i(B_{m,n} - E_{m,n})\right\} \\ C_{-m,-n} &= \frac{1}{4}\left\{(A_{m,n} - F_{m,n}) + i(B_{m,n} + E_{m,n})\right\} \end{aligned} \tag{2.32}$$

The modulus of $C_{m,n}$ gives the amplitude of the two dimensional wave with frequencies $\frac{m}{M\Delta x}$; $\frac{n}{N\Delta y}$

$$|C_{m,n}| = |C_{-m,-n}| = \frac{1}{4}\sqrt{(A_{m,n} - F_{m,n})^2 + (B_{m,n} + E_{m,n})^2} \tag{2.33}$$

$$|C_{-m,n}| = |C_{m,-n}| = \frac{1}{4}\sqrt{(A_{m,n} + F_{m,n})^2 + (B_{m,n} - E_{m,n})^2} \tag{2.34}$$

$$|C_{m,0}| = |C_{-m,0}| = \frac{1}{4}\sqrt{A_{m,0}^2 + E_{m,0}^2} \tag{2.35}$$

$$|C_{0,n}| = |C_{0,-n}| = \frac{1}{4}\sqrt{B_{0,n}^2 + F_{0,n}^2} \tag{2.36}$$

The amplitudes are seen to depend on whether m and n have the same or opposite sign. Therefore only two quadrants of $C_{m,n}$ are required to specify the amplitudes of all waves, that is half of the frequency domain, while the remaining two quadrants express the phase. Analogously in one dimension positive wavelengths only are required to specify amplitude.

Geometrically two dimensional waves can be represented by contoured diagrams. From fig. 2 we can see that the planar wave in fig. 3 a is the result of

$$A_{m,n} = -F_{m,n}, \quad = 0 \text{ except for a particular } m \text{ and } n . \tag{2.37}$$
$$B_{m,n} = E_{m,n}, \quad = 0 \text{ except for a particular } m \text{ and } n .$$

This is also derived from eqn. (2.31)

$$g_{r,s} = A_{m,n}\left\{\cos(rm\xi + sn\zeta) + \sin(rm\xi + sn\zeta)\right\} \tag{2.38}$$

showing that $g_{r,s}$ is constant along any line

$$rm\xi + sn\zeta = \text{const.} \tag{2.39}$$

Similarly the planar waves in fig. 3b, c and d are seen to be caused by the waves in fig. 2 cancelling out or amplifying each other.

This is expressed generally by putting eqn. (2.31) into the form

$$q_{n,s} = \sum_{m} \sum_{n} \left\{ \begin{array}{l} \left(\frac{A_{m,n} - F_{m,n}}{2}\right) \cos(\pi m\xi + sn\zeta) \\ + \\ \left(\frac{B_{m,n} + E_{m,n}}{2}\right) \sin(\pi m\xi + sn\zeta) \\ + \\ \left(\frac{A_{m,n} + F_{m,n}}{2}\right) \cos(\pi m\xi - sn\zeta) \\ - \\ \left(\frac{B_{m,n} - E_{m,n}}{2}\right) \sin(\pi m\xi - sn\zeta) \end{array} \right\} \quad (2.40)$$

Swartz (1956) discussed the application of these waves to trend analysis.

Communication theory may now be brought to bear on the analysis of the two-dimensional waves forming $q_{n,s}$.

At this point we consider an important limitation in the transformed frequency domain data.

2.3.1 Bandwidth

A well-known fact from the study of light waves is that (Ditchburn, 1963) it is impossible to propagate light waves continuously. As a result frequency broadening of an otherwise discrete spectral line occurs. This is measured in terms of the bandwidth Δf over which the amplitude density is greater than $2/\pi$ times its maximum value. Δf is related to the average wave train length $c\Delta t$ (c is the velocity of light) by

$$\Delta f = 1/2\pi \Delta t \quad (2.41)$$

PLANAR WAVES

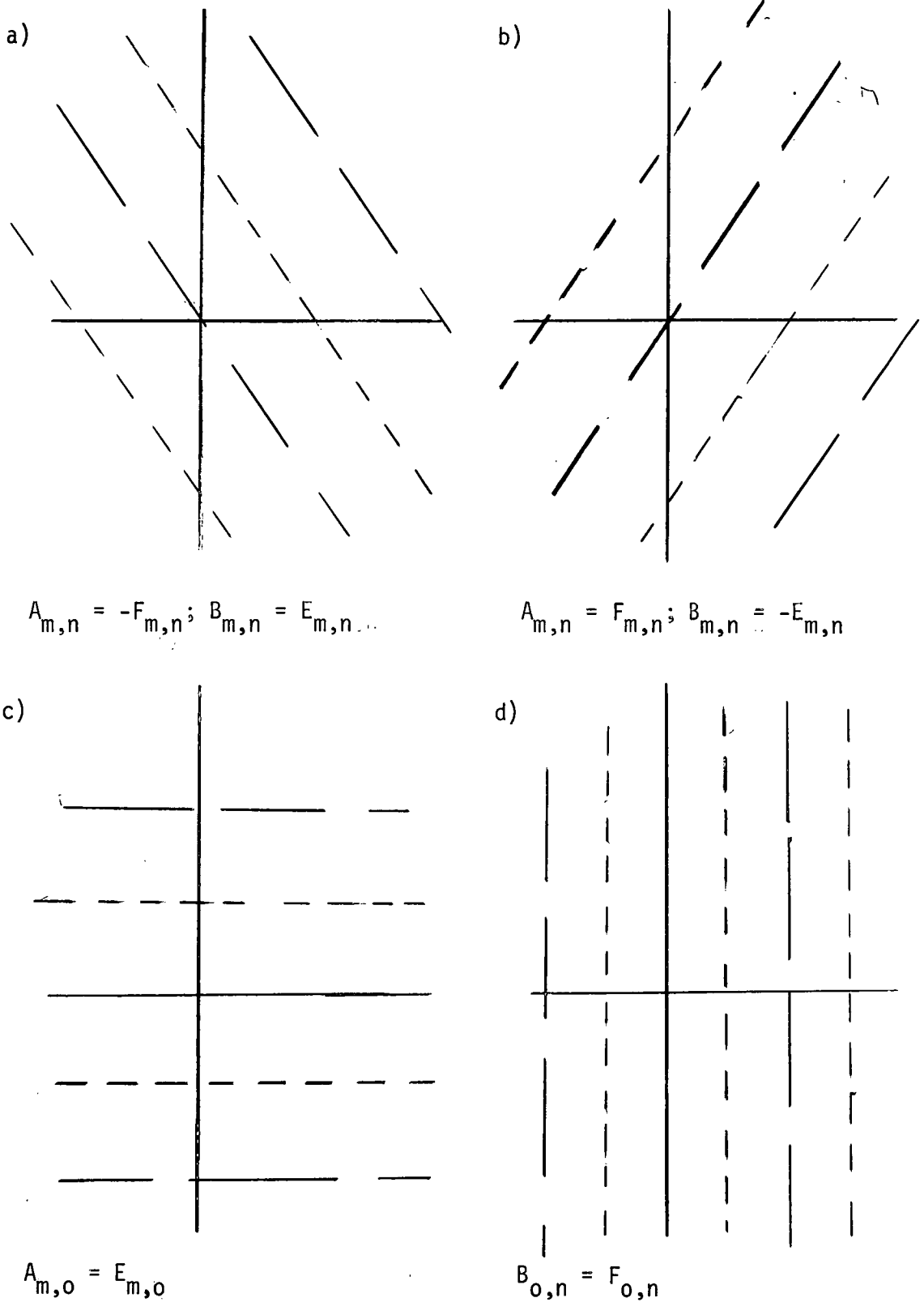

FIGURE 3.

where Δt is the finite time that a wave train is received at a given point. This is closely analogous to the Uncertainty Principle of quantum mechanics. We may consider this phenomenon as the uncertainty of a measured frequency being directly related to the time over which it is recorded.

Similarly in the spacial domain, it is only possible to measure the gravity field $\underset{\sim}{g}$ over a finite area or length. Uncertainty therefore exists in the N discrete spacial frequencies $n/N\Delta x$ assumed to represent $\underset{\sim}{g}$ in the frequency domain by eqn. (2.25).

As the Fourier Transform exactly transforms between the two domains we find the exact spectrum of

$$g_z(x) = C_n \, e^{i 2\pi n x / N\Delta x} \tag{2.42}$$

by equation (2.13).

As nothing is known of $g_z(x)$ beyond the area of measurement we put

$$g_z(x) = 0 \quad \text{for } |x| > \frac{N\Delta x}{2}$$ (see eqn. (2.14) and (2.24)

in order to investigate the uncertainty of the frequency $f_n = n/N\Delta x$, by finding the amplitude density spectrum $G(u)$.

$$G(u) = C_n \int_{-\frac{N\Delta x}{2}}^{\frac{N\Delta x}{2}} e^{-i\left(u - \frac{2\pi n}{N\Delta x}\right)x} \, dx \tag{2.43}$$

$$= 2C_n \sin\left\{\left(u - \frac{2\pi n}{N\Delta x}\right)\frac{N\Delta x}{2}\right\} \Big/ \left(u - 2\pi n/N\Delta x\right)$$

$$= 2\,C_n \sin\left\{\frac{N\Delta x}{2}\,\Delta u\right\} \Big/ \Delta u \tag{2.44}$$

where $\Delta u = u - 2\pi n / N\Delta x$

Thus $G(u) = N\Delta x\, C_n$ when $\Delta u = 0$

i.e. when $u = 2\pi n / N\Delta x$

$= \frac{2}{\pi} N\Delta x\, C_n$ when $\Delta u = \pm \frac{\pi}{N\Delta x}$

i.e. when $u = \frac{2\pi(n \pm \frac{1}{2})}{N\Delta x}$

Hence the bandwidth

$$\Delta u_B = 2\pi / N\Delta x \qquad (2.45)$$

and $\Delta f = \frac{1}{N\Delta x}$

Thus each discrete frequency f_n making up the gravity field contains information in the frequency range

$$\frac{n - \frac{1}{2}}{N\Delta x} \leqslant f_n \leqslant \frac{n + \frac{1}{2}}{N\Delta x}$$

and we say that the amplitude C_n predominantly represents the magnitude of gravity potential field over this segment of F.

This limitation of using discrete frequencies to represent what in reality is a continuous spectrum should be especially noted when rapidly varying filter functions such as the downward continuation filter is used. As is seen from the limits of integration in equation (2.43) bandwidth is a result of the uncertainty of the gravitational field intensity beyond the survey limits. As will be seen in chapter 3 this uncertainty causes most distortion near the edge of a survey.

2.4 Vertical Continuation and Communication Theory

We now proceed to apply communication theory to the analysis of various methods of gravity field processing.

In particular we consider vertical continuation as it has many interesting applications yet has been a difficult method to use judging by the many different techniques so far proposed. Communication theory offers an excellent medium by which to examine its intricacies.

2.4.1 Practical Applications of Vertical Continuation

The vertical continuation method can be very useful in interpreting gravity and magnetic anomaly maps. Basically this method computes the anomaly at some height or depth from the plane of measurement.

Downward continuation is able to directly calculate, at a known depth, the surface-contrast density producing a given anomaly, from the relationship:

$$\sigma_h(x,y) = \frac{1}{2\pi G}\, g_z(x,y,h) \qquad (2.46)$$

where $\sigma_h(x,y)$ is the surface contrast density at (x,y) and depth h; g(x,y,h) is the anomaly at (x,y,h) and G is the gravitational constant.

The role of downward continuation in magnetic interpretation is seen in the determination of structure from

$$\mathcal{F}(x,y,z) = \frac{\mu_0}{4\pi}\int_\tau \underset{\sim}{I}(\alpha,\beta,\gamma)\cdot \underset{\sim}{\nabla}\left(\frac{1}{r}\right) d\tau \qquad (2.47)$$

assuming unit relative permeability where $F(x,y,z)$ is the anomalous scalar magnetic field potential due to the intensity of magnetization $\underset{\sim}{I}(\alpha,\beta,\gamma)$ at (α,β,γ) over the volume τ, and

$$r = \{(x-\alpha)^2 + (y-\beta)^2 + (z-\gamma)^2\}^{1/2}$$

can be derived (see Appendix A) the relationship that the undulating magnetic basement surface $z = f(x,y)$ of infinite depth and horizontal extent is related to $H_z(\alpha,\beta,\gamma)$ the vertical anomalous field intensity at (α,β,γ) by

$$f(x,y) = \frac{1}{2\pi\mu_0 I_z} \iint_S \frac{H_z(\alpha,\beta,h)\, d\alpha\, d\beta}{\{(x-\alpha)^2 + (y-\beta)^2\}^{1/2}} \qquad (2.48)$$

where the surface integral is over the surface S and I_z is the vertical component of the intensity of magnetisation.

The surface integral can be approximated by a double summation, giving the structure by a direct computation from a grid

$$f(x,y) = \frac{1}{2\pi\mu_0 I_z} \sum_{i=-N}^{N} \sum_{j=-N}^{N} \frac{H_z(i\Delta x, j\Delta y)}{\{(x-i\Delta x)^2 + (y-j\Delta y)^2\}^{1/2}} \qquad (2.49)$$

where $\Delta x, \Delta y$ are unit grid lengths in the x and y direction and N is a value beyond which the truncation error is negligible.

Upward continuation may also be used to bring ground and airborne vertical magnetic anomaly results to the same reference plane. However, as will be seen later, this process can never be perfect.

2.4.2 Filter Response

As Tarklov and Sidorov (1960) have pointed out the regional field,

random errors and other unwanted influences on the geophysical data are interference. Processing geophysical data mathematically is the elimination of interference and the ordering and collecting of the existing information. In spite of the great diversity of mathematical methods used in processing geophysical data, they are all basically filtration methods that operate like electronic filters and have the object of detecting the anomaly (the signal) in the background of more or less intense interference (the noise). In these methods the intensity is not necessarily increased, in fact, it may be decreased. However, due to a certain decrease in the unwanted information (the noise), the anomaly to interference ratio is increased.

The principles of communication theory underlie these data processing methods. Operations on geophysical data are merely various types of space filters.

Dean (1958) proved the following results:

(1) If h is the distance of vertical continuation, taking the positive direction as down, then the theoretical frequency response of the upward and downward vertical continuation process is:

$$e^{h\sqrt{u^2+v^2}} \tag{2.50}$$

where u and v are frequency parameters in the x and y direction such that $u = 2\pi f$ where f is the frequency of an anomaly in the cycles per unit length. $\lambda = \Delta x/f$, where λ is the wavelength of the anomaly in the x-direction. An analogous relation can be derived for v.

Thus it can be seen that if the anomalous field intensity varies only

in the x-direction then the frequency response of the vertical continuation process is

(2) The frequency response of a general coefficient set $C_{m,n}$ where $C_{m,n}$ is the coefficient at the point $(m\Delta x, n\Delta y)$, assuming a uniform grid with station spacing in the x- and y-direction Δx and Δy respectively, is

$$\sum_{m=-\infty}^{\infty} \sum_{n=-\infty}^{\infty} C_{m,n}\, e^{-i(u m \Delta x + v n \Delta y)} \tag{2.51}$$

In practice we would run over m and n only up to N where for $|m|$ and $|n| > N$ the truncation error would be negligible.

Thus in the one dimensional case assuming $C_n = C_{-n}$ the filter response would be

$$C_0 + 2 \sum_{n=1}^{N} C_n \cos(u n \Delta x) \tag{2.52}$$

This is like a Fourier series which repeats itself with frequency $u\Delta x$. The period is

$$\frac{-\pi}{\Delta x} \leqslant u \leqslant \frac{\pi}{\Delta x} \tag{2.53}$$

Thus the maximum frequency at which the frequency response can be specified is

$$u_{max} = 2\pi f_{max} = \frac{2\pi}{2\Delta x} = \frac{\pi}{\Delta x} \tag{2.54}$$

where the maximum frequency $1/2\Delta x$ follows directly from the sampling theorems of communication theory (Goldman, 1955). The main effect of

digitalizing data is to limit the high frequency response to one half cycle per station spacing so that the frequency response of the coefficient set need only be considered up to $f = 1/2\Delta x$ or $\lambda = 2\Delta x$. This makes vertical continuation possible.

Thus in the analyses of vertical continuation coefficient sets which follows, the coefficient sets frequency response will be compared to the theoretical response by examining the equality of

$$e^{h|\mu|} = C_0 + 2\sum_{n=1}^{N} C_n \cos(\mu n \Delta x) \qquad (2.55)$$

2.4.3 Error Control

In any analysis of an interpretation technique the influence of errors must also be considered. Elkins (1952) and Fajklewicz (1965) both discuss the problem, Elkins showing how errors can give rise to erroneous derivative maps while Fajklewicz shows how the error introduced by a regional with extrema near local variations can cause problems.

Consider a set of random numbers η_r representing the noise component of gravity intensity measurements. In accordance with definition the η_r's are independent. We find that when transformed into the frequency domain the random numbers produce random frequency amplitudes.

From eqn. (2.26)

$$C_n = \frac{1}{N}\sum_r \eta_r e^{-i r n \xi}$$

$$|C_n| = \frac{1}{N}\sum_r \eta_r \left|e^{-i r n \xi}\right| = \frac{1}{N}\sum_r \eta_r a_{rn}$$

Thus the C_n are merely linear combinations of the η_n and hence must also be random. The spectrum of a set of random numbers is seen in figure 4. This shows that random errors (or noise) can be expected at all frequencies with no systematic decrease in the higher or lower frequencies.

Also in the special case where, for example, a tare occurs in a gravitymeter, the resulting error could be represented by a step function which is equivalent to the presence of all frequencies.

From its theoretical frequency response, downward vertical continuation is seen to be unstable in its high frequencies. Physically downward continuation is questionable because it appears that more detail is being squeezed out of the data than it contains.

The fallacy of using a coefficient set which has the theoretical response is seen by the effect on errors - the high frequency data would be greatly magnified in relation to the low frequency data so that high frequency noise would swamp low frequency information (or signal).

To overcome this problem distortion must be introduced into the frequency response over the high frequency range. The distortion used is smoothing which controls the high frequency errors.

In the analysis which follows, the various methods proposed in the literature are discussed according to their filter response and error control.

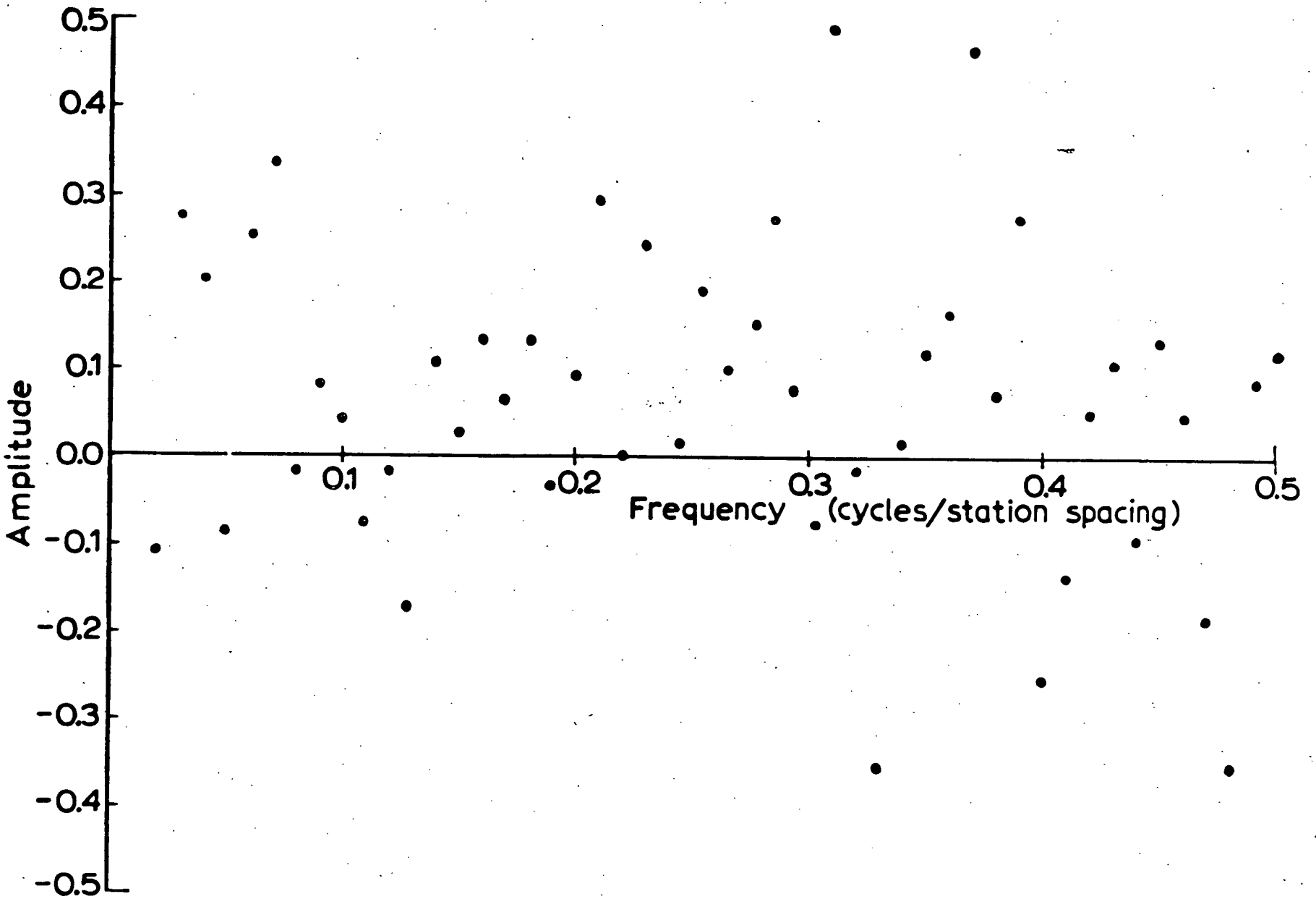

Fig. 4. Amplitude of random noise spectrum.

2.5 Some Previous Vertical Continuation Coefficient Sets Analysed

In the analysis of the downward continuation coefficient sets which follows, the anomaly is assumed, for simplicity, to vary only in one direction. For the various ring techniques the coefficients are projected onto the x-axis. In this analysis it is assumed that anomalies have already been put on a grid before interpretation begins. Fig. 5, 6 and 7 and Tables I and II show the normalised filter responses of various coefficient sets proposed in the literature.

As discussed in Dampney (1964), Bullard and Cooper's (1948) coefficient set is only one-dimensional and can, therefore, only be used for interpreting profiles.

Bullard and Cooper in deriving the relationship between smoothed gravity $\bar{g}_z(x)$ at x on the line at depth z and $g_0(x)$ use smoothing related to the error function

$$\bar{g}_z(\alpha) = \frac{1}{\pi}\int_{-\infty}^{\infty}\int_{-\infty}^{\infty} g_0(x)\, e^{-p^2/4\beta}\, e^{pz}\cos p(\alpha - x)\, dx\, dp$$

$$= \int_{-\infty}^{\infty} g_0(x)\,\lambda(x-\alpha)\, d\alpha$$

$$= \sum_{-\infty}^{\infty} g_0(n\Delta x)\,\lambda(n\Delta x - \alpha)\,\Delta x \qquad (2.56)$$

Thus $$C_n = \lambda(n\Delta x - \alpha)\,\Delta x$$

They smooth by

$$\bar{g}_0(\xi) = \sqrt{\frac{\beta}{\pi}}\int_{-\infty}^{\infty} g_0(x)\, e^{-\beta(x-\xi)^2}\, dx \qquad (2.57)$$

where β is a smoothing parameter determining the severity of smoothing. The function is simply related to the error function by

$$\bar{g}_0(0) = \sum_{n=-\infty}^{\infty} \sqrt{\frac{\beta}{\pi}}\, g_0(n\Delta x) \int_{\Delta x(n-\frac{1}{2})}^{\Delta x(n+\frac{1}{2})} e^{-\beta x^2} dx$$

$$= \sum_{n=-\infty}^{\infty} W_n\, g_0(n\Delta x)$$

where

$$W_n = \frac{1}{2}\left[erf\left\{\sqrt{\beta}\,\Delta x(n+\tfrac{1}{2})\right\} - erf\left\{\sqrt{\beta}\,\Delta x(n-\tfrac{1}{2})\right\}\right] \quad (2.58)$$

In Fig. 5 their suggested set of coefficients is analysed using a station spacing of 0.125 units, over the range $0 \leq u \leq \pi$.

This normalised filter response was worked out for both average and middle values in each range. Only variation of the order of 5% was noted between the two responses.

The normalised filter responses in Fig. 5 and Table I were calculated for various depths. Bullard and Cooper use a parameter βh^2 in their computation where h is the depth of continuation. As in both Fig. 5 and Table I the parameter was unity, the filter response was worked out for various depths namely for h = 0.1; 0.125; 0.2; 0.5; 1; 2 and 10 units corresponding to β = 100; 64; 25; 4; 1; 0.25; 0.01. Thus the severity of smoothing is increased with depth satisfying error control.

Fig. 5 and Table I show the similarity in the variation of the filter responses. In fact, it was calculated for other station spacings,

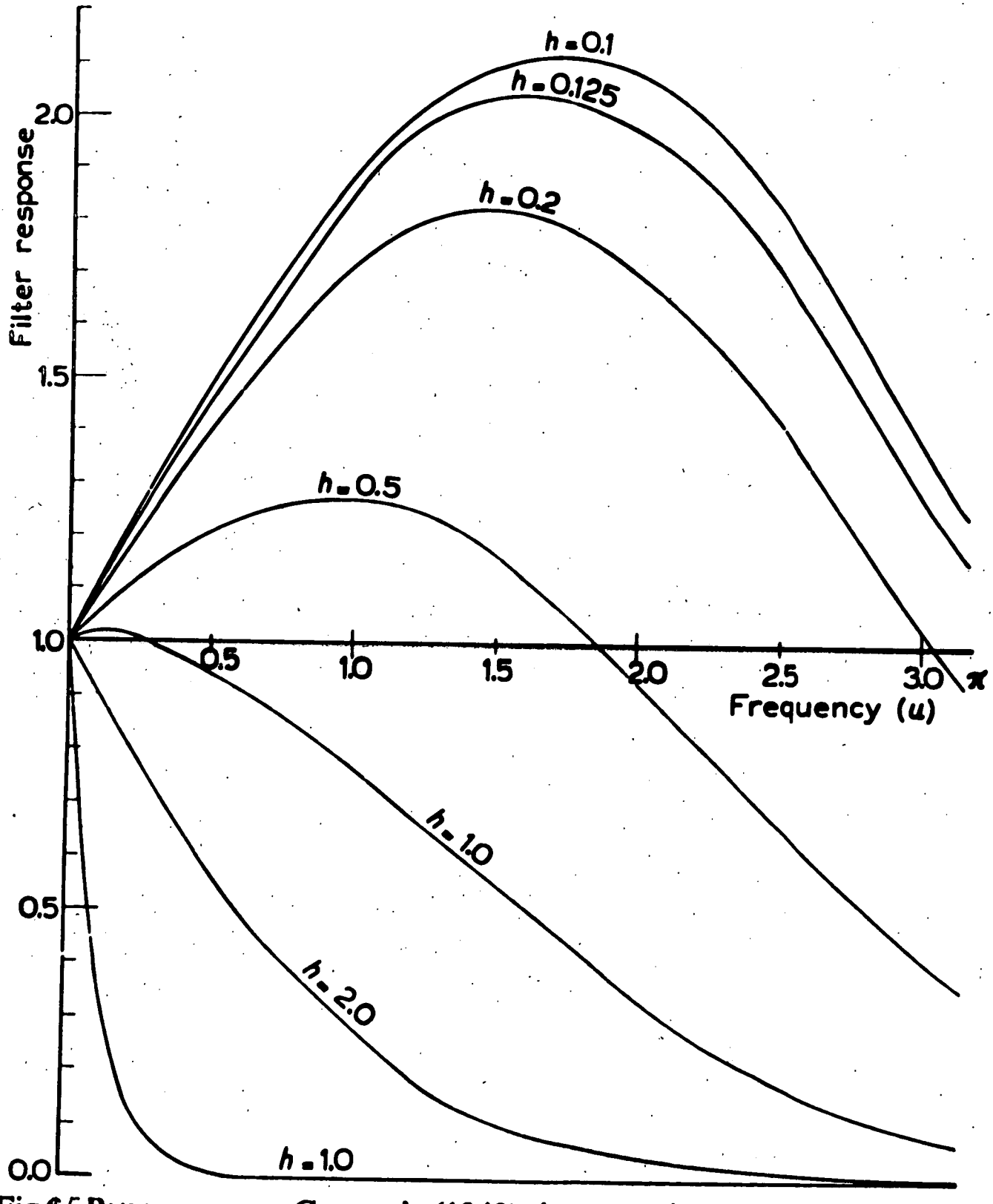

Fig. 65. BULLARD AND COOPER's (1948) downward continuation filter response

TABLE I

BULLARD AND COOPER'S (1948) COEFFICIENT SET FILTER RESPONSE[1]

10	*2*	*1*	*0.5*	*0.2*	*0.125*	*0.1*	*radians*
1.0101	1.0101	1.0101	1.0101	1.0101	1.0101	1.0101	0.0000
0.4932	0.9245	1.0000	1.0401	1.0649	1.0711	1.0733	0.0785
0.2417	0.8491	0.9936	1.0748	1.1266	1.1400	1.1445	0.1571
0.1181	0.7778	0.9845	1.1076	1.1887	1.2099	1.2170	0.2356
0.0576	0.7106	0.9729	1.1384	1.2509	1.2807	1.2908	0.3142
0.0280	0.6471	0.9584	1.1663	1.3122	1.3514	1.3647	0.3927
0.0135	0.5872	0.9407	1.1906	1.3714	1.4207	1.4376	0.4712
0.0065	0.5308	0.9198	1.2109	1.4280	1.4881	1.5087	0.5498
0.0031	0.4782	0.8964	1.2273	1.4818	1.5533	1.5779	0.6283
0.0015	0.4295	0.8708	1.2399	1.5328	1.6163	1.6451	0.7069
0.0007	0.3844	0.8432	1.2487	1.5805	1.6764	1.7096	0.7854
0.0003	0.3430	0.8137	1.2533	1.6241	1.7328	1.7706	0.8639
0.0002	0.3049	0.7825	1.2535	1.6632	1.7850	1.8275	0.9425
0.0001	0.2702	0.7501	1.2498	1.6977	1.8328	1.8802	1.0210
0.0000	0.2387	0.7169	1.2422	1.7277	1.8762	1.9285	1.0996
0.0000	0.2103	0.6830	1.2309	1.7527	1.9147	1.9719	1.1781
0.0000	0.1846	0.6487	1.2159	1.7727	1.9479	2.0100	1.2566
0.0000	0.1616	0.6142	1.1974	1.7873	1.9756	2.0427	1.3352
0.0000	0.1411	0.5799	1.1758	1.7970	1.9980	2.0698	1.4137
0.0000	0.1228	0.5460	1.1515	1.8017	2.0151	2.0917	1.4923
0.0000	0.1066	0.5128	1.1247	1.8017	2.0270	2.1081	1.5708
0.0000	0.0923	0.4803	1.0956	1.7969	2.0336	2.1192	1.6493
0.0000	0.0797	0.4487	1.0646	1.7878	2.0351	2.1249	1.7279
0.0000	0.0687	0.4183	1.0321	1.7746	2.0320	2.1259	1.8064
0.0000	0.0591	0.3891	0.9986	1.7578	2.0248	2.1225	1.8850
0.0000	0.0507	0.3613	0.9643	1.7379	2.0136	2.1149	1.9635
0.0000	0.0434	0.3348	0.9294	1.7150	1.9989	2.1036	2.0420
0.0000	0.0372	0.3098	0.8944	1.6897	1.9810	2.0889	2.1206
0.0000	0.0317	0.2862	0.8595	1.6626	1.9607	2.0715	2.1991
0.0000	0.0271	0.2642	0.8251	1.6341	1.9385	2.0521	2.2777
0.0000	0.0231	0.2436	0.7914	1.6046	1.9148	2.0309	2.3562
0.0000	0.0197	0.2245	0.7584	1.5745	1.8899	2.0085	2.4347
0.0000	0.0167	0.2068	0.7265	1.5442	1.8645	1.9854	2.5133
0.0000	0.0143	0.1904	0.6958	1.5142	1.8391	1.9622	2.5918
0.0000	0.0121	0.1753	0.6664	1.4848	1.8140	1.9393	2.6704
0.0000	0.0103	0.1615	0.6384	1.4563	1.7897	1.9170	2.7489
0.0000	0.0088	0.1488	0.6118	1.4288	1.7663	1.8957	2.8274
0.0000	0.0075	0.1372	0.5866	1.4026	1.7442	1.8756	2.9060
0.0000	0.0064	0.1266	0.5628	1.3779	1.7235	1.8571	2.9845
0.0000	0.0055	0.1169	0.5405	1.3547	1.7046	1.8402	3.0631
0.0000	0.0047	0.1080	0.5194	1.3330	1.6872	1.8251	3.1416

[1] Each column is headed by the distance of vertical continuation in units of station spacings (Station spacing = 1.0 unit), or by "radians" which is given in units of frequency. The unit of the normalised filter response for a given distance of vertical continuation and frequency is dimensionless.

and displayed the same characteristics. However, at the smaller depths, the coefficient set filter response does not match up with the theoretical response over the lower frequencies.

The normalised filter response of Henderson's (1960) coefficient set, is shown in Fig. 6 and Table II. Henderson's (1960) downward continuation can be seen to have smooth error control in relation to the filter response increasing, as required with depth. Henderson's method is able to most often satisfy error control and filter response requirements.

Fig. 7 shows the normalised filter response of Peters' (1949), Henderson and Zeitz (1949) and the finite differences (Bullard and Cooper, 1948) coefficient sets for the indicated values of h, with unit station spacing. The first 80 coefficients were used for the finite differences method and the first 23 coefficients in the rapidly convergent Henderson and Zeitz method. All these filter responses appear unsatisfactory, except the downward continuation finite differences coefficient set. Upward continuation coefficient sets tend to oscillate and do not, in any case, match the theoretical response, in the low-frequency range.

Upward vertical continuation is by contrast a very stable process. Gravity and magnetic data have predominantly low frequencies even near their source. Away from the source, upward continuation favours low frequencies because it is a low mass filter (see eqn. (2.50)). The low frequencies are essential for defining all gravity and magnetic anomalies. The higher frequencies are relatively more important for the smaller sharper anomalies and for defining details.

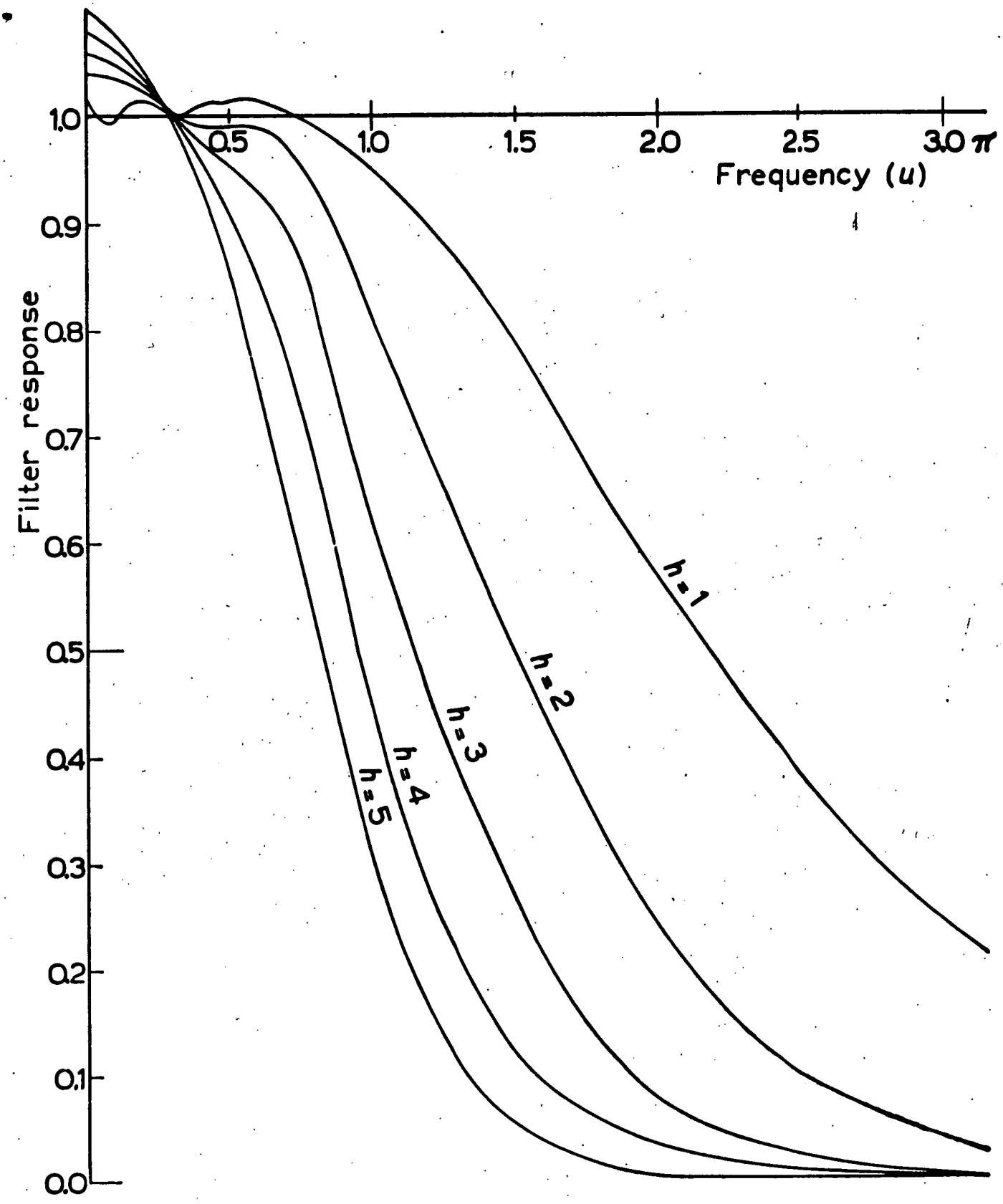

Fig. 6. HENDERSON's (1960) downward continuation filter response.

TABLE II

HENDERSON'S (1960) COEFFICIENT SET FILTER RESPONSE[1]

−5.0	*−4.0*	*−3.0*	*−2.0*	*−1.0*	*1.0*	*2.0*	*3.0*	*4.0*	*5.0*	*radians*
0.9019	0.9210	0.9404	0.9601	0.9800	1.0199	1.0398	1.0595	1.0790	1.0983	0.0000
1.0442	1.0318	1.0214	1.0128	1.0057	0.9953	0.9912	0.9874	0.9836	0.9794	0.0785
0.8704	0.9068	0.9371	0.9624	0.9832	1.0130	1.0221	1.0275	1.0291	1.0269	0.1571
0.8972	0.9256	0.9495	0.9698	0.9866	1.0098	1.0158	1.0177	1.0154	1.0085	0.2356
1.0658	1.0232	1.0027	0.9957	0.9961	1.0043	1.0067	1.0050	0.9976	0.9832	0.3142
0.9103	0.9276	0.9485	0.9685	0.9860	1.0091	1.0114	1.0040	0.9853	0.9542	0.3927
0.5527	0.7408	0.8577	0.9293	0.9732	1.0130	1.0111	0.9917	0.9538	0.8983	0.4712
−0.1267	0.4272	0.7226	0.8773	0.9581	1.0150	1.0040	0.9660	0.9027	0.8192	0.5498
−0.6403	0.2334	0.6544	0.8554	0.9528	1.0112	0.9858	0.9244	0.8333	0.7233	0.6283
1.3180	1.0650	0.9974	0.9638	0.9797	0.9971	0.9530	0.8666	0.7497	0.6193	0.7069
5.6484	2.6375	1.4962	1.1100	1.0099	0.9819	0.9161	0.8029	0.6626	0.5181	0.7854
10.5983	4.1176	1.8761	1.1840	1.0182	0.9698	0.8788	0.7376	0.5771	0.4250	0.8639
13.9335	4.7438	1.8995	1.1391	0.9997	0.9592	0.8398	0.6711	0.4955	0.3424	0.9425
3.3950	1.1110	0.7090	0.7926	0.9271	0.9518	0.8007	0.6059	0.4203	0.2717	1.021
−8.9543	−2.5160	−0.3416	0.5154	0.8750	0.9366	0.7542	0.5393	0.3510	0.2120	1.100
41.3289	9.9167	2.4477	1.0549	0.9550	0.9047	0.6968	0.4712	0.2879	0.1625	1.178
113.263	24.8208	5.1729	1.4652	1.0012	0.8756	0.6423	0.4092	0.2341	0.1232	1.257
−2.5687	−4.2193	−1.6220	0.0740	0.7978	0.8627	0.5980	9.3562	0.1898	0.0928	1.335
−284.999	−63.9689	−13.4577	−1.9886	0.5395	0.8472	0.5531	0.3075	0.1524	0.0692	1.414
−389.193	−83.6603	−16.9052	−2.4989	0.4957	0.8151	0.5023	0.2614	0.1208	0.0510	1.492
−258.901	−60.4736	−13.0092	−1.8937	0.5790	0.7762	0.4516	0.2202	0.0949	0.0373	1.571
−69.0811	−29.6844	−8.3660	−1.2556	0.6581	0.7383	0.4047	0.1846	0.0741	0.0271	1.649
247.358	16.3920	−2.2226	−0.5213	0.7382	0.7009	0.3614	0.1540	0.0575	0.0195	1.728
477.795	43.8706	0.5372	−0.2865	0.7680	0.6655	0.3219	0.1280	0.0445	0.0140	1.806
517.737	40.6837	−1.1287	−0.5800	0.7555	0.6315	0.2860	0.1095	0.0342	0.0100	1.885
1019.64	83.8747	1.6006	−0.4692	0.7764	0.5971	0.2529	0.0871	0.0261	0.0071	1.963
1272.97	82.0746	−1.6236	−0.9501	0.7604	0.5640	0.2230	0.0715	0.0199	0.0050	2.042
−38.1514	−89.1489	−20.9338	−2.6827	0.6789	0.5325	0.1963	0.0584	0.0151	0.0035	2.121
−3629.34	−450.100	−53.3778	−5.0615	0.5864	0.5017	0.1723	0.0476	0.0114	0.0025	2.199
−14042.0	−1302.00	−116.400	−8.9480	0.4498	0.4722	0.1509	0.0387	0.0086	0.0017	2.278
−20779.4	−1664.00	−128.600	−8.5916	0.5605	0.4412	0.1314	0.0313	0.0064	0.0012	2.356
16439.4	1277.12	88.8265	5.6824	1.2921	0.4070	0.1133	0.0252	0.0048	0.0008	2.435
81484.4	5697.48	369.627	21.5187	1.9954	0.3759	0.0977	0.0202	0.0036	0.0006	2.513
64480.0	4431.96	282.778	16.3556	1.8107	0.3522	0.0849	0.0162	0.0027	0.0004	2.592
−29810.7	−1150.00	−26.2928	1.2789	1.3123	0.3309	0.0737	0.0130	0.0020	0.0003	2.670
−37579.0	−1566.00	−45.6933	0.6764	1.3634	0.3078	0.0635	0.0104	0.0015	0.0002	2.749
33939.6	1819.16	106.070	6.9501	1.6295	0.2852	0.0546	0.0083	0.0011	0.0001	2.827
43212.8	1906.43	97.8603	6.4648	1.6924	0.2647	0.0469	0.0066	0.0008	0.0001	2.906
−12578.8	−807.300	−19.3035	2.3692	1.6786	0.2456	0.0403	0.0052	0.0006	0.0001	2.985
−241570	−9903.00	−349.300	−7.7623	1.5538	0.2280	0.0345	0.0041	0.0004	0.0000	3.063
−604221	−22410.0	−739.300	−17.8794	1.4840	0.2112	0.0296	0.0033	0.0003	0.0000	3.142

[1] Each column is headed by the distance of vertical continuation in units of station spacings (Station spacing = 1.0 unit), or by "radians" which is given in units of frequency. The unit of the normalised filter response for a given distance of vertical continuation and frequency is dimensionless.

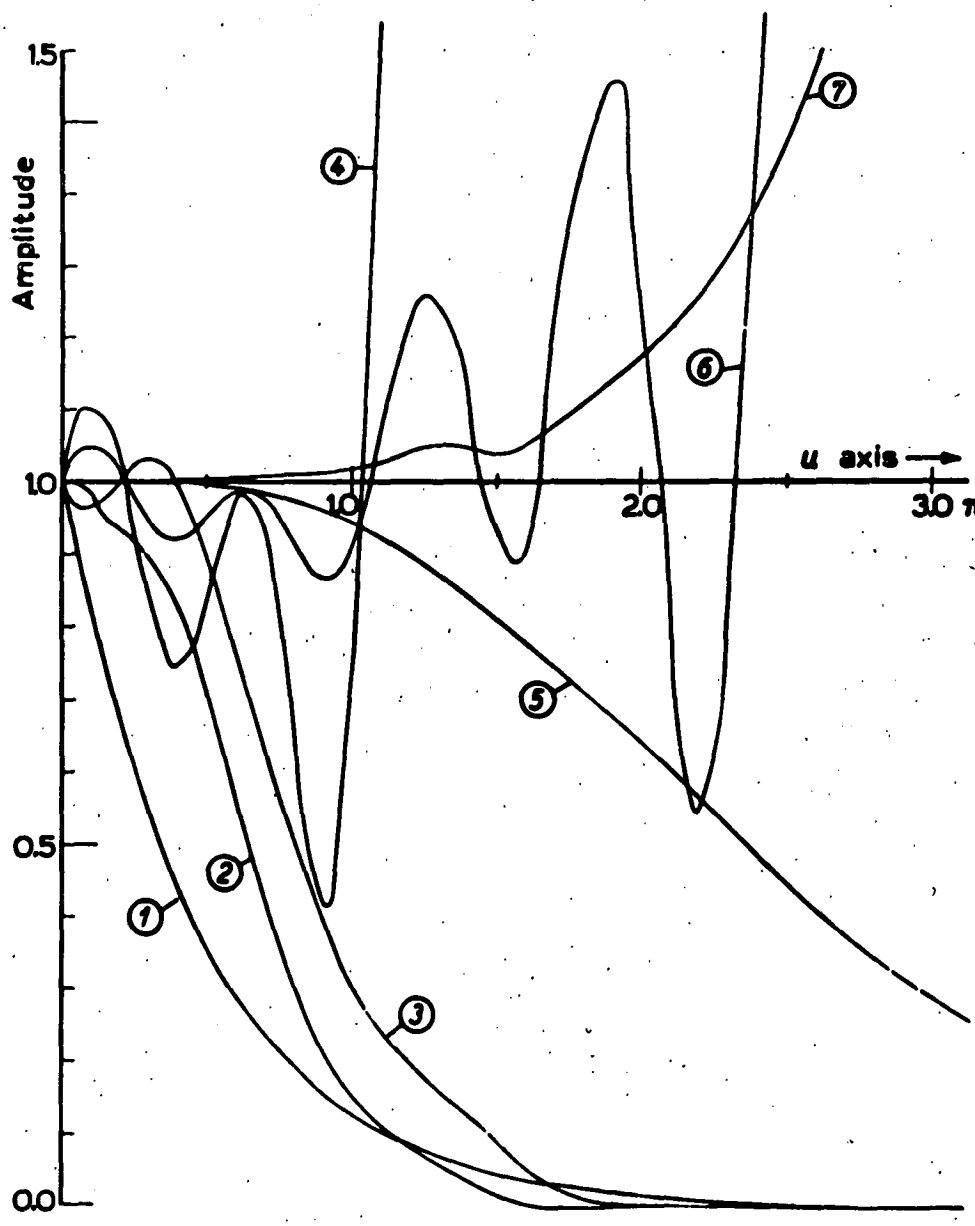

Fig. 7. Filter response of indicated coefficient sets. *1* = Finite difference method, $h = 1$; *2* = PETER's (1949) method, $h = 2$; *3* = PETER's (1949) method, $h = 1$; *4* = PETER's (1949) method, $h = -2$; *5* = finite difference method, $h = -1$; *6* = PETER's (1949) method, $h = -1$; *7* = HENDERSON AND ZEITZ' (1949) method, $h = -1$.

Upward vertical continuation smooths down the higher frequencies, reducing information in this range. Low-frequency noise in a perfect response coefficient set swamps high frequency information. Generally this does not matter, so that error control is not nearly as important in this process.

The normalised filter response of Henderson's (1960) coefficient sets for various negative values of h with unit station spacing are shown in Table II. The mismatch in the high frequencies is at once noticeable, but the filter response decreases correctly in the important low-frequency range preserving the regional information. However, Henderson's method would allow high-frequency information to be vastly accentuated beyond their theoretical amplification, producing a derived anomaly map containing all frequencies and thus looking correct, but in actual fact not possessing the correct relationship to its original data.

The upward continuation process can therefore be only really useful as a numerical filter. As errors occurring in magnetometers and gravity-meters can not be made frequency dependent, it is not yet possible to match up ground and airborne anomaly results through all the frequencies simultaneously in the spacial domain.

Henderson's coefficient set for continuing upwards a theoretical anomaly of a particular body, which, by definition, has no error, would be highly unsatisfactory.

Strakhov (e.g. 1961, 1962a, 1962b, 1963a, 1963b, 1963c, 1964) and Strakhov and Lapina (1962 and 1963) have written many articles on potential field analysis including various methods and analysis of second-derivative and vertical continuation methods. The articles are generally intensely

mathematical using many unfamiliar inequalities and equalities of harmonic analysis, though their truth is undoubted.

Strakhov's approach in his articles is fundamentally different as he uses the Fourier Transform to translate his information into the frequency domain. This requires interpolation between his data points and he thus derives optimum formula to carry out this process. However, it is felt here that using the Fourier Transform is unnecessarily complicated because the assumption that there are no frequencies in the field greater than

$$f_{max} = \frac{1}{2\Delta x} \tag{2.59}$$

allows the direct use of coefficient sets derived by expanding eqn. (2.55) to the two-dimensional case. In fact at some point in the development of the Fourier Transform approach, a series of some sort has to be substituted for an integral so that the discrete points can be used. This may as well be done immediately.

The reader is especially referred to his article, "The derivation of optimum numerical methods for the transformation of potential fields," (Strakhov, 1963c) as an excellent list of references, especially of many Russian authors, is included.

Elkins (1952) showed the effect of taking the second derivative, using his own coefficient sets, of a grid of random normally distributed errors. The appearance of the anomalies he gets can be explained by the filter response unequally affecting all the frequencies in the data.

Danes and Ondrey (1962) have analysed second derivative methods and

compared them to the theoretical second derivative filter response of $e^{\sqrt{u^2+v^2}}$ in a similar fashion to the preceding vertical continuation analysis. They do not consider the effect of errors in this comparison, however. As it turns out (see later), there is no need to consider error control because the theoretical frequency response of second derivative methods does not increase sufficiently.

3. DERIVATION OF COEFFICIENT SETS

Assuming that the measurements of the gravitational field intensity are such that the frequencies present beyond the cut-off frequency are negligible then the coefficient sets which follow, perfectly carry out the analytical process they are supposed to.

The purpose of deriving these coefficient sets is to allow a closer analysis of their effect on data and to demonstrate their limitations.

3.1 Noise Level

Error control must first be satisfied in any process by cutting out the high-frequency data with frequency greater than $|u_o|$ beyond which the errors are greater than the lowest-frequency information in the data.

The noise to signal (information) ratio in the data, assumed to be on a grid, can be taken as being the ratio

$$\frac{\text{standard deviation of anomaly}}{\text{standard deviation of error}} = x$$

The error or noise in gravity data may be estimated from the loop misclosures. However in calculating the Bouguer Anomaly further errors are introduced into the data by the following assumptions.

(a) The Free Air Correction increases linearly with height above the reference spheroid (the International Ellipsoid).

(b) In calculating the Bouguer Correction the earth is assumed to be flat.

The errors introduced by these assumptions are systematic and in particular for the Derby Survey are of the order of 10^{-3} mgal. between stations.

The main source of error however is the topographic correction. Even an observer of normal mass has a gravitational attraction of the order of 10^{-2} mgal. which affects the gravitymeter when he stoops over to read it. This emphasizes the difficulty of allowing for the small but unfortunately important local topographic variations. Hammer's (1943) terrain correction tables for instance ignore the region within eight feet of the meter as being too variable to be accounted for.

Gravitymeter drift introduces errors. Tides (lunar and solar) cause regular variations in the gravity field and may be allowed for, but atmospheric disturbances moving great masses of air can, as Romanyuk (1959) points out, result in gravity field fluctuations of a similar magnitude and hence errors of the order of 10^{-1} of a mgal. In fact, the onset of a storm will often cause erratic drift in the gravitymeter due to this latter effect. All these influences contribute to the noise level. In the Derby-Winnaleah survey discussed in chapter 6 for example we assumed, giving consideration to the highly variable topography, a noise level of the order of 0.25 mgal.

Gravity surveys are usually composed of a number of loops around each of which a series of measurements are taken. Generally misclosures occur, allowing an estimate of the errors due to drift and other time dependent effects to be made at each point. Assuming topography and the co-ordinates of each point of measurement to have been exactly defined we can take the standard deviation of these errors as the noise level. The

standard deviation of the anomaly is taken as the signal level. This ratio is taken without any pretence of mathematical rigour, but is sufficiently representative for practical purposes.

Thus if the distance of downward continuation is h then the frequency above u_0 must be filtered out where

$$e^{hu_0} = x \tag{3.1}$$

because above this value of u_0 the amplification of the errors will be greater than the amplification of the zero frequency information.

Using this fact, the maximum anomaly size that can be interpreted from downward continued data for a signal to noise ratio of 200 is shown in fig. 8.

3.2 Smoothing

A numerical filter is therefore required which will cut out these high frequencies. Smoothing by an erf function as used by Bullard and Cooper (1948) would be suitable, but, for simplicity, a two-dimensional symmetrical step function is used in the frequency domain.

The coefficient set which has the required filter response is calcualted. Put

$$\sum_{m=-\infty}^{\infty}\sum_{n=-\infty}^{\infty} C_{m,n}\, e^{-i(um\Delta x + vn\Delta y)} = f(u,v) \tag{3.2}$$

where $f(u,v)$ is a symmetric function with respect of u and v about 0. Suppose $\Delta x = \Delta y = 1$ then

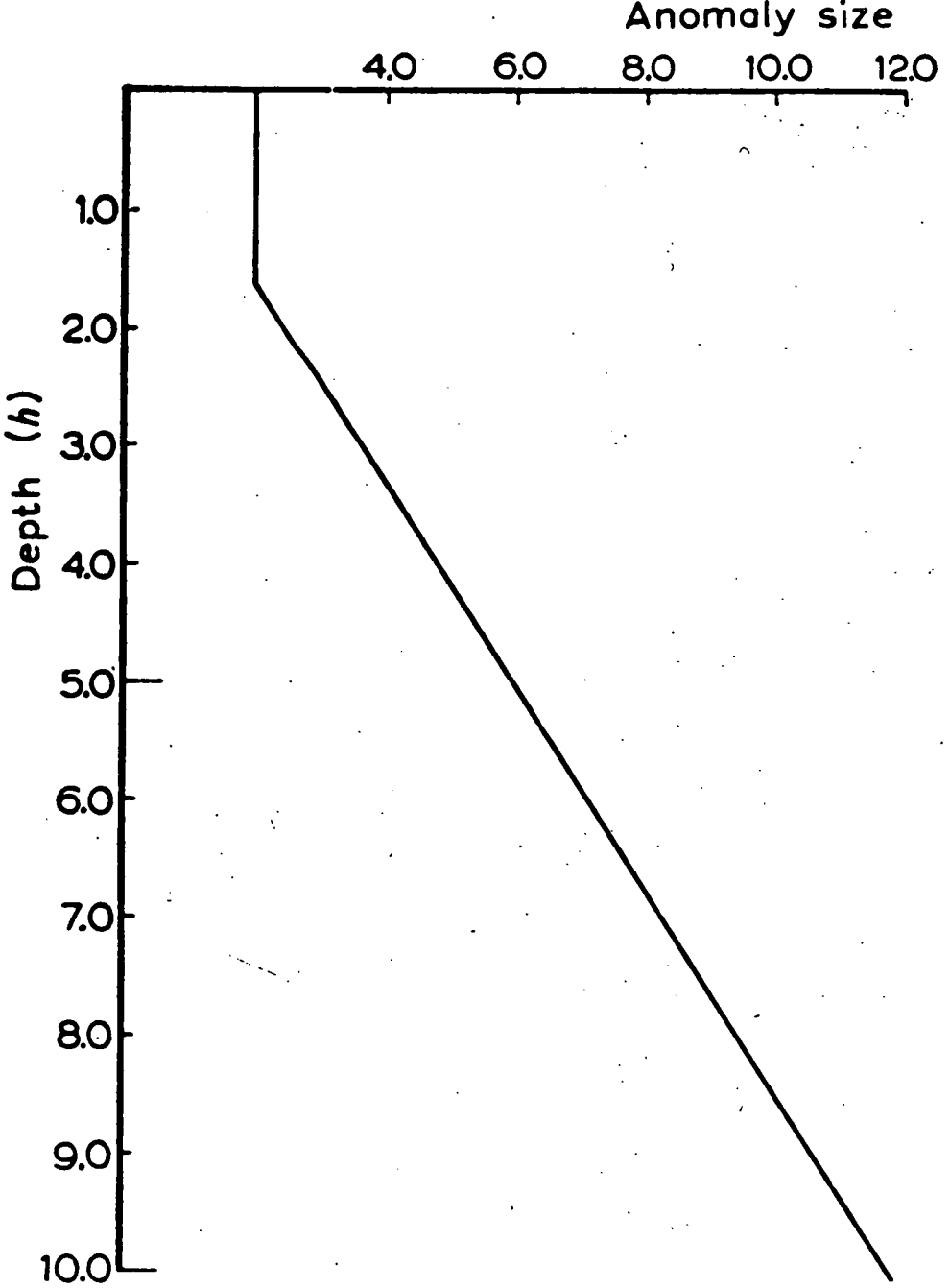

Fig.8. Minimum anomaly size detectable at depth h in units of station spacing.

$$C_{m,n} = \frac{1}{4\pi^2}\int_{-\pi}^{\pi}\int_{-\pi}^{\pi} f(u,v)\, e^{i(um+vn)}\, du\, dv$$

$$= \frac{1}{4\pi^2}\int_{-\pi}^{\pi}\left(\int_{0}^{\pi} + \int_{-\pi}^{0}\right) f(u,v)\, e^{i(um+vn)}\, du\, dv$$

In the range 0 to $-\pi$ put $v = -v$

$$\therefore C_{m,n} = \frac{1}{4\pi^2}\int_{-\pi}^{\pi} du\, e^{ium}\int_{0}^{\pi} 2\cos(vn)\cdot f(u,v)\, dv$$

as $f(u,v) = f(u,-v)$

$$C_{m,n} = \frac{1}{\pi^2}\int_{0}^{\pi}\int_{0}^{\pi} f(u,v)\cos(um). \qquad (3.3)$$

as $f(u,v) = f(-u,v)$. Thus the coefficient set with the required filter response is found.

The two dimensional symmetric step function is given by:

$$f(u,v) = 1$$

$-u_0 \leq u \leq u_0$; $-u_0 \leq v \leq u_0$ or = 0 otherwise

Therefore

$$C_{m,n} = \frac{1}{\pi^2}\int_{0}^{u_0}\cos(um)\int_{0}^{u_0}\cos(vn)\, du\, dv$$

$$= \frac{1}{\pi^2} \times \frac{1}{nm}\sin(u_0 m)\sin(u_0 n) \qquad (3.4)$$

Note that $C_{m,n} = C_{m,-n} = C_{m,n} = C_{-m,-n} = C_{n,m} = C_{n,-m} = C_{-n,m} = C_{-n,-m}$

that is $C_{m,n}$ is eight-fold symmetric.

Example: Suppose for a survey we find that x = 112, which means that the errors are of the order of 0.1 mgal and the variations of the anomaly are about 11 mgal. We wish to continue this data downwards to a distance of five units

$$\therefore e^{hu_0} = 112$$

$$\therefore u_0 \approx 1.571 \approx \pi/2$$

Thus

$$\left.\begin{aligned} C_{m,n} &= \frac{1}{\pi^2} \times \frac{1}{nm} \sin\left(\frac{\pi m}{2}\right) \sin\left(\frac{\pi n}{2}\right) \\ C_{m,0} &= \frac{1}{2\pi} \times \frac{1}{m} \sin\left(\frac{\pi m}{2}\right) = C_{0,m} \\ C_{0,0} &= \frac{1}{4} \end{aligned}\right\} \quad (3.5)$$

Table III gives the right-hand quadrant of this coefficient set up to n = 10 and m = 10.

Smoothing is thus carried out on the data and then with no high frequencies present a downward continuation coefficient set can now be applied to the data.

3.3 Vertical Continuation

A vertical continuation coefficient set is found similarly to the smoothing coefficient set

$$C_{m,n} = \frac{1}{\pi^2} \int_0^{\pi} \int_0^{\pi} e^{h\sqrt{u^2+v^2}} \cos(mu)\cos(nv)\,du\,dv \quad (3.6)$$

TABLE III

SMOOTHING COEFFICIENT SET

n	$m = 0$	$m = 1$	$m = 2$	$m = 3$	$m = 4$	$m = 5$	$m = 6$	$m = 7$	$m = 8$	$m = 9$	$m = 10$
10	0.00000	0.00000	0.00000	0.00000	0.00000	0.00000	0.00000	0.00000	0.00000	0.00000	0.00000
9	0.01768	0.01126	0.00000	−0.00375	0.00000	0.00225	0.00000	−0.00161	0.00000	0.00125	0.00000
8	0.00000	0.00000	0.00000	0.00000	0.00000	0.00000	0.00000	0.00000	0.00000	0.00000	0.00000
7	−0.02274	−0.01447	0.00000	0.00482	0.00000	−0.00289	0.00000	0.00201	0.00000	−0.00161	0.00000
6	0.00000	0.00000	0.00000	0.00000	0.00000	0.00000	0.00000	0.00000	0.00000	0.00000	0.00000
5	0.03183	0.02026	0.00000	−0.00675	0.00000	0.00405	0.00000	−0.00289	0.00000	0.00225	0.00000
4	0.00000	0.00000	0.00000	0.00000	0.00000	0.00000	0.00000	0.00000	0.00000	0.00000	0.00000
3	−0.05305	−0.03377	0.00000	0.01126	0.00000	−0.00675	0.00000	0.00482	0.00000	−0.00375	0.00000
2	0.00000	0.00000	0.00000	0.00000	0.00000	0.00000	0.00000	0.00000	0.00000	0.00000	0.00000
1	0.15916	0.10132	0.00000	−0.03377	0.00000	0.02026	0.00000	−0.01447	0.00000	0.01126	0.00000
0	0.25000	0.15916	0.00000	−0.05305	0.00000	0.03183	0.00000	−0.02274	0.00000	0.01768	0.00000

TABLE IV

DOWNWARD CONTINUATION COEFFICIENT SET

n	$m = 0$	$m = 1$	$m = 2$	$m = 3$	$m = 4$	$m = 5$	$m = 6$	$m = 7$	$m = 8$	$m = 9$	$m = 10$
10	0.10615	−0.02190	0.00714	−0.00361	0.00188	−0.00141	0.00081	−0.00076	0.00044	−0.00047	0.00027
9	−0.13119	0.02660	−0.00918	0.00409	−0.00263	0.00146	−0.00124	0.00072	−0.00072	0.00042	−0.00047
8	0.16500	−0.03416	0.01107	−0.00565	0.00290	−0.00221	0.00126	−0.00117	0.00069	−0.00072	0.00044
7	−0.21547	0.04366	−0.01518	0.00669	−0.00436	0.00239	−0.00204	0.00120	−0.00117	0.00072	−0.00076
6	0.29011	−0.06043	0.01943	−0.01005	0.00510	−0.00389	0.00224	−0.00204	0.00126	−0.00124	0.00081
5	−0.41562	0.08427	−0.02962	0.01287	−0.00846	0.00467	−0.00389	0.00239	−0.00221	0.00146	−0.00141
4	0.63311	−0.13375	0.04254	−0.02226	0.01131	−0.00846	0.00510	−0.00436	0.00290	−0.00263	0.00188
3	−1.09070	0.22317	−0.07954	0.03454	−0.02226	0.01287	−0.01005	0.00669	−0.00565	0.00409	−0.00361
2	2.18630	−0.48546	0.15438	−0.07954	0.04254	−0.02962	0.01943	−0.01518	0.01107	−0.00918	0.00714
1	−5.84827	1.35202	−0.48546	0.22317	−0.13375	0.08427	−0.06043	0.04366	−0.03416	0.02660	−0.02190
0	15.78620	−5.84827	2.18630	−1.09070	0.63311	−0.41562	0.29011	−0.21547	0.16500	−0.13119	0.10615

$C_{m,n}$ has been calculated by Takeuchi and Saito (1964) for h = 1 which corresponds to a downward continuation of one station spacing. They interpret $C_{m,n}$ following Tsuboi and Tomoda (1958) as giving the surface mass density on square grid-points over a horizontal underground surface, depth D below the earth's surface, from a gravity field with unit gravity at the origin and zero gravity everywhere else on the earth's surface.

Takeuchi and Saito transform equation (3.6) to the form

$$C_{m,n} = \int_0^{\pi/4} f(\theta)\, d\theta \qquad (3.7)$$

using polar co-ordinates and then calculate $C_{m,n}$ using a Simpson approximation.

The right-hand upper quadrant of this coefficient set is given in Table IV.

The coefficient set for h = -1 was computed using a double Simpson approximation.

$$C_{m,n} = \frac{1}{\pi^2}\int_0^{\pi}\int_0^{\pi} e^{h\sqrt{u^2+v^2}} \cos(mu)\cos(nv)\,du\,dv$$

$$= \frac{1}{\pi^2}\sum_{j=0}^{m}\sum_{k=0}^{n}\int_{p1}^{p2}\int_{q1}^{q2} e^{h\sqrt{u^2+v^2}} \cos(mu)\cos(nv)\,du\,dv \qquad (3.8)$$

where $p1 = 0$ when $j = 0$

$$= \frac{\pi}{m}\left(j-\frac{1}{2}\right) \text{ otherwise.}$$

$p2 = \pi$ when $j = m$

$$= \frac{\pi}{m}\left(j+\frac{1}{2}\right) \text{ otherwise.}$$

$q1 = 0$ when $k = 0$

$= \frac{\pi}{m}\left(k - \frac{1}{2}\right)$ otherwise.

$q2 = \pi$ when $k = m$

$= \frac{\pi}{m}\left(j + \frac{1}{2}\right)$ otherwise.

We thus have to calculate the function shown in fig. 9.

As is seen the use of the Simpson approximation for each double integral in the summation over j and k is ideal.

In accordance with Forsythe (1964), the first integration with respect to v had to be more accurate than the second with respect to u. This was done by making the sensitivity of the first integration ten times smaller than the second integration.

Thus to calculate $C_{m,n}$ $(m+1)(n+1)$ integrations had to be made. To calculate all the square matrix of $C_{m,n}$ from $C_{0,0}$ to $C_{M,M}$ required

$$\frac{M(M+1)(M+2)(3M+5)}{12} \quad \text{integrations} \qquad (3.9)$$

= 3850 integrations for M = 10

As the program required 3600 seconds to calculate the matrix, we find that each integration requires 1 second.

The coefficient set is shown in Table V.

Second derivative

As Dean (1958) has shown the second differential theoretical filter

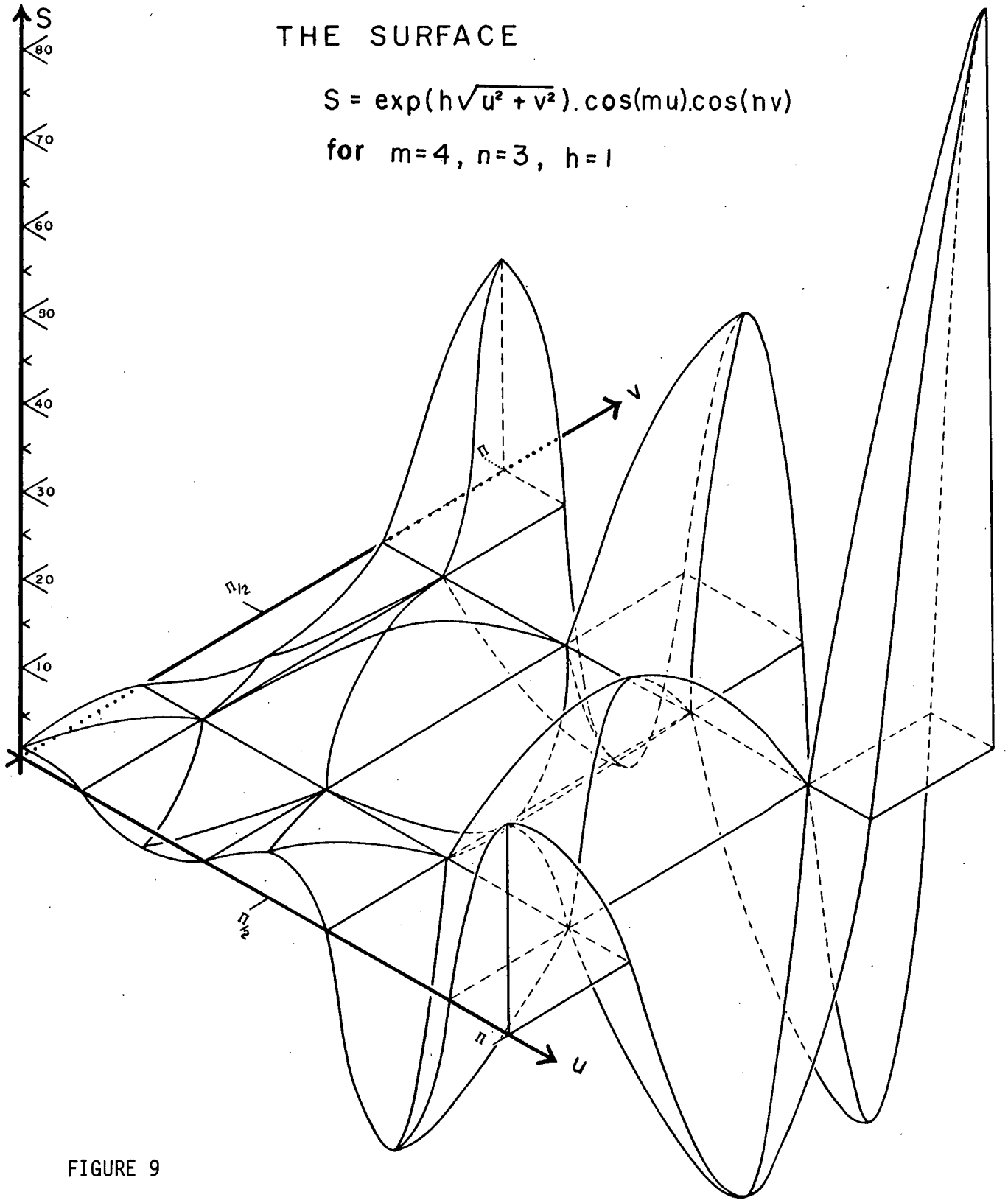
THE SURFACE
$S = \exp(h\sqrt{u^2 + v^2}).\cos(mu).\cos(nv)$
for m=4, n=3, h=1
S
80
70
60
50
40
30
20
10
V
U
Π
Π/2
Π/2
Π

FIGURE 9

TABLE V Upward Continuation Coefficient Set

n	m = 0	m = I	m = 2	m = 3	m = 4	m = 5	m = 6	m = 7	m = 8	m = 9	m = I0
I0	0.00007	0.000I3	0.000I5	0.000I4	0.000I3	0.000II	0.000I0	0.00009	0.00008	0.00006	0.00006
9	0.00032	0.00024	0.00020	0.000I8	0.000I6	0.000I4	0.000I2	0.000II	0.00009	0.00008	0.00006
8	0.000I7	0.00026	0.00028	0.00025	0.00022	0.000I9	0.000I6	0.000I3	0.000II	0.00009	0.00008
7	0.00062	0.00049	0.00040	0.00035	0.00030	0.00025	0.00020	0.000I6	0.000I3	0.000II	0.00009
6	0.00048	0.0006I	0.0006I	0.0005I	0.0004I	0.00033	0.00026	0.00020	0.000I6	0.000I2	0.000I0
5	0.00I53	0.00I23	0.00097	0.00077	0.00058	0.00044	0.00033	0.00025	0.000I9	0.000I4	0.000II
4	0.00I76	0.00I93	0.00I66	0.00I20	0.00084	0.00058	0.0004I	0.00030	0.00022	0.000I6	0.000I3
3	0.00590	0.00462	0.00303	0.00I93	0.00I20	0.00077	0.0005I	0.00035	0.00025	0.000I8	0.000I4
2	0.0I242	0.0I036	0.00590	0.00303	0.00I66	0.00097	0.0006I	0.00040	0.00028	0.00020	0.000I5
I	0.05965	0.03260	0.0I036	0.00462	0.00I93	0.00I23	0.00063	0.00049	0.00026	0.00024	0.000I3
0	0.I37I8	0.05965	0.0I242	0.00590	0.00I76	0.00I53	0.00048	0.00062	0.000I7	0.00032	0.00007

response is u^2+v^2. The highest frequency data is therefore amplified by a factor of $2\pi^2$. In all practical cases this value would be far below the signal to noise ratio and no account need be taken of error control, other than realising unequal amplification of errors.

Therefore a coefficient set having the perfect filter response would be best for this process.

$$C_{m,n} = \frac{1}{\pi^2}\int_0^{\pi} dv \cos(nv)\int_0^{\pi}(u^2+v^2)\cos(mu)\,du$$

$$= \frac{1}{\pi^2}\int_0^{\pi} dv \cos(nv)\int_0^{\pi} u^2\cos(mu)\,du + \frac{1}{\pi^2}\int_0^{\pi} dv \cos(nv)\,v^2\int_0^{\pi}\cos(mu)\,du$$

$$C_{0,n} = \frac{1}{\pi^2}\int_0^{\pi}\int_0^{\pi}(u^2+v^2)\cos(nu)\,du\,dv$$

$$= \frac{2}{n^2}\cos(n\pi)$$

$$C_{m,n} = 0 \quad (m,n \neq 0)$$

$$C_{0,0} = 2\pi^2/3 \qquad (3.10)$$

The upper quadrant of this coefficient set is found from Table VI.

TABLE VI

SECOND DERIVATIVE COEFFICIENT SET

n	$C_{o,n} = C_{n,o}$
10	0.02000
9	-0.02469
8	0.03125
7	-0.04082
6	0.05556
5	-0.08000
4	0.12500
3	-0.22222
2	0.50000
1	-2.00000
0	6.57972

3.3.1 Discussion of vertical continuation

From eqn. (3.6)

$$|C_{m,n}| = \frac{1}{\pi^2}\int_0^{\pi}\int_0^{\pi} e^{h\sqrt{u^2+v^2}}\cos(mu)\cos(nv)\,du\,dv$$

$$\begin{matrix}<\ (\text{if } h>0)\\ >\ (\text{if } h<0)\end{matrix}\left|\frac{1}{\pi^2}\int_0^{\pi}\cos(mu)\,e^{hu}\int_0^{\pi}\cos(nv)e^{hv}\,dv\right| \qquad (3.11)$$

$$\begin{matrix}>\ (\text{if } h>0)\\ <\ (\text{if } h<0)\end{matrix}\left|\frac{1}{\pi^2}\int_0^{\pi}\cos(mu)e^{hu}\,du\int_0^{\pi}\cos(nv)\,e^{-hv}\,dv\right| \qquad (3.12)$$

Now $$\frac{1}{\pi}\int_0^{\pi}e^{hu}\cos(mu)\,du = \frac{h}{\pi}\,\frac{(e^{\pi(h+im)}-1)}{(m^2+h^2)} \qquad (3.13)$$

$$\therefore\ |C_{m,n}| \begin{matrix}<\ (h>0)\\ >\ (h<0)\end{matrix}\left|\frac{h^2}{\pi^2}\left\{\frac{e^{h\pi}(-1)^m-1}{(m^2+h^2)}\right\}\left\{\frac{e^{h\pi}(-1)^n-1}{(n^2+h^2)}\right\}\right|$$

$$\begin{matrix}<\ (h>0)\\ >\ (h<0)\end{matrix}\left|\frac{h^2}{\pi^2}\left\{\frac{e^{2\pi h}(-1)^{m+n}-e^{h\pi}\left((-1)^m+(-1)^n\right)+1}{(m^2+h^2)(n^2+h^2)}\right\}\right|$$

$$|C_{m,n}| \begin{matrix}>\ (h>0)\\ <\ (h<0)\end{matrix}\left|\frac{h^2}{\pi^2}\left\{\frac{-(-1)^{m+n}+e^{-h\pi}(-1)^n+e^{h\pi}(-1)^m-1}{(m^2+h^2)(n^2+h^2)}\right\}\right|$$

if $h>0$

$$< \frac{h^2}{\pi^2}\,\frac{e^{2\pi h}}{(m^2+h^2)(n^2+h^2)}$$

$$|C_{m,n}| > \frac{h^2}{\pi^2}\,\frac{e^{\pi h}}{(m^2+h^2)(n^2+h^2)} \qquad (3.14)$$

if $h<0$

$$< \frac{h^2}{\pi^2}\,\frac{e^{-\pi h}}{(m^2+h^2)(n^2+h^2)}$$

$$|C_{m,n}| > \frac{h^2}{\pi^2}\,\frac{1}{(m^2+h^2)(n^2+h^2)} \qquad (3.15)$$

Table VII shows how this works with h = 1 and h = -1.

From these inequalities we can see that the farther the gravity field is continued up or down the larger are the number of data points required.

Physically this can be appreciated in the following way. The farther up an observer rises above the land surface, the larger is the volume of anomalous masses that can contribute significantly to his gravity field. In other words, while the intensity decreases with height, it is affected by a larger number of masses which now make smaller vertical angles with the point of observation.

Similarly the deeper a planar surface density source is, the greater the area over which gravity is affected on the surface. Thus the source

$$\sigma_h(x,y) = \frac{1}{2\pi G} g(x,y,h)$$

requires an increasing number of data points on the surface to specify it as the depth increases.

In other words the farther information is translated in distance above or below a finite number of data points the poorer the transmission.

While this method of Vertical Continuation is exact, it is never possible to fulfill the condition that $g(x,y,h)$ is known over an infinite area. Thus in any method of Vertical Continuation or Derivative Method the continuation of the data near the edge of the finite plane becomes poorer and poorer as h increases positively or negatively.

m	n	$C_{m,n}$					
		h = 1			h = -1		
		Lower bound	True value	Upper bound	Lower bound	True value	Upper bound
0	0	2.3495	15.7862	54.5100	0.1100	0.1372	2.3495
2	0	0.4698	2.1863	10.9000	0.0203*	0.0124	0.4698
3	1	0.1175	0.2232	2.7250	0.0051*	0.0046	0.1175
4	3	0.0138	0.0223	0.3200	0.0006	0.0017	0.0138
5	2	0.0181	0.0296	0.4190	0.0008	0.0010	0.0181
6	6	0.0017	0.0022	0.0390	0.0001	0.0003	0.0017
7	2	0.0094	0.0152	0.2180	0.0004	0.0004	0.0094
7	4	0.0028	0.0044	0.0640	0.0001	0.0003	0.0028
8	0	0.0361	0.1650	0.8390	0.0016*	0.0002	0.0361
8	1	0.0181	0.0342	0.4200	0.0007*	0.0003	0.0181
8	3	0.0036	0.0057	0.0840	0.0002	0.0003	0.0036
9	1	0.0143	0.0266	0.3320	0.0006*	0.0002	0.0143
9	2	0.0057	0.0092	0.1330	0.0002	0.0002	0.0057
9	9	0.0003	0.0004	0.0080	0.0000	0.0001	0.0003
10	5	0.0009	0.0014	0.0210	0.0000	0.0001	0.0009
10	8	0.0003	0.0004	0.0080	0.0000	0.0001	0.0003

*As $C_{m,n}$ is not monotonic the approximation in equation (3.15) is questionable and hence it breaks down for these cases. Note that $C_{m,n}$ is correct to 4 places. The lower bound however is correct providing m and n are both large for h = -1.

TABLE VII Selected coefficients illustrating equation (3.15).

This limitation we call the "edge effect" is an important restriction to the continuation of data and together with bandwidth shows why Bhattacharyya's (1965) theoretical continuation of a potential field due to a sphere breaks down near the sphere.

It is only possible to improve continuation by increasing the area over which the measurements are made, ensuring that the information which escapes in frequencies beyond the cut-off is negligible.

4. THE EQUIVALENT SOURCE TECHNIQUE

4.1 Review

As has been shown in the preceding chapters, the interpretation methods of vertical continuation and derivatives of potential fields are more accurately expressed in the frequency than the spacial domain.

In fact, it would be possible to exactly express these methods if the following three conditions were true:

(a) the data is known on a regular rectangular grid Δx by Δy which are the station spacings in the x and y directions.

(b) the data is infinite in extent over a horizontal plane.

(c) the data is sufficiently close spaced that no part of the potential field amplitude spectrum exists for frequencies greater than the cut-off frequency (see equation 2.54).

The first condition (a) is discussed in a following section. The remaining two conditions are necessary only to ensure that the spectrum is completely and continuously measured. Condition (b) implies from eqn. (2.25) that the infinite number of amplitudes C_n as $N \rightarrow \infty$ measure the spectrum continuously over the range

$$u = 2\pi n / N \Delta x ; \quad -\frac{N}{2} \leq n \leq \frac{N}{2}$$

Clearly this condition can never be satisfied, but provided we limit the distance of vertical continuation and the order of the derivative, we can assume the data has infinite extent - especially some distance in from the limits of the survey area as is seen from tables IV, V and VI.

It is not generally appreciated by many geophysicists that the Bouguer Anomaly, as described by Heiskanen and Vening- Meinesz (1956), should not be taken as being projected onto the geoid. This has been emphasized by Naudy and Newmann (1965) and Grant and Elsaharty (1962). The former proposed that

> "It is sufficient to consider the Bouguer anomaly, as the difference of two quantities, the first is the measurement at a station S amended by instrument corrections (such as drift); the second is the value of the gravitational field at the same point S of a model obtained by superimposing the ellipsoid and the topography at constant density. (Comment: There is no need to assume such a simple model.)
>
> "The significance of the Bouguer anomaly is thus ridden of ambiguity - it is the gravitational influence of the difference which exists between the real earth and the model. The point of application is at the station S and not the ellipsoid."

Figure 10 demonstrates the truth of this statement.

It is therefore necessary to vertically continue the individual potential field measurements at S from the rough topography onto a flat horizontal plane. This problem has received very little attention in the literature, except Strakhov, (1965) who applies his approach of using the Fourier Transform to manipulate discrete gravity information. As has been discussed in chapter 2 this approach is difficult to apply to gravity data.

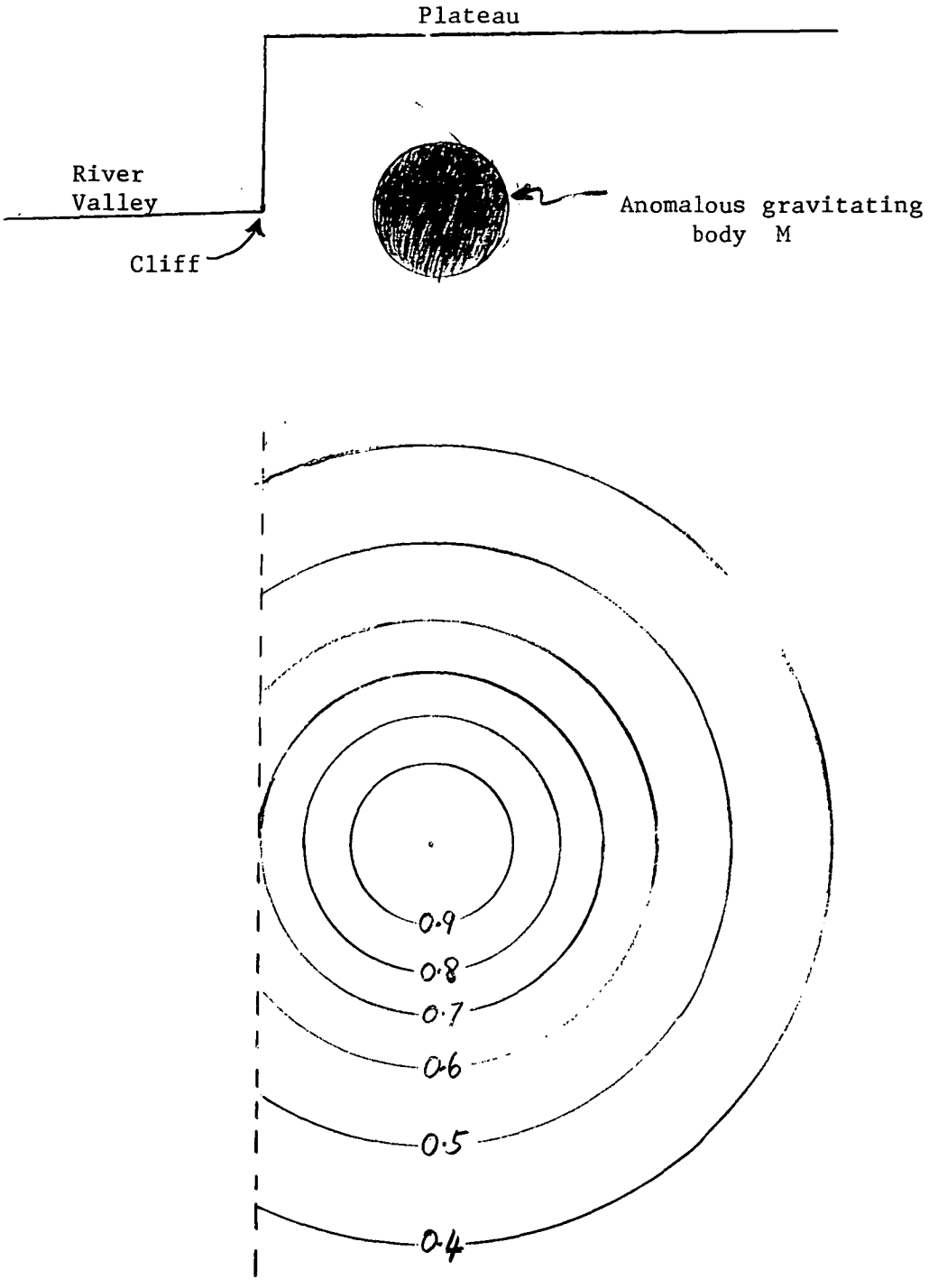

Bouguer Anomaly Contours in mgal due to M

FIGURE 10.

The equivalent source technique is therefore put forward as a method to vertically project data onto a plane.

By contrast, a great deal of attention has been focused onto the problem of projecting potential field information horizontally along a plane using interpolation. Measurements are usually made at convenient locations on the topography, so that if we assume it is flat, interpolation is required to project the information at these points onto a regular grid.

The mathematics of two-dimentional interpolation quickly becomes tedious when extending any of the conventional one-dimensional methods (for example Lagrange's Method, Neville's Method (Stafford, 1965)).

Kunz (1957) points out that a difficulty in bivariate and multivariate interpolation is that it has received only a very small amount of attention compared to that expounded on univariate interpolation. "Consequently one finds considerable arbitrariness, complexity of statement and notation, and even confusion in the various treatments of the subject.

Saltzer, particularly (1948), Grant (1957), Ho (1955) and Southard (1956), Benglsson and Norbeck (1964) have studied bivariate interpolation, all involving polynomial techniques. The extensive use of polynomial techniques in mathematical interpolation has been carried over to the geophysical literature. Brown (1955 and 1956) has given the most comprehensive application of polynomials to interpolation, vertical continuation and derivatives of the potential field. His method is complete in that he also estimates the errors involved in his least-polynomials method. Essentially Brown fits a polynomial curve to order n to k data points where

$$k \geq n$$

and then finds the standard deviation of the data points from the curve, thereby finding the expected errors. The method does have the advantage of minimizing random errors in the data. Other authors such as Jones (1956), Oldham and Sulterland (1955), Zilahi-Sebees (1964) and Grant and Elsaharty (1962) have used polynomial methods in processing potential field data.

As Kunz (1957) points out that probably the reason the greatest attention in univariate interpolation has been given to parabolic interpolation (the approximation of a function by a polynomial) is that polynomials are so nicely expressed in terms of elementary operations and very convenient to handle by differencing techniques. This same comment applies to bivariate interpolation, but this extension into the second dimension causes problems to arise. In particular, it becomes difficult to use polynomials of sufficient order, N, to even remotely represent the information contained over the entire array of data. If there are N measurements in a survey a polynomial

$$P_N(x,y) = \sum_{i=0}^{N} \sum_{j=0}^{N-i} a_{ij} x^i y^j \qquad (4.1)$$

of order N is required to represent and interpolate this data. Supposing each measurement to have an error of 1 % , then the resulting coefficient a_{ij} will have an error of N % if standard direct techniques are used to solve the resulting N by N system of equations by determinants.

Furthermore, there are numerical errors involved in representing the data points by a polynomial, the greatest of which is the Kunz Class A error - the magnitude of the remainder term in replacing the tabulated function f(x) by an interpolating polynomial $P_m(x)$. This remainder term involves

the $(m + 1)^{th}$ derivative of f(x). Thus "little can be said about the remainder term unless one specifies something about the function" Kunz (1957).

Danes (1961) has shown that the filter which represents the $(m + 1)^{th}$ derivative of the potential field has a response

$$(u^2 + v^2)^{\frac{m+1}{2}} \tag{4.2}$$

As this amplification of the various frequencies increases as m increases, there is no tendency for the $(m + 1)^{th}$ derivative and hence the remainder term to become negligible. Generally, a high Kunz Class A error must be expected for parabolic interpolation of potential field data.

This leads us to suspect that while potential fields are very well behaved in the frequency domain, polynomials are not by comparison.

Assume a 2-D potential field on a particular line represented by a polynomial

$$g(x) = \sum_{n=0}^{N} A_n x^n \; ; \; -L \leq x \leq L \tag{4.3}$$

The frequencies present in g(x) can be found by taking the Fourier Transform over $-L \leq x \leq L$ as $g(x) = 0, |x| > L$

$$\therefore G(u) = C_1 \sum_{n=0}^{N} \int_{-L}^{L} A_n x^n e^{-iux} dx$$

where C_1 is the normalization factor.

Consider the zeroth, first and second terms.

$$G(u) = A_0\left[\frac{e^{-iux}}{iu}\right]_{-L}^{L} + A_1\left[\frac{x e^{-iux}}{iu}\right]_{-L}^{L} + A_1\left[\frac{e^{-iux}}{u^2}\right]_{-L}^{L} + \ldots\ldots\ldots\ldots$$

Hence by induction

$$G(u) = \frac{A_0'}{u}\sin(uL) + \frac{A_1'}{u^2}\sin(uL) + \ldots\ldots + \frac{A_n'}{u^{n+1}}\sin(uL)$$

where $A_0', A_1' \ldots\ldots\ldots A_n'$ are linear combinations of the $A_0, A_1 \ldots A_n$ in equation (4.3).

$$\therefore G(u) = \sin(uL)\left\{\frac{A_0'}{u} + \frac{A_1'}{u^2} + \ldots + \frac{A_n'}{u^n}\right\} \quad (4.4)$$

as u becomes large $G(u)$ becomes small as

$$G(u) = O\left(\frac{1}{u}\right) \quad (4.5)$$

which in comparison with eqn. (2.12) is not sufficiently fast for potential fields.

An interpolation method is thus sought which will match potential field behaviour in the frequency domain.

For instance the form

$$g(x,y) = \sum_m \sum_n C_{m,n}\, e^{\frac{imx}{2\pi M} + \frac{iny}{2\pi N}} \quad (4.6)$$

is a direct measure of the spectrum of $g(x,y)$ as has already been shown in Chapter 2, and must therefore have its frequency domain characteristics.

We find that

$$C_{m,n} = \rho \iint g(x,y)\, e^{-\frac{i m x}{2\pi M} - \frac{i n y}{2\pi N}} dx\, dy \qquad (4.7)$$

(ρ is the normalization constant).

Bhattacharyya (1965) uses this approach as discussed in chapter 2 to transform his data into the frequency domain. He initially interpolates his data onto a grid from the contours drawn around his original points of measurement. By using hand contours his method is subject to personal bias. However as he deals with aero-magnetic anomalies the assumption of measurements being on a flat plane is reasonable.

The problem of "aliasing", however, arises in the determination of $C_{m,n}$ by exact application of equation (4.7). Moreover the limiting assumption of flat topography for gravity measurements is often not justifiable.

It is therefore desirable that a technique be developed which can compute the Bouguer Anomalies on a regular gridded horizontal plane from measurements at unsystematically scattered points on rough topography, yet stand up to analysis in the frequency domain. The equivalent source technique described in the following sections is put forward as fulfilling these requirements.

4.2 Equivalent Source Technique

4.2.1 First Form

We first assume that the potential field values are on a regular grid on non-planar topography.

This field can be caused by an infinite variety of surface density distributions which give rise to the ambiguity in geophysical interpretation. Using the relationship

$$g(x,y,z) = G\int_{-\infty}^{\infty}\int_{-\infty}^{\infty} \frac{\sigma_z(\alpha,\beta)(z-\gamma)\,d\alpha\,d\beta}{\{(x-\alpha)^2+(y-\beta)^2+(z-\gamma)^2\}^{3/2}} \qquad (4.8)$$

we find the surface density $\sigma_h(x,y)$ on any plane z = h, given the set of values g(x,y,z) at the points (x,y,z). This was discussed in Dampney (1964).

Thus we may represent a particular gravity field by the σ_h (x,y) which we call the Equivalent Source.

The following theorem and proof is given to show that the depth of the source is immaterial.

Theorem. The gravitational field intensity measurements on a regularly gridded infinite horizontal plane can be exactly represented by an equivalent surface density source on a lower infinite horizontal plane at any depth assuming no frequencies are present beyond the cut-off frequency.

Proof.

We prove this by finding $g(x,y,h_2)$ from two different sources on planes B and C in fig. 11 which both synthesize the field g(x,y,o) on plane A. If $g(x,y,h_2)$ is the same in both cases the theorem is proved.

For simplicity consider the problem in two dimensions. The gravity g(x,h) is related to the line density $\lambda(\alpha,h_2)$ on plane C by

$$g(x,h) = 2k(h-h_2)\int_{-\infty}^{\infty} \frac{\lambda(\alpha,h_2)\,d\alpha}{\{(x-\alpha)^2+(h-h_2)^2\}} \qquad (4.9)$$

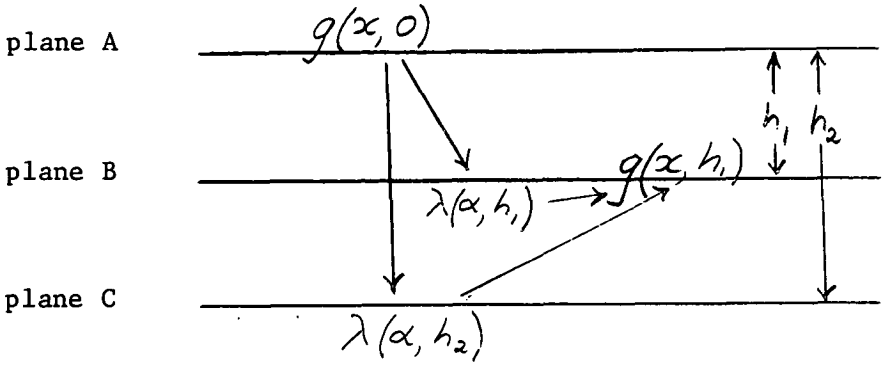

Both sources $\lambda(\alpha, h_1)$ and $\lambda(\alpha, h_2)$ synthesize the field originally measured as $g(x, 0)$ in precisely the same way in theory. In practice, imperfections in the data place necessary restrictions on the depth of the equivalent source to reduce error distortions.

FIGURE 11.

using "k" instead of "G" to represent the gravitational constant to avoid confusion.

Take Fourier Transforms ; $h = 0$

$$\int_{-\infty}^{\infty} g(x,0)\, e^{-iux}\, dx = 2k \int_{-\infty}^{\infty} \lambda(\alpha, h_2)\, d\alpha \int_{-\infty}^{\infty} \frac{-h_2\, e^{-iux}\, dx}{\{(x-\alpha)^2 + h_2^2\}}$$

$$= 2k \int_{-\infty}^{\infty} \lambda(\alpha, h_2)\, e^{-i\alpha u}\, d\alpha \int_{-\infty}^{\infty} \frac{-h_2\, e^{-iuX}\, dX}{\{X^2 + h_2^2\}}$$

where $X = x - \alpha$

$$\therefore G(u,0) = 2\pi k L(u, h_2)\, e^{-h_2|u|} \qquad (4.10)$$

where $G(u,0)$ and $L(u,h_2)$ are the Fourier Transforms of $g(x,0)$ and $\lambda(x,h_2)$ respectively.

Now as $G(u,0) = 0$ for $u > \pi$

$\therefore$ $L(u,h_2) = 0$ for $u > \pi$

Also for every value of u that G = 0, L = 0.

Thus the equivalent source only contains the frequencies present in the gravity field.

Hence $g(x,0)$ is approximated to as being made up of the discrete frequencies

$$u = \frac{n}{N\Delta x} \quad \text{where } n = -\frac{N}{2} - 1 \text{ to } \frac{N}{2} \ (N \text{ even})$$

$$\therefore \lambda(\alpha, h_2) = \sum_{n=N/2}^{N/2} C_n^c\, e^{i2\pi n\alpha/N\Delta x} \qquad (4.11)$$

Hence from equation (4.9)

$$g(x, h_1) = 2\pi k(h_1 - h_2)\int_{-\infty}^{\infty} \sum_{n=-a}^{b} C_n^c \frac{e^{i2\pi n\alpha/N\Delta x}\, d\alpha}{\{(x-\alpha)^2 + (h_1 - h_1)^2\}}$$

$$= 2\pi k \sum_{n=-a}^{b} C_n^c e^{+i2\pi mn/N} e^{-|(h_1 - h_1)2\pi n/N\Delta x|} \tag{4.12}$$

where $x = m\Delta x$

$$g(m\Delta x, 0) = 2\pi k \sum_{n=-a}^{b} C_n^c e^{+\frac{i2\pi mn}{N}} e^{-h_2\left|\frac{2\pi n}{N\Delta x}\right|} \tag{4.13}$$

gives C_n^c

Hence the gravity on plane B is given by

$$g(m\Delta x, h_1) = \sum_{n=-a}^{b} C_n^c 2\pi k\, e^{\frac{i2\pi mn}{N}} e^{-(h_2 - h_1)\left|\frac{2\pi n}{N\Delta x}\right|} \tag{4.14}$$

Also we have analagous to eqn. (4.13)

$$g(m\Delta x, 0) = 2\pi k \sum_{n=-a}^{b} C_n^B e^{\frac{i2\pi mn}{N}} e^{-h_1\left|\frac{2\pi n}{N\Delta x}\right|} \tag{4.15}$$

where on B

$$\lambda(\alpha, h_1) = \sum_{n=-a}^{b} C_n^B e^{i\frac{2\pi \alpha n}{N}} \tag{4.16}$$

taking $\alpha = m\Delta x$ and using eqn. (2.46) in one dimension

$$g(m\Delta x, h_1) = 2\pi k \sum_{n=-a}^{b} C_n^B e^{i\frac{2\pi nm}{N}}$$

From eqn. (4.10) $L(u, h_2) = L(u, h_1)\, e^{-(h_2 - h_1)u}$

hence for a specific value of $u = n/N\Delta x$ we have

$$C_n^B = C_n^C e^{-(h_2 - h_1)(2\pi n / N\Delta x)} \tag{4.17}$$

Then the two equivalent sources give precisely the same results and hence the theorem is proved.

Thus as $\sigma_h(x,y) = \frac{1}{2\pi k} g(x,y,h)$

We can put (from chapter 2)

$$\sigma_h(x,y) = \sum_{m=-a_x}^{b_x} \sum_{n=-a_y}^{b_y} C_{m,n} e^{-i\frac{2\pi m x}{M\Delta x} - i\frac{2\pi n y}{N\Delta y}}$$

$$u = \frac{2\pi m}{M\Delta x}, \quad v = \frac{2\pi n}{N\Delta y}$$

Thus from equation (4.8),

$$g(x,y,z) = G \int_{-\infty}^{\infty}\int_{-\infty}^{\infty} \sum\sum \frac{C_{m,n} e^{-i\frac{2\pi m\alpha}{M\Delta x} - i\frac{2\pi n\beta}{N\Delta y}} d\alpha d\beta (z-h)}{\{(x-\alpha)^2 + (y-\beta)^2 + (z-h)^2\}^{\frac{3}{2}}}$$

Then using a result from Erdelyi et al, 1954 a combination of equation (7) page 11 and equation (44) page 56

$$= G \sum\sum C_{m,n} e^{\left(i\frac{2\pi m x}{M\Delta x} + i\frac{2\pi n y}{N\Delta y}\right)} \times e^{2\pi(h-z)\sqrt{\left(\frac{m}{M\Delta x}\right)^2 + \left(\frac{n}{N\Delta y}\right)^2}} \tag{4.18}$$

Putting $G C_{m,n} \exp\left\{2\pi(h-z)\sqrt{\left(\frac{m}{M\Delta x}\right)^2 + \left(\frac{n}{N\Delta y}\right)^2}\right\} = C'_{m,n}$

we can find $C'_{m,n}$ extending equation (2.25) to two dimensions.

Thus we can find $C_{m,n}$ and hence the equivalent source $\sigma_h(x,y)$ or more particularly $g(x,y,h)$ now projected onto a horizontal plane of height h.

This equivalent source should exactly represent the gravity field provided conditions (b) and (c) enunciated at the beginning of the chapter are obeyed. If a direct measurement of the vertical derivations, as has been done by S. Thiesson Bornemisza (1965) for example, disagrees with the theoretical result; the difference will be due to two causes

(i) the effect of bandwidth as discussed in chapter 2

(ii) missing information in the gravity spectrum if condition (c) is not true. This can be overcome by closing the station spacing so that the small bodies previously undetected show up on the gravity record.

However, very rarely in practice is $g(x,y,z)$ measured at grid points on the topography. Physical considerations in the field such as swamps, cliffs, rivers, vegetation make it impossible to measure gravity at regular pre-determined locations.

If the points of measurement are scattered unsystematically on the topography, the $C'_{m,n}$ in eqn. (4.18) cannot be immediately expressed as a linear combination of the g(x,y,z) but become MN coefficients satisfying MN equations. Again, as with the polynomial technique a large matrix has to be manipulated - thereby limiting the number of gravity measurements in a survey if a conventional solution by determinants is carried out.

"Aliasing" is a more immediate problem, however. In any ordinary survey station density is not uniform, inevitably resulting in some small region having a high station density. To examine the consequences of this consider three points on a particular travers line unusually close together. Then if the middle point has an error in it, a sudden local jump would be present

in the gravity field as measured. The smaller the area in which the jump is contained, the greater are the amplitudes of the high frequencies present causing a few stations to have an unduly large influence on the values of the $C_{m,n}$. This phenomenon of aliasing is well known in geomagnetism where the problem of having unevenly scattered measurements due to the restricted distributions of continents becomes acute in spherical harmonic analysis.

Also with data no longer on a regular grid the number of frequencies present in the x and y direction are not uniquely defined. As shown in fig. 12 it would be possible in the extreme to make MN frequencies in either the x or y directions fit the data where MN is the total number of survey stations. These disadvantages make it impossible to apply eqn. (4.18) directly to the transformation of gravity data to the frequency domain.

A new approach is required to overcome these difficulties.

4.2.2 Second Form

Equation (2.5) shows that if we have a point mass m at a point $(\alpha, \beta, 0)$ then

$$g(x,y,z) = -G m z / \{(x-\alpha)^2 + (y-\beta)^2 + z^2\}^{3/2} \qquad (4.19)$$

Therefore the spectrum of g from eqn. (2.50)

$$= G m \varepsilon_n e^{-z\sqrt{u^2+v^2}} \qquad (4.20)$$

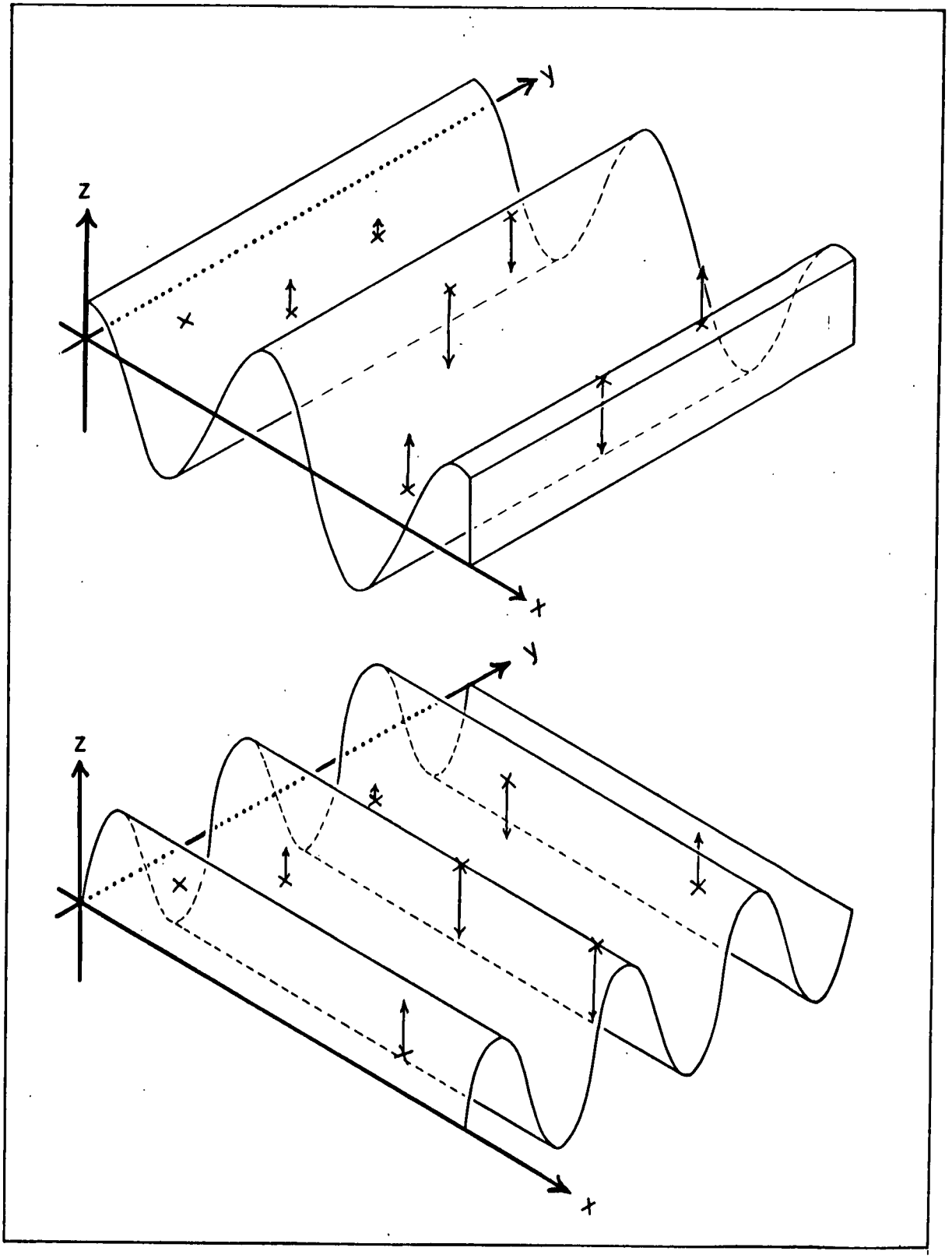

The ambiguity of fitting a two-dimensional Fourier Series to points on a plane.

FIGURE 12.

where $|\varepsilon_n| = |e^{-i\alpha u - i\beta v}| \leq 2$

Putting $u = 2\pi f_x$

$v = 2\pi f_y$

where f_x, f_y are frequencies measured in cycles per metre in the m.k.s. system.

From eqn. (2.59)

$$f_{x_{max}} = 1/2\Delta x$$

In eqn. (4.20) if z is large enough the amplitude of the spectrum beyond the cut-off frequencies can be made arbitrarily small. The spectrum can be made to satisfy the condition (c) necessary to exactly represent g in the frequency domain. Hence it is possible to replace $\sigma_k(x,y)$ by a series of point masses to synthesize the Bouguer Anomalies. This approximation to a continuous equivalent source is sufficiently accurate provided this discrete equivalent source is at a sufficient depth below the surface. Otherwise the field at the surface resulting from these masses will be distorted compared to the real field.

For instance consider the extreme case of the point source being at the surface. Then the vertical component of the gravity field would be zero everywhere surrounding the source except directly above it. Clearly there would be large amplitudes in the spectrum beyond the cut-off frequency so that the vertical continuation and derivatives of this field would bear no relationship to reality. In fact from table IV and V it can be seen that only one coefficient in the transforming matrices for these processes would be needed.

Thus if we have n data points we can find n point masses m_k at a suitable depth giving the equivalent source.

Thus $(G \equiv 1)$

$$
\begin{aligned}
g_1 &= a_{11} m_1 + a_{12} m_2 + \ldots + a_{1k} m_k + \ldots + a_{1n} m_n \\
g_2 &= a_{21} m_1 + a_{22} m_2 + \ldots + a_{2k} m_k + \ldots + a_{2n} m_n \\
&\vdots \\
g_i &= g_{i1} m_1 + a_{i2} m_2 + \ldots + a_{ik} m_k + \ldots + a_{in} m_n \\
&\vdots \\
g_n &= g_{n1} m_1 + a_{n2} m_2 + \ldots + a_{nk} m_k + \ldots + a_{nn} m_n
\end{aligned}
\tag{4.21}
$$

where the

$$
a_{ik} = \frac{(z_i - h)}{\left\{ (x_i - x_k)^2 + (y_i - y_k)^2 + (z_i - h)^2 \right\}^{3/2}} \tag{4.22}
$$

and z = h is the horizontal plane containing the point masses m_k at (x_k, y_k, h). (x_i, y_i, z_i) is the position of g_i.

This can be written vectorially

$$
\underset{\sim}{g} = \underset{\approx}{A}\, \underset{\sim}{m} \tag{4.23}
$$

The matrix $\underset{\approx}{A}$ tends to become ill-conditional if the equivalent source is too far below the surface; that is if z - h is too large in the eqn. (4.21).

Mathematically A is ill-conditioned if det A $\longrightarrow$ 0

Thus if h is very large relative to the dimensions of the survey then

$$a_{11} \longrightarrow a_{12} \longrightarrow \ldots \longrightarrow a_{ik} \longrightarrow \ldots \longrightarrow a_{nn} \longrightarrow a$$

where $$a = \lim_{(z_i - h) \to +\infty} \frac{-(z_i - h)}{\{(x_i - x_k)^2 + (y_i - y_k)^2 + (z_i - h)^2\}^{3/2}}$$

$$= \lim_{h \to -\infty} \frac{-1}{(z - h)^2}$$

and det A $\longrightarrow$ 0

resulting in great variation between the values of the m_i as is seen from

$$m_k = \begin{vmatrix} a_{11} \ldots a_{1k-1} & a_{1k+1} \ldots a_{1n} & g_1 \\ \ldots\ldots & \ldots\ldots & \ldots \\ a_{k1} \ldots a_{kk-1} & a_{kk+1} \ldots a_{kn} & g_k \end{vmatrix} \Big/ \det A$$

$$= g_1 \frac{\det(A'_{1k})}{\det A} + g_2 \frac{\det(A'_{2k})}{\det A} + \ldots \qquad (4.24)$$

Therefore any variations in g will induce large variations in m.

Wild fluctuations will also result from the anomalous source being near the points of measurement relative to the station spacing. As Bullard and Cooper (1948) point out when g is continued below the level of the anomalous source large fluctuations occur in the values of g along a profile. If h is too large in relation to the depth of the anomalous source, then the values of m will vary in amplified sympathy with the values of g below the source. Therefore h must be chosen to lie between these two limits of being too small or too large. It seems empirically, judging from the area interpreted (chapter 6), that

$$4 \times \frac{\Delta x + \Delta y}{2} < (z_{av} - h) < 8 \times \frac{\Delta x + \Delta y}{2}$$

z_{av} is the average height of the survey area.

Substituting the lower value of $z_{a.s.} - h$ into eqn. (2.10) we find

$$G(u) < G m \varepsilon_n \times 10^{-8}, \quad u_1 > u_{max}; v > v_{max}.$$

Therefore condition (c) is almost satisfied.

The next step is to solve equation (4.23) which was carried out as follows.

4.2.2.1 Solution of $\underset{\sim}{g} = \underset{\approx}{A}\,\underset{\sim}{m}$

An iterative method which reduced the influence of random errors in $\underset{\sim}{g}$ on m was sought as direct solutions are unsuitable because of their tendency to accumulate round-off errors and magnify random errors already present. Generally speaking, an iterative method for solving an equation or set of equations is a rule for operating upon any approximate solution $\underset{\sim}{x}^{(p)}$ of the equation $\underset{\sim}{y} = \underset{\approx}{A}\,\underset{\sim}{x}$ in order to obtain an improved solution $\underset{\sim}{x}^{(p+1)}$ and such that sequence $\{x^{(p)}\}$ so defined has the solution x in the limit (Householder 1953, p. 45).

Zidarov (1965) has put forward a method which finds a system of masses in a spherical earth, satisfying a given gravity field, using iteration. Zidarov's scheme uses "the method of steepest descent" which is based on the geometric notion that the equation

$$\underset{\approx}{A}\,\underset{\sim}{x} = \underset{\sim}{b} \tag{4.25}$$

can be solved by minimising

$$R = (\underset{\sim}{b} - \underset{\approx}{A}\,\underset{\sim}{x})^T (\underset{\sim}{b} - \underset{\approx}{A}\,\underset{\sim}{x}) \tag{4.26}$$

This is done by choosing a direction $\underset{\sim}{v}$, along the line of maximum change of R and along which the initial vector $\underset{\sim}{x}^{(1)}$ is moved a distance λ to get $\underset{\sim}{x}^{(2)}$. "Distance" and "direction" are meant in the sense of Ralston

(1965) (page 44) for a hyperspace of dimension N where N is the number of variables x_i .

In general

$$\underset{\sim}{x}_{i+1} = \underset{\sim}{x}_i + \lambda_i \underset{\sim}{v}_i \qquad (4.27)$$

Naturally the minimization of R to zero by $\underset{\sim}{x}$ would give the solution of equation (4.25).

Geometric considerations

Let $\underset{\sim}{x}^t = [x_1^t, x_2^t \ldots x_N^t]$ be the true solution of $\underset{\approx}{A}\underset{\sim}{x} = \underset{\sim}{b}$ and let

$$\underset{\sim}{x} = \underset{\sim}{x}^t + \underset{\sim}{\varepsilon} \quad ; \underset{\sim}{\varepsilon} = (\varepsilon_1, \ldots \varepsilon_N)$$

For this $\underset{\sim}{x}$.

$$R = (\underset{\sim}{b} - \underset{\approx}{A}(\underset{\sim}{x}^t + \underset{\sim}{\varepsilon}))^T (\underset{\sim}{b} - \underset{\approx}{A}(\underset{\sim}{x}^t + \underset{\sim}{\varepsilon}))$$

$$= \underset{\sim}{b}^T\underset{\sim}{b} - \underset{\sim}{b}^T\underset{\approx}{A}(\underset{\sim}{x}^t + \underset{\sim}{\varepsilon}) - (\underset{\sim}{x}^t + \underset{\sim}{\varepsilon})^T\underset{\approx}{A}^T\underset{\sim}{b} + (\underset{\sim}{x}^t + \underset{\sim}{\varepsilon})^T\underset{\approx}{A}^T\underset{\approx}{A}(\underset{\sim}{x}^t + \underset{\sim}{\varepsilon})$$

$$= \underset{\sim}{b}^T\underset{\sim}{b} - \underset{\sim}{b}^T\underset{\sim}{b} - \underset{\sim}{b}^T\underset{\approx}{A}\underset{\sim}{\varepsilon} - \underset{\sim}{b}^T\underset{\sim}{b} - \underset{\sim}{\varepsilon}^T\underset{\approx}{A}^T\underset{\sim}{b} + \underset{\sim}{b}^T\underset{\sim}{b} + \underset{\sim}{b}^T\underset{\approx}{A}\underset{\sim}{\varepsilon} + \underset{\sim}{\varepsilon}^T\underset{\approx}{A}^T\underset{\sim}{b} + \underset{\sim}{\varepsilon}^T\underset{\approx}{A}^T\underset{\approx}{A}\underset{\sim}{\varepsilon}$$

$$= \underset{\sim}{\varepsilon}^T\underset{\approx}{A}^T\underset{\approx}{A}\underset{\sim}{\varepsilon}$$

The matrix $\underset{\approx}{C} = \underset{\approx}{A}^T\underset{\approx}{A}$ must be symmetric.

$$R = \underset{\sim}{\varepsilon}^T\underset{\approx}{C}\underset{\sim}{\varepsilon} = \sum_{i=1}^{N}\sum_{j=1}^{N} C_{ij}\varepsilon_i\varepsilon_j \qquad (4.28)$$

The surface

$$R = \text{const.}$$

is therefore a hyperellipsoid in the variables $\varepsilon_1, \ldots \varepsilon_N$ with centre at $\underset{\sim}{\varepsilon} = 0$ (i.e. the solution of $\underset{\approx}{A}\underset{\sim}{x} = \underset{\sim}{b}$ in the $x_1, \ldots x_N$ co-ordinate system). Now because $\underset{\approx}{C}$ is symmetric, there exists an orthogonal matrix $\underset{\approx}{P}$ such that

$$P^T C P = D \tag{4.29}$$

where D is a diagonal matrix with the eigen-values of C on the diagonal.

The eigenvalues $\beta_1 \ldots \beta_N$ are the solutions of the characteristic equation

$$|A - \beta I| = 0$$

Corresponding to each distinct eigenvalue β_i there exists a solution of

$$\begin{aligned}
\underset{\approx}{A}\,\underset{\sim}{\varepsilon} &= \beta_i\,\underset{\sim}{\varepsilon} \\
\underset{\sim}{\varepsilon}^T \underset{\approx}{A}^T \underset{\approx}{A}\,\underset{\sim}{\varepsilon} &= \beta_i\,\underset{\sim}{\varepsilon}^T \underset{\sim}{\varepsilon}\,\beta_i \\
\underset{\sim}{\varepsilon}^T \underset{\approx}{C}\,\underset{\sim}{\varepsilon} &= \beta_i^2\,\underset{\sim}{\varepsilon}^T \underset{\sim}{\varepsilon} \\
\underset{\approx}{C}\,\underset{\sim}{\varepsilon} &= \beta_i^2\,\underset{\sim}{\varepsilon}
\end{aligned} \tag{4.30}$$

Thus each eigenvalue of C correspond to the square of each of the eigenvalues of A.

Making the change of variables

$$\underset{\sim}{\xi} = P^T \underset{\sim}{\varepsilon} \quad , \quad \underset{\sim}{\xi} = (\xi_1 \; \ldots \; \xi_N)$$

then

$$\begin{aligned} \underset{\approx}{R} &= \underset{\sim}{\varepsilon}^T \underset{\approx}{C} \underset{\sim}{\varepsilon} \\ &= \underset{\sim}{\varepsilon}^T \underset{\approx}{P} \underset{\approx}{P}^T \underset{\approx}{C} \underset{\approx}{P} \underset{\approx}{P}^T \underset{\sim}{\varepsilon} = \underset{\sim}{\xi}^T D \underset{\sim}{\xi} \\ &= \sum_{i=1}^{N} \beta_i^2 \xi_i^2 \end{aligned} \tag{4.31}$$

Therefore the hyperellipsoid R = const. has axes in the direction $\underset{\sim}{\xi}_i$ of length proportional to $1/\beta_i$. Ralston (1965) has shown that the condition of a matrix is represented by how nearly its hyperellipsoid (4.31) approaches a hypersphere. An ill-conditioned matrix has an "elongated" hyperellipsoid.

In the method of steepest descent if A is ill-conditioned the direction of maximum change of R must point in a direction very differently from the direction of the centre of the hyperellipsoid.

This is shown diagrammatrically in fig. 13 for the system.

$$\begin{aligned} 0.5x_1 + x_2 &= 1.5 \\ 0.52x_1 + x_2 &= 1.52 \end{aligned}$$

for which the true solution is $x_1 = 1, x_2 = 1$

The eigenvalues are given by the determinant

$$\begin{vmatrix} 1-\beta & 0.5 \\ 1 & 0.52-\beta \end{vmatrix} = 0$$

$$(1-\beta)(0.52-\beta) - 0.5 = 0$$

producing

$$\begin{aligned} \beta &= \tfrac{1}{2}(1.26 \pm \sqrt{1.5476}) \\ &= 1.252; \; 0.008 \end{aligned}$$

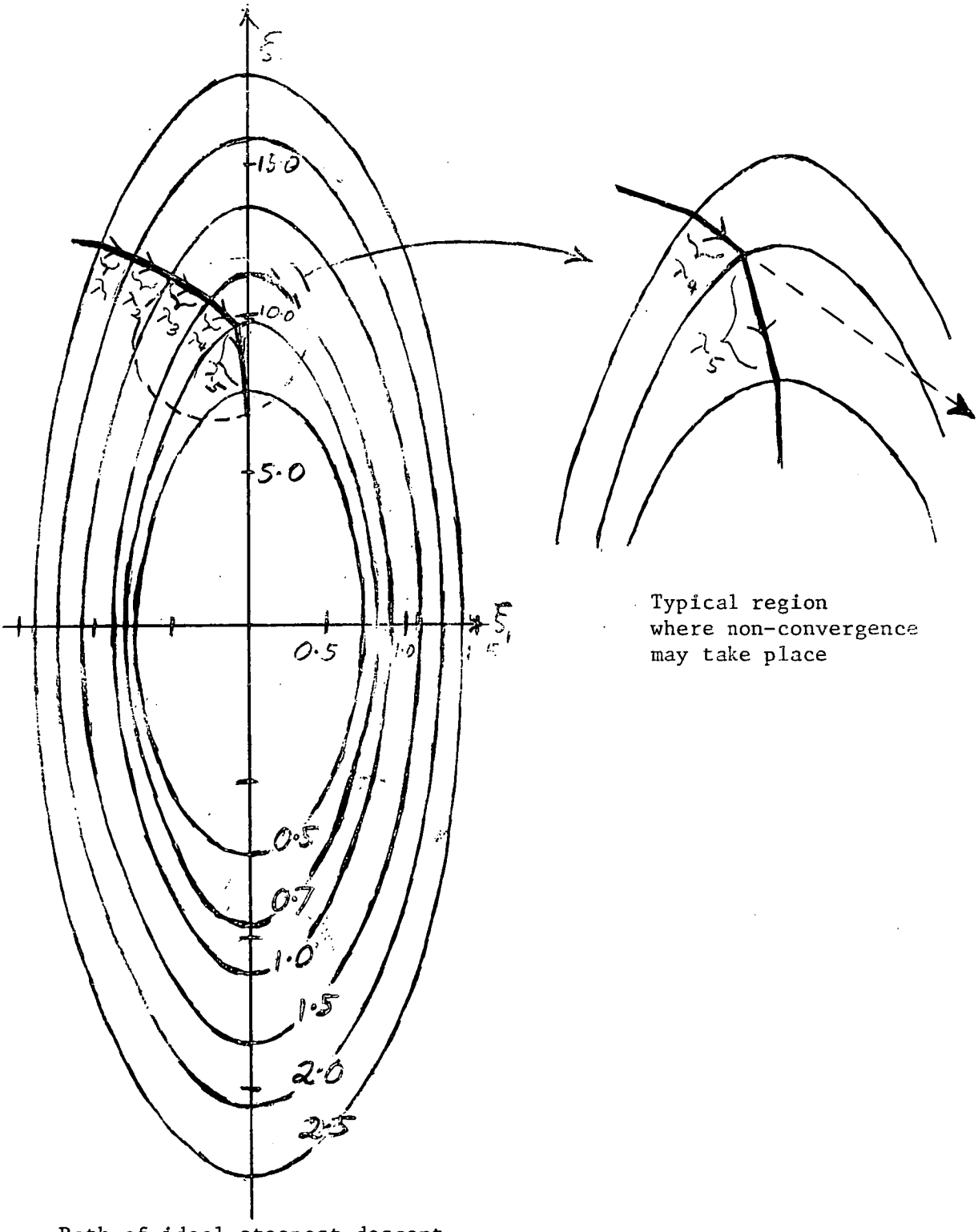
ξ
15·0
10·0
5·0
0·5
1·0
ξ1
0·5
0·7
1·0
1·5
2·0
2·5
λ1
λ2
λ3
λ4
λ5
Typical region
where non-convergence
may take place
Path of ideal steepest descent
solution

FIGURE 13.

This system is therefore ill-conditioned.

The equation of the ellipse is

$$(0.008\xi_2^2 + 1.2525\xi_1^2) = C$$

C = constant

In fig. 13 this ellipse is plotted for various values of C with the scale ξ_1 expanded in relation to ξ_2 so that the true ellipse is even more elongated than shown.

For ideal convergence the magnitude of $\lambda_1, \lambda_2 \ldots$ giving successive iterations from the first approximation is shown. However in the region encircled an incorrect value of λ will throw the process of convergence out and the solution diverges for that iteration.

Physically one sees in the solution of $g = A m$ that if the true value of m_k is greatly different to the other m's then the hyperellipsoid is very elongated along the m_k axis. This will occur if m_k is in a position where the actual source is shallow. In chapter 5 a region of non-convergence will be described in the solution of

$$\underset{\sim}{g} = \underset{\approx}{A}\,\underset{\sim}{m}$$

as the iteration procedure passes through a region in hyperspace with geometric characteristics analogous to fig. 13.

We minimise

$$(\underset{\sim}{g} - \underset{\approx}{A}\,\underset{\sim}{m})^T(\underset{\sim}{g} - \underset{\approx}{A}\,\underset{\sim}{m}) = U$$

to find the solution of m is equation (4.23).

The direction of maximum change of U with respect to m_i is given by $-\frac{\partial U}{\partial m_i}$ the ith component of ∇U with respect to $\underset{\sim}{m}$.

Thus following Zidarov (1965)

$$U = \sum_{i=1}^{N} \left[g_z(M_i) - g_z^{(n)}(m_i) \right] \tag{4.32}$$

$$g_z^{(n)} = \sum_{k=1}^{N} m_k \frac{\cos(\hat{R_{ik}z})}{R_{ik}^2} \tag{4.33}$$

where $$R_{ik} = \left\{ (x_i - x_k)^2 + (y_i - y_k)^2 + (z_i - z_k)^2 \right\}^{1/2}$$

$g_z(M_i)$ is the measured field due to the true masses M_i and $g_z^{(n)}(m_i)$ is the nth approximation of g_z from the approximate masses m_i .

We restrict the position of discrete masses m_i to positions (x_i, y_i, h) where the N co-ordinates (x_i, y_i) correspond to the N positions of the measured g and h is the level of the horizontal plane for this equivalent source. Thus each discrete mass lies vertically underneath one of the N data points making up the survey. This restriction gives U a unique solution. We assume nothing about the matrix in eqn. (4.23) except that it is square and its elements real.

Therefore

$$\frac{\partial U}{\partial m_i} = \sum_{k=1}^{N} 2 f_k \frac{\partial f_k}{\partial m_i} \quad ; \frac{dU}{d\underset{\sim}{m}} = 2 \underset{\sim}{f} \frac{d\underset{\sim}{f}}{d\underset{\sim}{m}} \tag{4.34}$$

where

$$f_k = g_z(M_i) - \sum_{i=1}^{N} \frac{m_i \cos(\hat{R_{ik}z})}{R_{ik}^2}$$

that is $$U = \sum_{i=1}^{N} f_i^2 \tag{4.35}$$

We find following equation (4.27) that

$$m_k^{(p)} = m_k^{(p-1)} - \lambda \frac{\partial U}{\partial m_k} \tag{4.36}$$

where $m_k^{(p)}$ is a closer approximation to the true value of m_k than $m_k^{(p-1)}$.

Therefore

$$U = U\left(m_1^{(p)} - \lambda \frac{\partial U}{\partial m_1}, \ldots\ldots\ldots, m_n^{(p)} - \lambda \frac{\partial U}{\partial m_n}\right)$$

is less than $U = U\left(m_1^{(p)}, \ldots\ldots\ldots m_n^{(p)}\right)$

To find λ we maximise

$$\varphi(\lambda) = U\left(m_1^{(p)} - \lambda \frac{\partial U}{\partial m_1}, \ldots, m_n^{(p)} - \lambda \frac{\partial U}{\partial m_n}\right) \tag{4.37}$$

In this way U will converge most rapidly for λ obeying this condition.

Developing $\varphi(\lambda)$ as a power series in λ from Taylor's Theorem, and taking into consideration only the first two terms (as $\frac{d^3 U}{dm^3} = 0$ from equation 4.34) we obtain

$$\varphi(\lambda) = U - \lambda \frac{dU}{d\underset{\sim}{m}} \frac{dU}{d\underset{\sim}{m}} + \frac{\lambda^2}{2!}\left(\frac{dU}{d\underset{\sim}{m}}\right)^2 \frac{d^2 U}{d\underset{\sim}{m}^2} \tag{4.38}$$

$$\frac{d^2 U}{d\underset{\sim}{m}^2} = 2\left(\frac{d\underset{\sim}{f}}{d\underset{\sim}{m}}\right)^2 + 2\underset{\sim}{f}\frac{d^2 \underset{\sim}{f}}{d\underset{\sim}{m}^2} \tag{4.39}$$

Now $\frac{d^2 \underset{\sim}{f}}{d\underset{\sim}{m}^2} = 0$ from equation (4.34)

$$\therefore \phi(\lambda) = \underset{\sim}{f}^2 - 4\lambda \underset{\sim}{f}^2 \left(\frac{d\underset{\sim}{f}}{d\underset{\sim}{m}}\right)^2 + 4\lambda^2 \underset{\sim}{f}^2 \left(\frac{d\underset{\sim}{f}}{d\underset{\sim}{m}}\right)^4 \quad (4.40)$$

$\phi(\lambda)$ will have a maximum when $\frac{d\phi}{d\lambda} = 0$

Thus

$$4\underset{\sim}{f}^2 \left(\frac{d\underset{\sim}{f}}{dm}\right)^2 - 8\lambda \underset{\sim}{f}^2 \left(\frac{d\underset{\sim}{f}}{d\underset{\sim}{m}}\right)^4 = 0 \quad (4.41)$$

Hence $$\lambda = \underset{\sim}{f}^2 \left(\frac{d\underset{\sim}{f}}{dm}\right)^2 \Big/ 2\underset{\sim}{f}^2 \left(\frac{d\underset{\sim}{f}}{d\underset{\sim}{m}}\right)^4$$

$$= \underset{\sim}{f} \frac{d\underset{\sim}{f}}{d\underset{\sim}{m}} \frac{dU}{dm} \Big/ \left(\frac{d\underset{\sim}{f}}{d\underset{\sim}{m}}\right)^2 \left(\frac{dU}{d\underset{\sim}{m}}\right)^2$$

$$= \frac{\sum_{i=1}^{N} f_i \sum_{k=1}^{N} \frac{\partial f_i}{\partial m_k} \frac{\partial U}{\partial m_k}}{\sum_{i=1}^{N} \left(\sum_{k=1}^{N} \frac{\partial f_i}{\partial m_k} \frac{\partial U}{\partial m_k}\right)^2} \quad (4.42)$$

which is Zidarov's (1965) equation (2) with m_k substituted for θ_{jk}

This method assumed U only has one minimum. The condition for a minimum is that $dU/dm = 0$

Suppose that $\frac{dU}{dm} = 0$ for some value of U other than $U = 0$. Then for some value of U, $d^2U/dm^2 = 0$

but $$\frac{d^2U}{dm^2} = 2\left(\frac{df}{dm}\right)^2 > 0 \quad (4.43)$$

Hence $\frac{d^2U}{dm^2} \neq 0$ and hence U only has one minimum. This is also seen from

$$\frac{d^3U}{dm^3} = 0 \tag{4.44}$$

Thus $\frac{d^2V}{dm^2}$ cannot change sign.

Thus it is possible fo find the equivalent source of a gravitational field in terms of discrete masses. In the limit it is seen that the second form approaches the first form. Suppose the gravitational field is known at a number of points infinitesimally close together, then the discrete masses would be infinitesimal distances apart and in the limit would become a continuous surface density distribution.

Having found the equivalent source one then is able to calculate the anomalous field at any point in space restricted by

(a) areal extent of the survey

(b) minimum height above equivalent source at which $e^{h\sqrt{u^2+v^2}}$ is negligible for $u \gg 2\pi f_{x_{max}}$; $v \gg 2\pi f_{y_{max}}$

In this way the field can be calculated at regular grid points on a horizontal plane at some height above the source.

In order to conserve the amount of information present in the gravity measurements, the number of grid points calculated should not significantly exceed the number of data points.

This result should be nearly exact

if

(a) no frequencies are present in the actual field beyond cut-off frequency.

(b) no information is missed by having non-uniform sampling over the area.

It should be noted here that a significant difference in the two forms is that the second form of the equivalent source technique assumes the field asymptotically approaches zero beyond the area, the first form assumes periodic continuation horizontally.

5. APPLICATION OF THE EQUIVALENT SOURCE TECHNIQUE

The fundamental assumption in using the equivalent source technique is that the data points (points of measurement) sample sufficient of the field for the purpose at hand. Thus a survey must have sufficient measurements over its area that the amplitude of frequencies missed by the station spacing is negligible for the structure being sought.

With this assumption the gravitational field at any point in space can be found as shown in the last chapter. However, it is to be noted that no more accurate way is available than actually measuring the field at a particular point in space. Thus Thyssen-Bornemisza and Stackler (1956) measured gravity at two heights at each survey point to obtain the gradient. In theory, the most accurate means available for finding the gradient is to measure it directly (providing the topography is flat). But as this requires twice the number of readings the equivalent source technique is more economical to use. In any case the accuracy of measuring the gradient directly is restricted by the small height differences over which gravity may be measured.

The data used for the equivalent source technique must be corrected for extraneous influences. That is the theoretical gravitational field intensity g_T due to the earth (particularly the surrounding terrain and geological stratigraphic units) should be computed and then subtracted from the practical measurement g_p, thus forming the Bouguer Anomaly $g_p - g_T$.

Corrections for all the known geology of the area must be included in g_p in order to further our knowledge of the deeper structures

underlying the surface features. Essentially all available information is used to "strip" away the effect of the shallow structures in the sense of Hammer (1963).

In chapter 6 this is done using a method modified from Bott's (1962) "Use of Electronic Computers for the Evaluation of Gravimetric Terrain Corrections".

The Bouguer Anomalies $g[k]$ found in this way make up the data required for the Equivalent Source Technique. The only further information needed is the depth h of the masses $m[k]$ which has to satisfy equation (4.24). For convenience we make the horizontal co-ordinates of the $m[k]$ the same as the data points, thus saving the amount of information required for the technique.

Using this method of steepest descent the resulting $N \times N$ system of equations in $m[k]$ is solved, keeping in mind that a minimum amount of computer space should be used so as not to restrict the technique to impractically small surveys.

From equation (4.42) it is seen that to calculate λ, the variables $\partial f_i / \partial m_k$, f_i and $\partial U / \partial m_k$ must be known.

Recall that

$$f_i = \left[g_i - \sum_{k=1}^{N} \frac{m_k (z_i - h)}{\{(x_i - x_k)^2 + (y_i - y_k)^2 + (z_i - h)^2\}^{3/2}} \right] \quad (5.1)$$

$$\frac{\partial f_i}{\partial m_k} = \frac{-(z_i - h)}{\{(x_i - x_k)^2 + (y_i - y_k)^2 + (z_i - h)^2\}^{3/2}} \quad (5.2)$$

$$\frac{\partial U}{\partial m_k} = 2 f_i \frac{\partial f_i}{\partial m_k} \qquad (5.3)$$

f_i and $\frac{\partial U}{\partial m_k}$ both depend on m_k and therefore have to be recomputed for each determination of λ. $\partial f_i / \partial m_k$ however does not depend on m_k; but it has $N \times N$ values. Suppose N = 1000 then 10^6 computer spaces would be required to store the $\partial f_i / \partial m_k$ - clearly impractically large for most computers. The computer used, an Elliott 503 had 8000 spaces with an additional 16,000 in a core backing store. As the program took up about 3,000 spaces 21,000 spaces all told were left for data storage.

Therefore $\partial f_i / \partial m_k$ or more particularly the kernel

$$\frac{(z_i - h)}{\{(x_i - x_k)^2 + (y_i - y_k)^2 + (z_i - h)^2\}^{3/2}}$$

was recomputed each time it was required.

The program was thus split up into three major loops as shown in table VIII where

$$dU[i] = \partial U / \partial m_i = \sum_{k=1}^{N} 2 f_k \partial f_k / \partial m_i$$

The program structure is seen in the flow diagram fig. 14. Therefore seven arrays viz.

$$g, \; m, \; x, \; y, \; z, \; f, \; dU. \qquad (5.4)$$

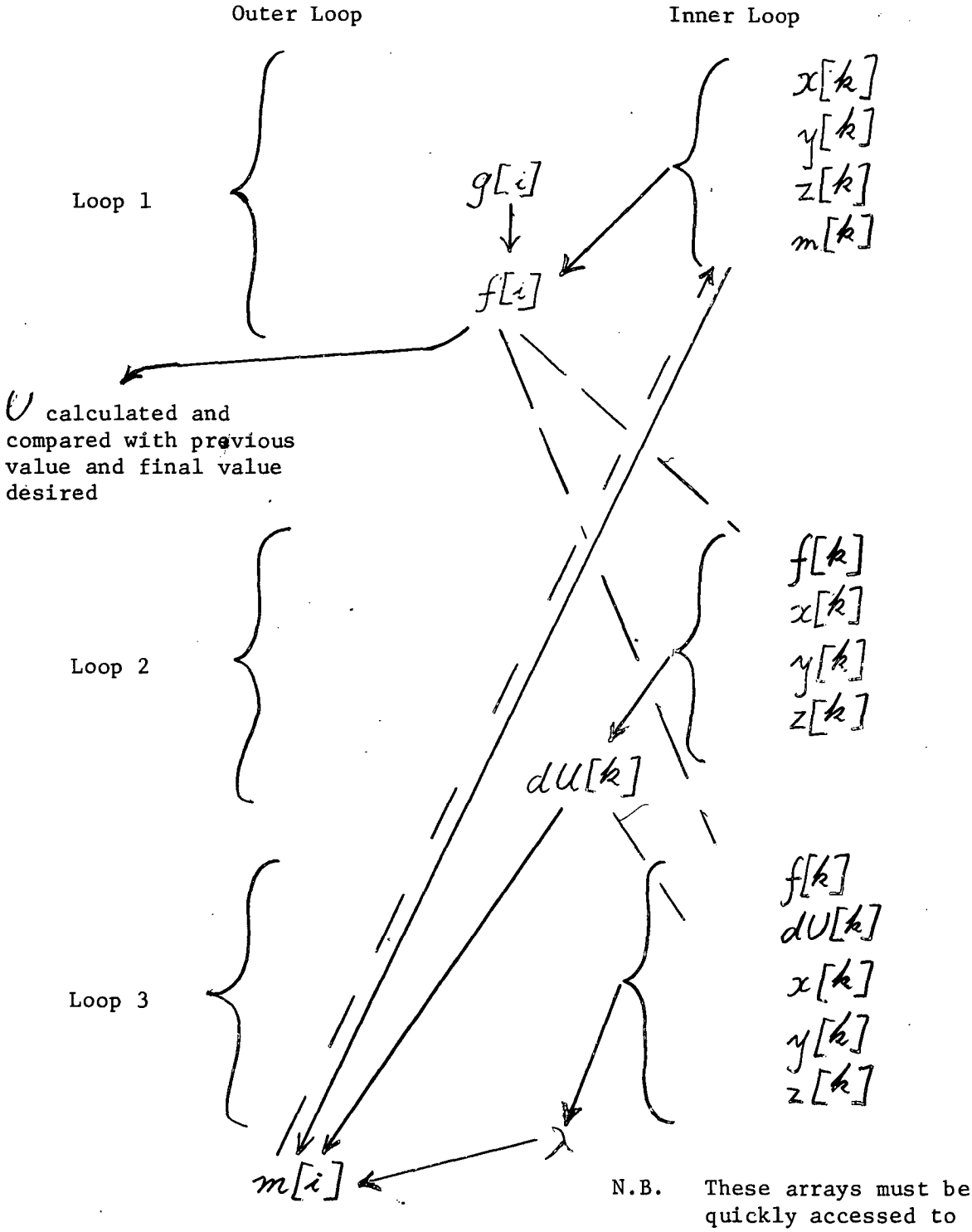

TABLE VIII Arrays required in equivalent source computation

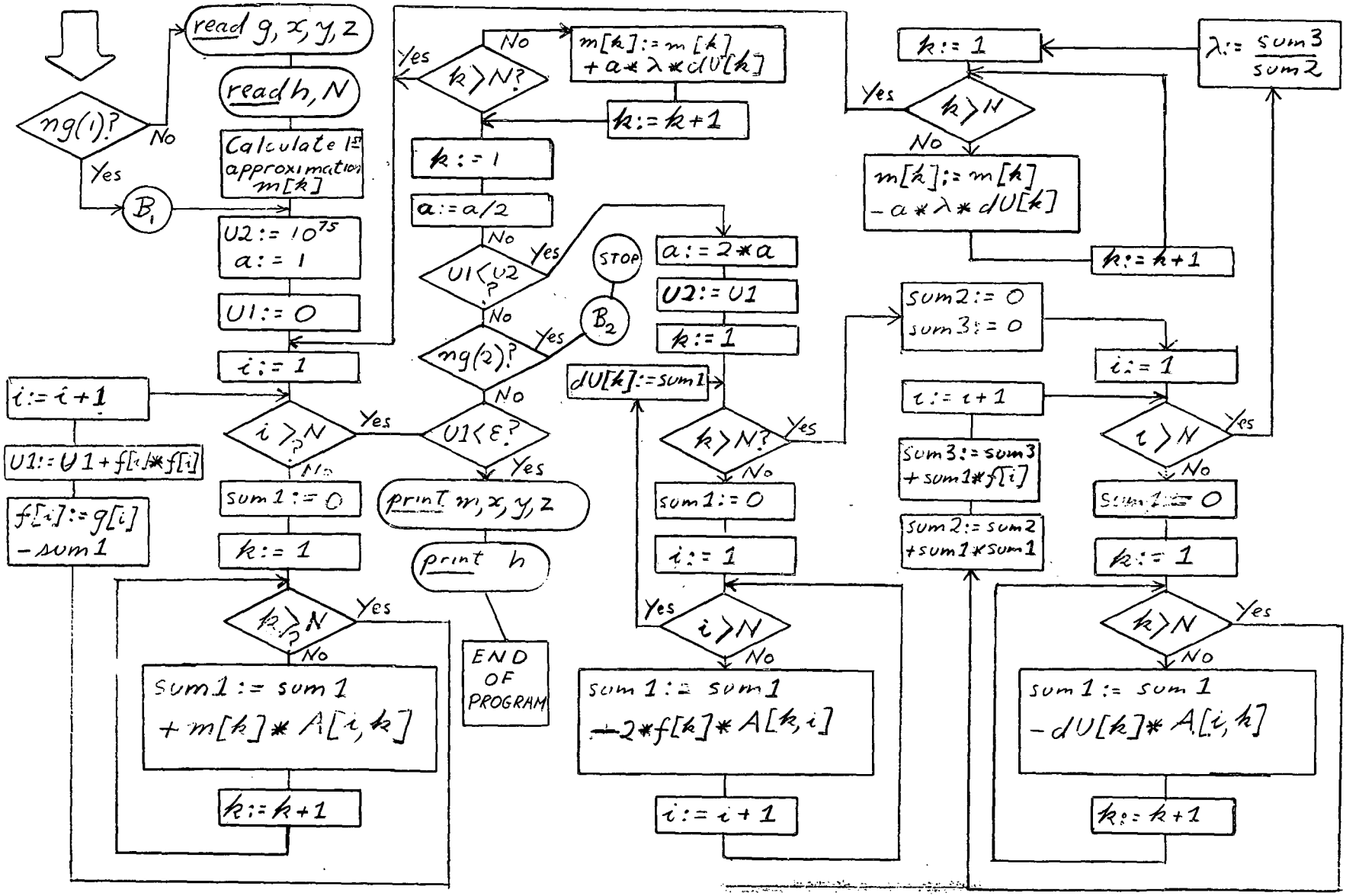

Fig. I4. Flow chart for equivalent source program. $A[i,k] = \partial f_i / \partial m_k$ in eqn.(5.2) and is computed each time it is used. See fig.I5 for details. At B_1 the program continues with data obtained at B_2. This is controlled by external switches ng(I) and ng(2) respectively, allowing a break in computation.

are necessary to compute λ . These arrays required $7N$ storage locations, a considerable saving on the N^2 locations required to store $\partial f_i/\partial m_k$.

As seems inevitable in science, a saving at one point means a loss somewhere else. Here the loss was in terms of computer time - to the extent that 99% of the total program time was devoted to calculating the $\partial f_i/\partial m_k$. Even so computation time was reasonable.

Each loop required, to within 1%, the same computing time T, found to be given by the equation

$$T = N^2/1000 \quad \text{secs.} \qquad (5.5)$$

where N is the dimension of the arrays.

To achieve this the major loops were programmed into the machine code of the Elliott 503 rather than the normal Algol - resulting in a 400% improvement in calculating time efficiency.

The square root procedure used in the final step of calculating the kernel

$$\{(x_i - x_k)^2 + (y_i - y_k)^2 + (z_i - z_k)^2\}^{1/2}$$

took up a large proportion of each kernel's 1 millisecond (eqn. 5.5) time requirements. This was concluded from the fact that dispite a varying number (12 - 16) of similar machine code instructions in the three loops apart from the square root operation, the same time (to within 1%) was spent in each loop.

In the first loop the $f[i]$ were squared and summed to form U (equation 4.35). At the end of the first loop U was compared with its previous value to ensure convergence was taking place. It was found that the rate of convergence tended to slow down as the computation progressed. In order to speed up convergence a factor was introduced into equation 4.36 forming

$$m^{(p)}[k] = m^{(p-1)}[k] - a\lambda \frac{\partial U}{\partial m_k} \qquad (5.6)$$

where "a" is the introduced factor.

By putting $a > 1$ it was possible to speed up convergence (in fact make the method "over-relax" in the sense of Ralston (1965)). However this led to the danger that the solution may become non-convergent.

This was overcome by reducing "a" successively by a factor of 2 until U did converge when the solution entered a region of non-convergence. Successive values of U are shown in Tables IX a and b for a small test area of the Derby-Winnaleah survey and the whole survey respectively.

By forcing the convergence to over-relax, it became possible to take the solution quickly through values of U where the hyperellipsoid (see fig. 13) was elongated.

The bracketed portions in Table IX are attributed to regions in the hyperspace of the solution where a small number of the dimensions of $m[k]$ dominate the gradient $dU[k]$. However once this region was passed convergence continued quickly until U became less than a predetermined

TABLE IX

a) Derby-Winnaleah Area

	$\sum_{i=1}^{N}(q_i - q_i^{\nu})^2$	Iteration ν	Convergence
	3887.4597	1	
	1562.7364	2	con
	1063.3290	3	con
	739.07411	4	con
Note slow convergence	556.31239	5	con
	556.31232	6	con
Region of non-convergence	2896.7126	7	not con
	556.31234	8	not con
Note fast convergence	263.76229	9	con
	139.69104	10	con
	86.758592	11	con
	59.154730	12	con
	44.441891	13	con

b) Test Area

	1197.9390	1	
	384.77229	2	con
	214.14105	3	con
	118.76362	4	con
Note slow convergence	84.163410	5	con
	84.163409	6	con
Region of non-convergence	467.92798	7	not con
	84.163406	8	con
	84.163423	9	not con
Note fast convergence	30.586830	10	con
	19.190139	11	con

value.

While theoretically it is possible to minimise U to zero, it would require a large number of convergences and would be in practice unnecessary. As U tends to follow the path of steepest descent in hyperspace the random errors ε_i of g_i would tend to cancel out and not influence the gradient. In accordance with normal practice (e.g. Kempthorne, 1952, p. 129) we assume the ε_i normal with mean zero and variance σ.

$$\frac{\partial U}{\partial m_k} = \sum_{i=1}^{N} 2 f_i \frac{\partial f_i}{\partial m_k}$$

$$= 2 \sum_{i=1}^{N} \varepsilon_i \frac{\partial f_i}{\partial m_k} + 2 \sum_{i=1}^{N} f_i^T \frac{\partial f_i}{\partial m_k} \qquad (5.7)$$

where $f_i^T = g_i^T - \sum_{k=1}^{N} m_k (z_i - h) \Big/ \left\{ (x_i - x_k)^2 + (y_i - y_k)^2 + (z_i - h)^2 \right\}^{3/2}$

and g_i^T is the true value of g_i stripped of its random error ε_i.

i.e. $g_i = g_i^T + \varepsilon_i$

$\therefore f_i = f_i^T + \varepsilon_i$

As $\partial f_i / \partial m_k < 0$ for all i and k

then $\sum_{i=1}^{N} 2 \varepsilon_i \frac{\partial f_i}{\partial m_k} \approx K \sum \varepsilon_i \longrightarrow 0 \qquad (5.8)$

as $N \longrightarrow \infty$

from the property of ε_i having a zero mean.

Thus a value ε was chosen so that when

$$U < \varepsilon \tag{5.9}$$

the program terminated.

ε was worked out on the criterion that the random error in each Bouguer Anomaly was of the order of 0.25 milligals for the Derby-Winnaleah survey. This is a reasonable value in view of the precipitous topography of part of the area and the associated difficulty of making exact topographic corrections. Also by assuming this relatively large random error it is possible to smooth out small unwanted surface features that we regard as noise in the data.

Thus

$$U = \sum_{i=1}^{N} f_i^2$$

$$= \sum_{i=1}^{N} (\varepsilon_i + f_i^T)^2$$

As $f_i^T \rightarrow 0$ as $U \rightarrow 0$ despite the influence of the random numbers ε_i

$$U = \sum_{i=1}^{N} (\varepsilon_i)^2 \quad ; f_i^T = 0$$

Thus there is no point in reducing U much below the value $\sum_{i=1}^{N} \sigma^2$ where σ^2 is the variance of the errors - i.e.

$$\sigma^2 = \frac{1}{N} \sum_{i=1}^{N} (\varepsilon_i)^2$$

Thus the process of iteration should continue until

$$U < N\sigma^2 \qquad (5.10)$$

From the preceding discussion $\sigma^2 = (0.25)^2$

Hence $U < 45$ when N = 860 (Table IXa)

< 20 when N = 330 (Table IXb)

As the computer locations remaining after the equivalent source technique program was compiled was 5000 location it was necessary to use the core backing store when N = 860 (for the entire survey).

However it was only necessary to transfer 4 of the 7 arrays between the core backing store and the computer without even disrupting the three major inner loop computations. In this way no significant time was lost due to this information transfer.

By analysing each double loop it is seen from Table VIII that except for loop 1 only 5 variables are necessary in the computation process. In loop 1, g had to be transferred in the outer loop between the backing store and computer.

Thus the equivalent source for the 860 data points making up the Derby-Winnaleah survey could be stored within 5 x 860 = 4300 computer locations.

As is seen from B_1 and B_2 in the flow chart (fig. 14) the program was designed so that it could be switched off at any stage and the output would contain all necessary information for computation to proceed at a later date without loss of time.

Fig. 15 shows the flow chart for Program "Gravtwo part B" which

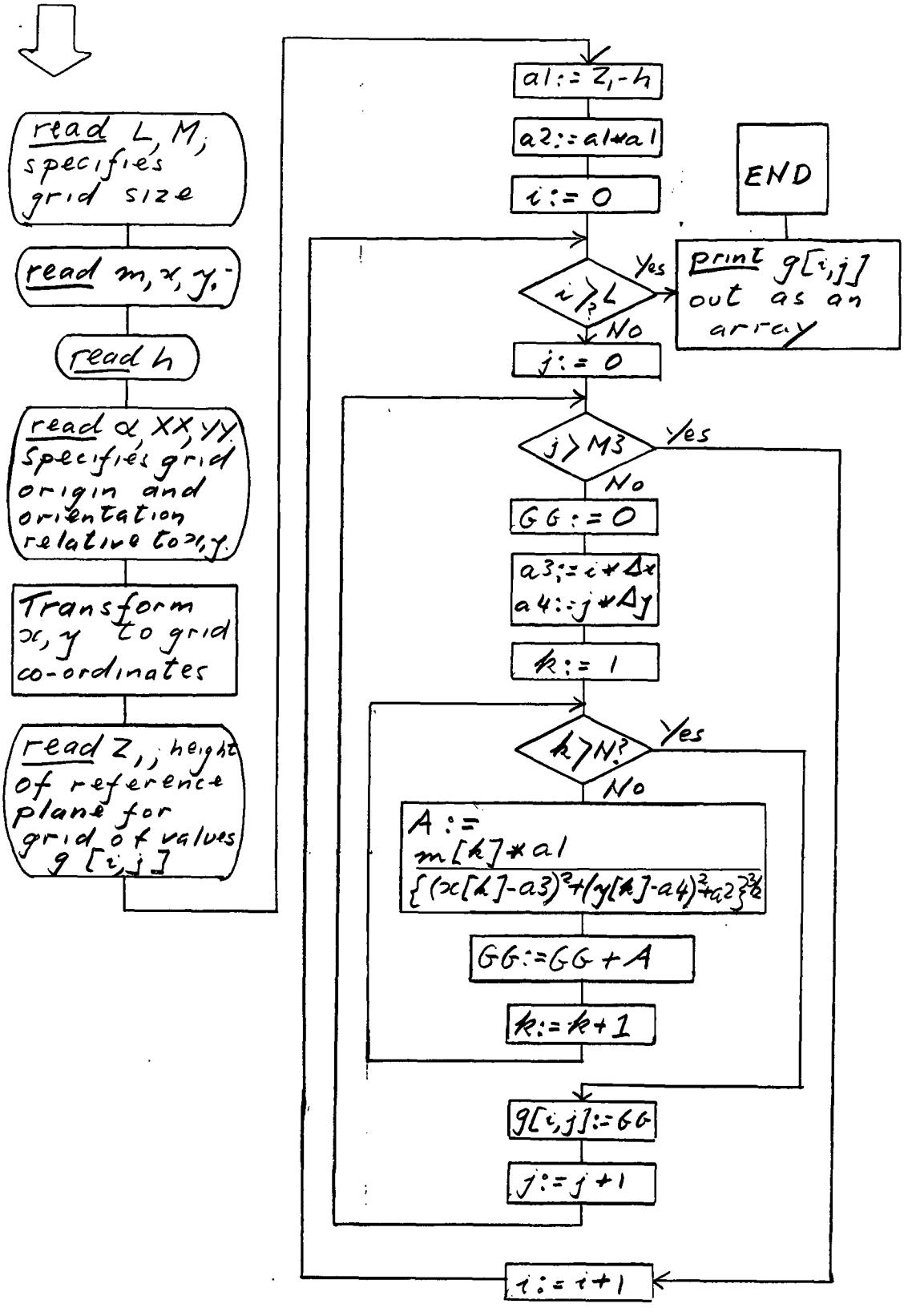

FIGURE 15. Flow chart for program calculating gravity on a flat horizontal grid. Residual is found by making two computations at different heights (Z_1) and subtracting.

computed the Bouguer Anomalies on a regularly gridded horizontal plane from the equivalent sources $m[k]$. The program required one major loop very similar in character to each of the major loops in "Gravtwo part A". By inputting the equivalent source $m[k]$ and the positions $x[i], y[j]$ on a plane at depth h it is possible to compute the gravity $g[i,j]$ at regular points $(i\Delta x, j\Delta y)$ where Δx and Δy are station spacing in the x and y direction. Computing time for this program was exactly one-third of the computing time for each convergence in "part A".

Using the equivalent source it was possible to compute the field at any height (with the restrictions as pointed out in chapter 3). In this way it is possible to vertically continue the gravitational field in either direction.

The "Regional" and "Residual" gravity fields

As already pointed out the "regional" field is a purely relative term. However, if we measure gravity at steadily increasing height above a certain point, we are being influenced by anomalous bodies over a steadily increasing horizontal area. Also the deeper larger bodies underlying the survey area have a larger relative influence on the gravity field. Thus we can consider that the field at height Z_1 is "regional" relative to the field at height Z_2 if $Z_1 > Z_2$. In chapter 6 we find the "residual" field by vertically continuing the field upwards to 500 metres and then subtracting it from the original field at 250 metres.

Comparison with exact techniques

If the field is known on a regularly gridded horizontal plane it may

still be more economical in terms of computer time to use the equivalent source technique. Bhattacharyya (1966) has shown how the two-dimensional spacial frequency components of a field may be found.

To compute each frequency component requires a double summation of trigonometrical functions times g each over N terms. The field is then continued vertically by filtering the frequency coefficients in the appropriate manner. However, as $\cos\theta$ and $\sin\theta$ are comparatively slow processes for the computer, the method of computing the field from an equivalent source may well be faster. In fact once the equivalent source is found for any field further processing such as vertical continuation and finding the residual will be very economical.

Analogue Technique

If the gravity field is known as a continuous function on a horizontal plane then it is possible fo find its derivatives and vertically continue the field by the following Analogue device (Green, 1966).

The field is first represented by a film having transmissibility properties proportional to the magnitude of g_z. The intensity of monochromatic and coherent light passed through the film, then focussed, is found at the focal plane to be given by

$$I(u,v) = \int_{-\infty}^{\infty}\int_{-\infty}^{\infty} g(x,y)\, e^{-iux - ivy}\, dx\,dy \qquad (5.11)$$

Thus appropriate filters at the focal plane can be made to attenuate the light according to either vertical continuation i.e. $e^{h\sqrt{u^2+v^2}}$ or derivative $(u^2+v^2)^{n/2}$. The resultant processed field appears at

the image plane. A similar method using diffraction is discussed by Jackson (1965) for seismological interpretation.

This optical method would greatly speed up gravity interpretation once the film representing the field is made.

6. DERBY-WINNALEAH GRAVITY SURVEY

Description of Plates 1-7

The development of the Residual Bouguer Anomaly from the original measurements on the topography is shown on the following plates.

Note - all contours are in units of milligals.

Plate 1. Geology of the area. Note all elevation contours are in units of feet above mean sea level.

Plate 2. The Free Air Anomaly

Plate 3. The Simple Bouguer Anomaly with density = 2.67 gms/cc.

Plate 4. The Bouguer Anomaly with terrain correction using densities shown on plate 1 for the topography.

Plate 5. The Bouguer Anomaly (as in plate 4) projected onto a reference plane 250 metres above mean sea level.

Plate 6. The Bouguer Anomaly projected onto a reference plane 500 metres above mean sea level which we define as the regional.

Plate 7. The Residual Bouguer Anomaly at 250 metres with interpretation of old river paths.

All maps drawn with reference to the Tasmanian Grid with the position of the base station (see fig. 18) taken as 566,438 yds. East; 932,670 yds. North.

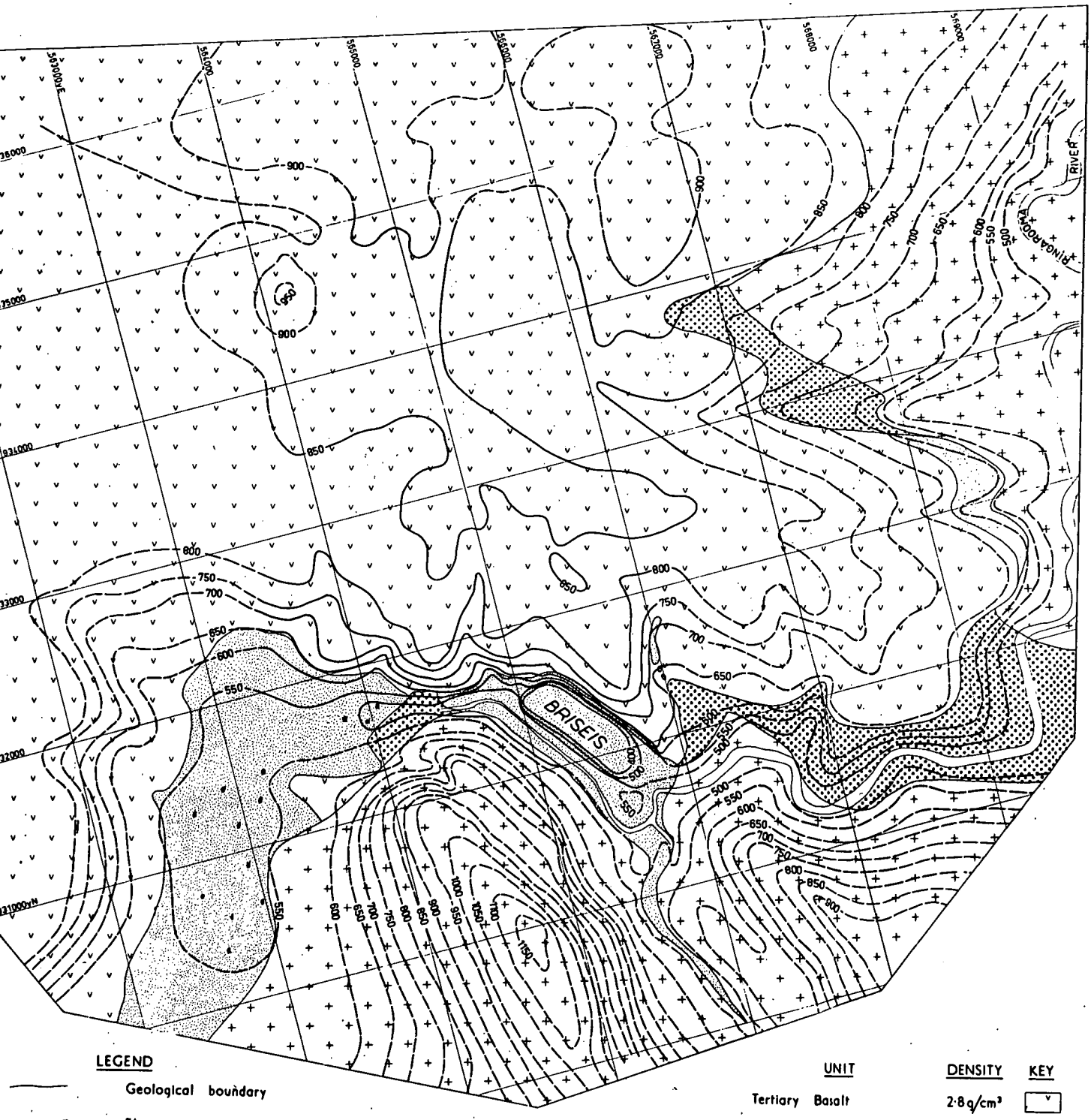

LEGEND

Geological boundary

Elevation contours AMSL

(inferred from air photos)

Swamp

UNIT	DENSITY	KEY
Tertiary Basalt	2·8g/cm³	
Devonian Granite	2·6g/cm³	+
Mathinna Group Sandstone	2·6g/cm³	
Tertiary Gravels	2·0g/cm³	

GEOLOGY and TOPOGRAPHY of DERBY

PLATE 1

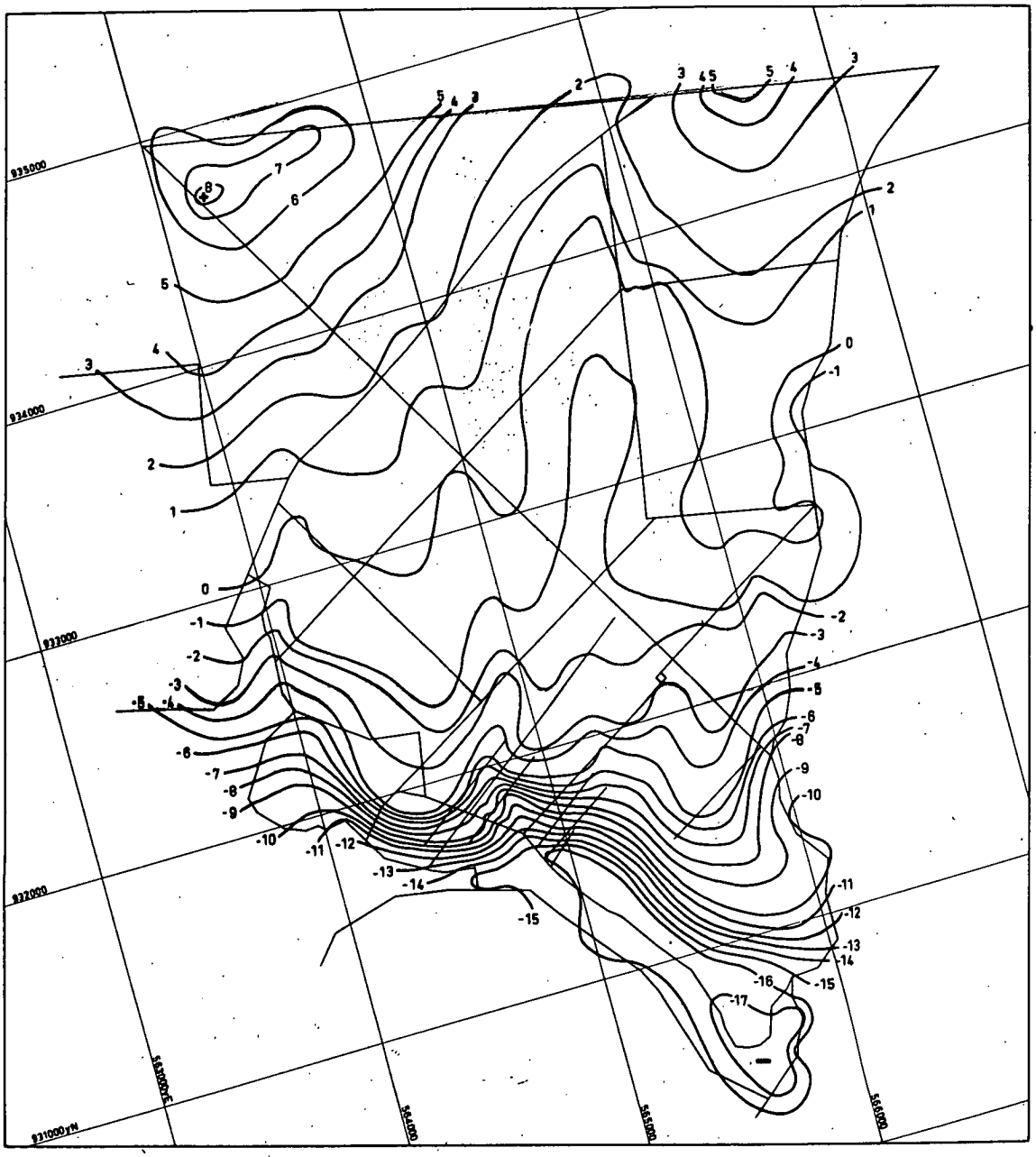
935000
934000
933000
932000
931000mN
563000mE
564000
565000
566000

PLATE 2

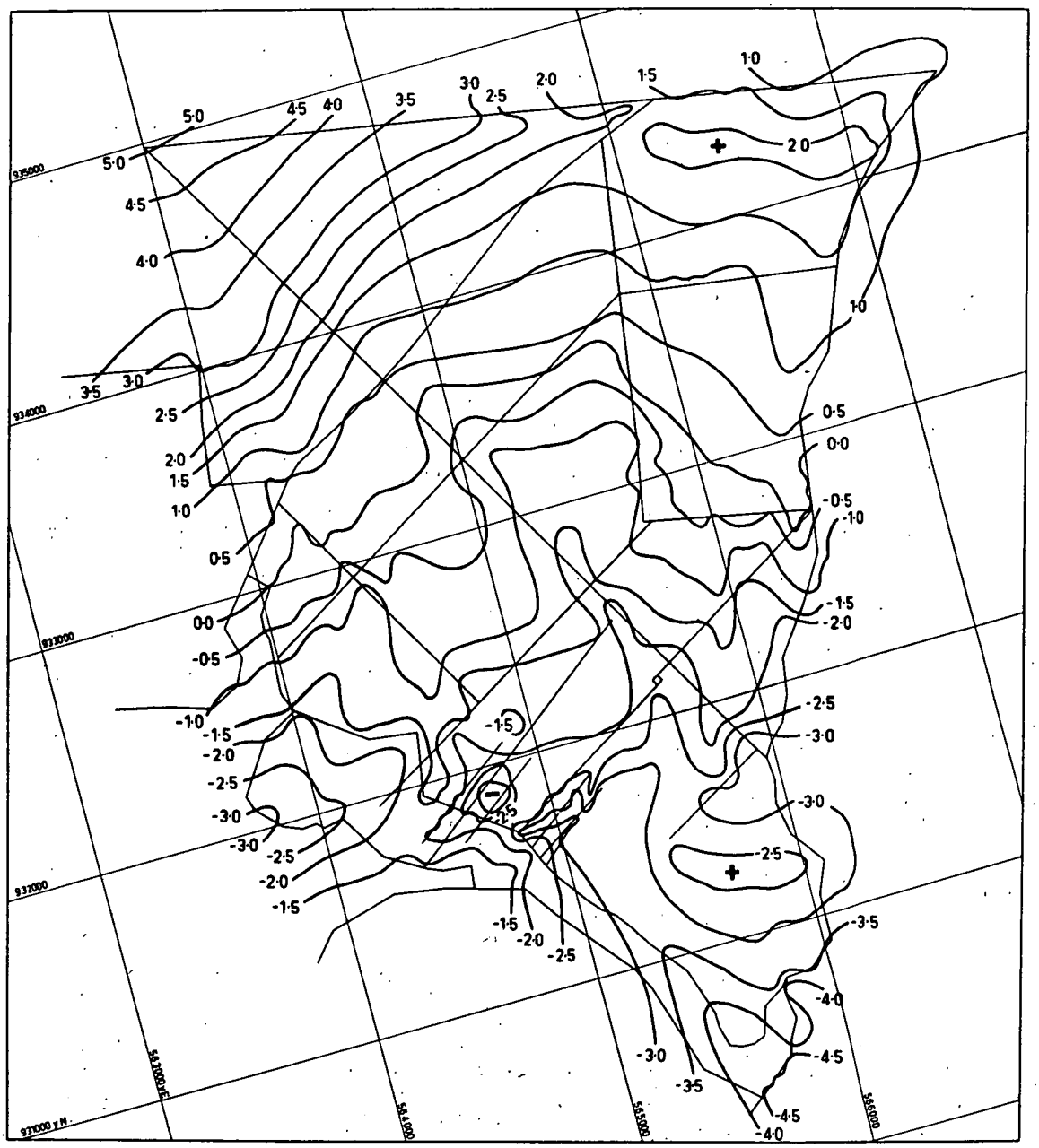
935000
934000
933000
932000
931000 E
931000 N
564000
565000
566000
5·0
4·5
4·0
3·5
3·0
2·5
2·0
1·5
1·0
0·5
0·0
-0·5
-1·0
-1·5
-2·0
-2·5
-3·0
-3·5
-4·0
-4·5

PLATE 3

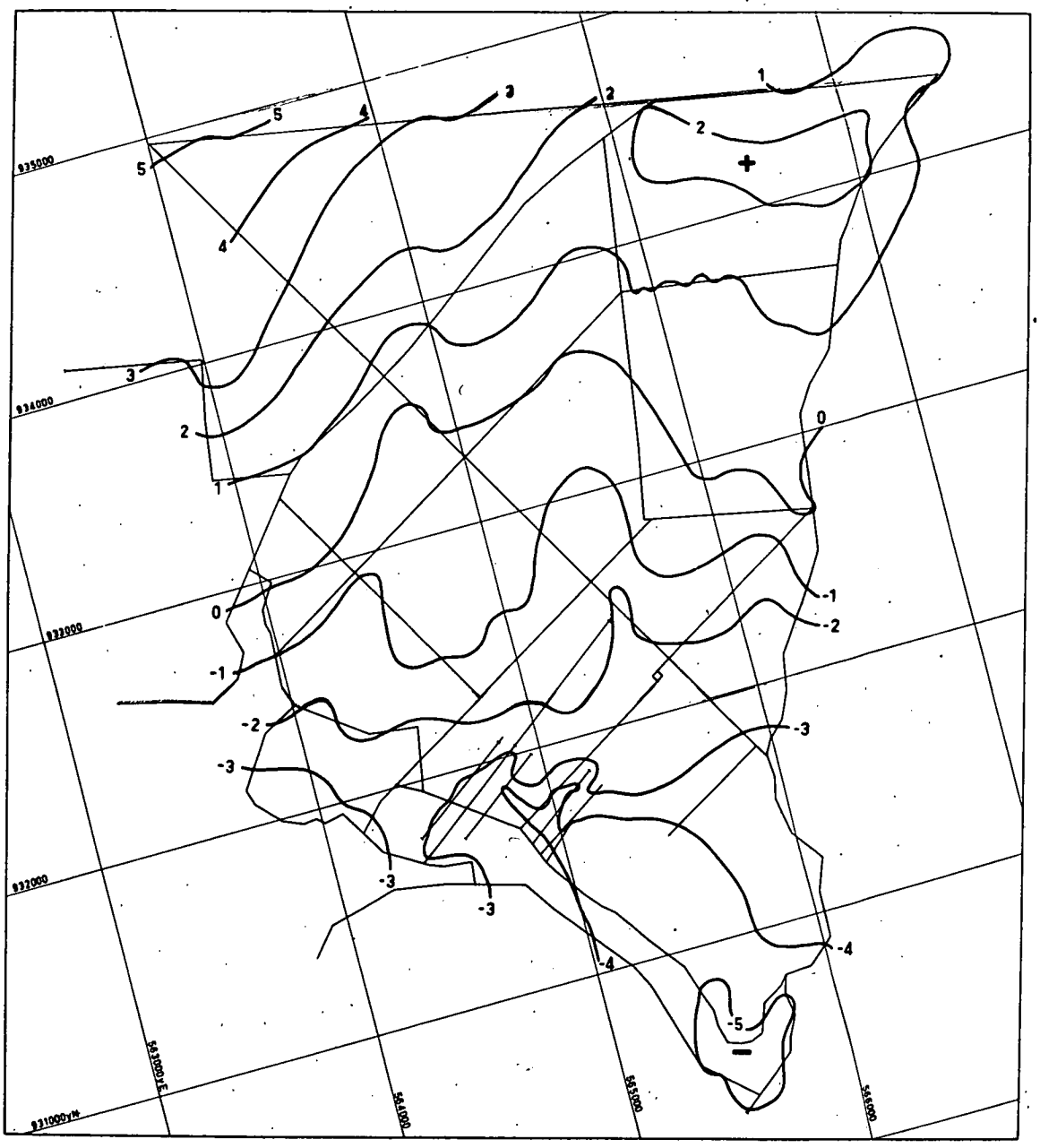
935000
934000
933000
932000
931000mN
565000E
566000
565000
565000
5
4
3
2
1
0
-1
-2
-3
-4
-5
+
−

PLATE 4

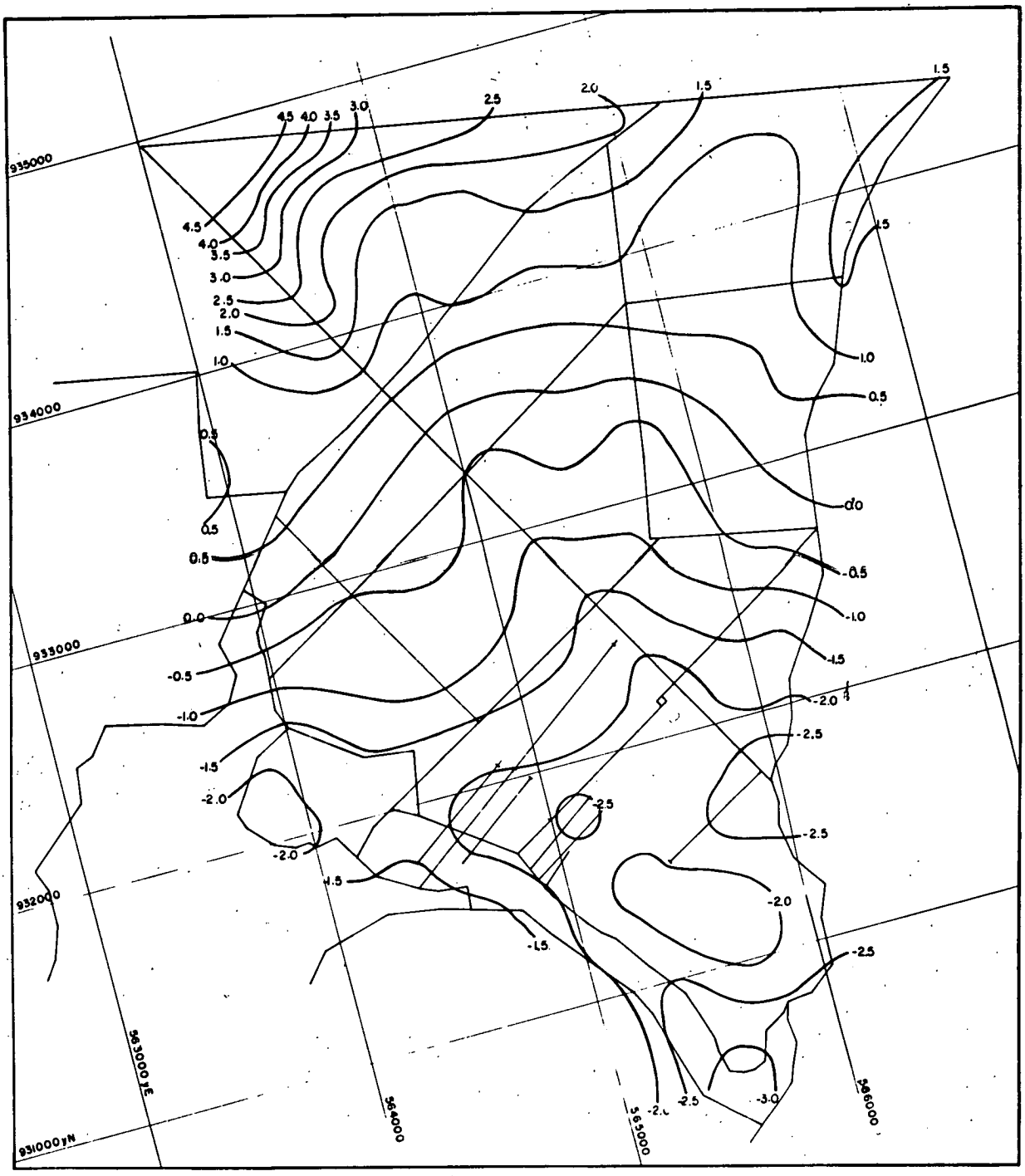
935000
934000
933000
932000
931000 N
563000 E
564000
565000
566000
4.5
4.0
3.5
3.0
2.5
2.0
1.5
1.0
0.5
0.0
-0.5
-1.0
-1.5
-2.0
-2.5
-3.0

PLATE 5

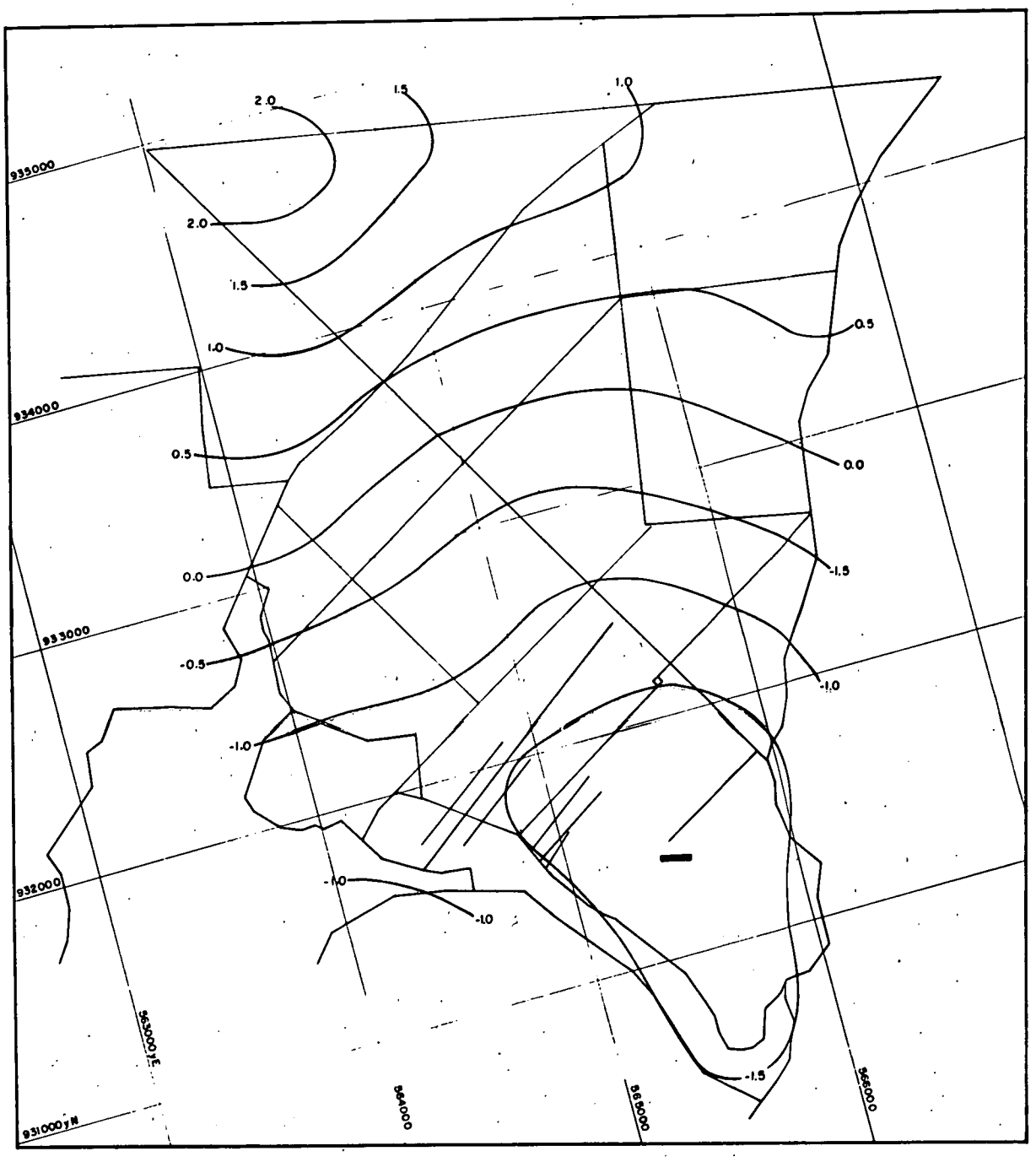
2.0
1.5
1.0
2.0
1.5
1.0
0.5
0.5
0.0
0.0
-0.5
-1.5
-1.0
-1.0
-1.0
-1.0
-1.5
935000
934000
933000
932000
931000 N
563000 E
564000
565000
566000

PLATE 6

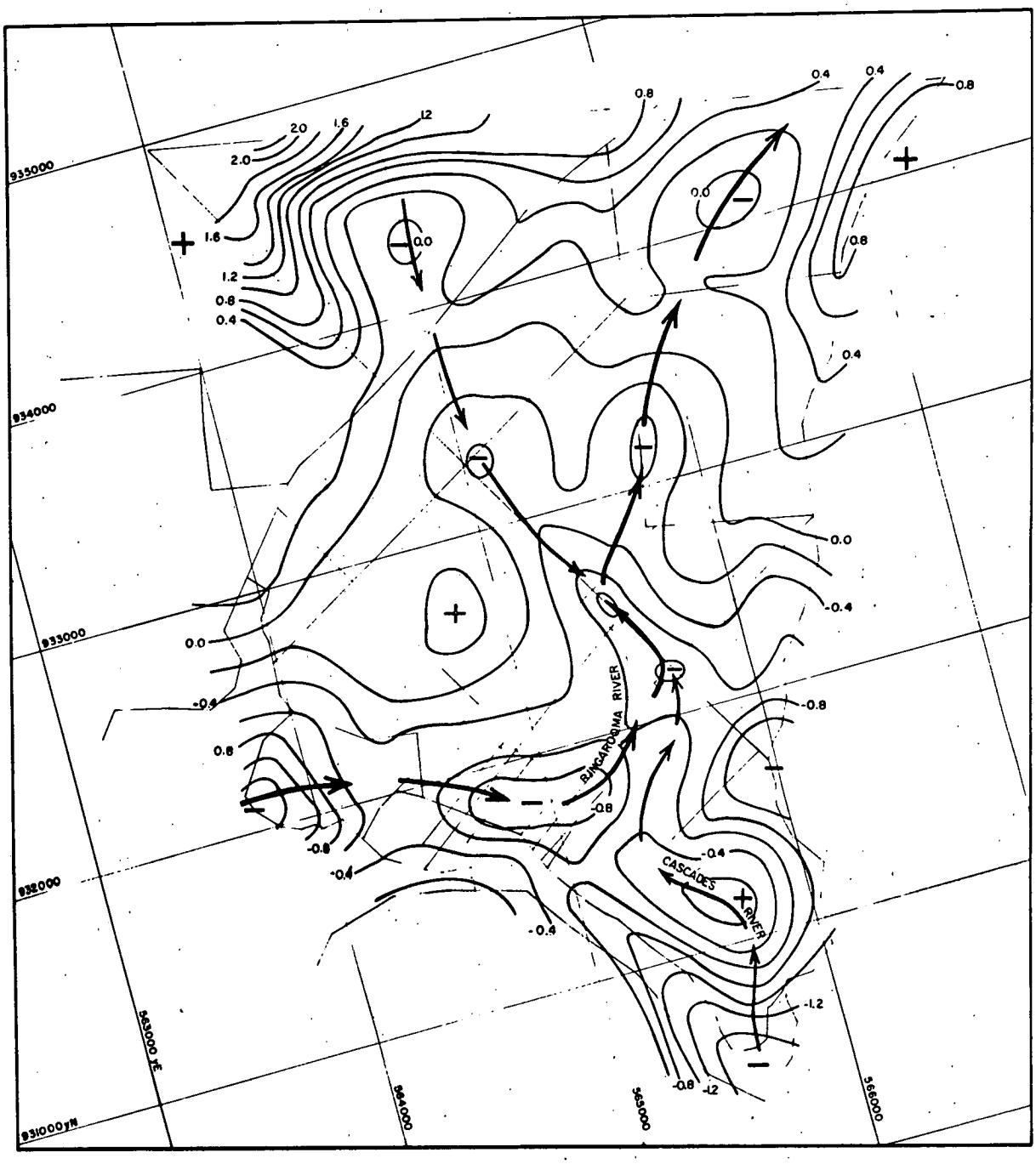
935000
934000
933000
932000
931000 mN
563000 mE
564000
565000
566000
2.0
1.6
1.2
0.8
0.4
0.0
-0.4
-0.8
-1.2
BJNCAROMA RIVER
CASCADES
RIVER

PLATE 7

The data from this survey was chosen as the area topographically (see Frontispiece and fig. 16) was precipitous to the extent that the gravity measurements should be projected analytically onto a horizontal plane. The location of the survey is shown in fig. 17.

6.1 Geology of the area.

The geology of the Ringarooma Valley area which embraces the area surveyed has been described in detail by Nye (1925). The geology in plate 1 (also reproduced on a larger scale map 1 - inside back cover) is due to Nye. Howland-Rose, however, observed an additional outcrop of Mathinna Sandstone in the region at 934,500yN and 564,000yE on the map. These two outcrops were found to show up very clearly on the Bouguer Anomaly Residual map plate 7.

The oldest rocks of the survey area are the slates and sandstones making up the Silurian Mathinna Group. This group was deposited over a large area of Tasmania.

Deposition was brought to a close by a period of diastrophism which intensely folded and faulted the Mathinna Sandstone leading up to the intrusion of granite in Devonian times. The intrusions are extensive in the area and at Derby now make up a group of relatively high hills to the south.

The granite is thought to be part of the batholith of N.E. Tasmania.

Fig. 16. The plateau and the sharp cliffs leading down to the water-filled Briseis Mine are shown above and below on the following page.

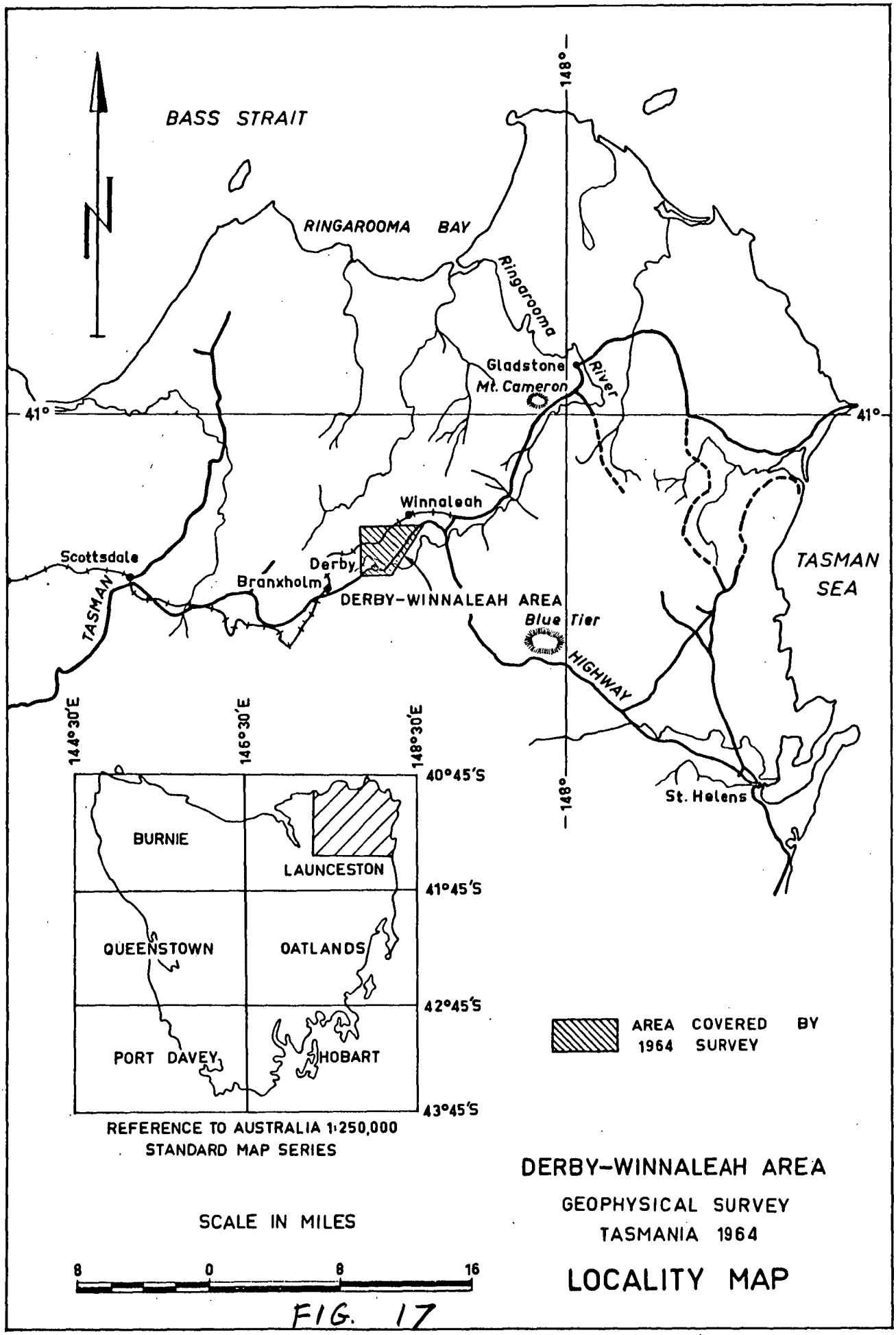

DERBY-WINNALEAH AREA

GEOPHYSICAL SURVEY
TASMANIA 1964

LOCALITY MAP

FIG. 17

As the granite magma cooled its residual vapours and fluids resulted in the formation of tin lodes in veins. These veins are the source of the alluvial tin deposited in later times as the granite was eroded away. Generally the granite ranges from the fine-grained to coarsely porphyritic.

Following the granitic intrusions a very long period of erosion, followed interspersed with periods of marine sedimentation which were subsequently eroded away. Permo-Carboniferous sedimentation is known to the north and south of the Ringarooma Valley and so it is concluded the Ringarooma River system which was now developing eroded them away.

This erosion and stream development continued until Lower Tertiary times as the then Ringarooma River developed its course. The ancient Ringarooma River according to Nye (1925) followed the present one from Branxholm to Derby, but then took a more northerly course west of the west end of the Mt. Cameron Range. So far as the survey area is concerned Nye appears to have been right to the first approximation.

The outcrops of Mathinna Sandstone found by Howland-Rose (1964) suggest that the course of the old Ringarooma River was controlled by these two ancient elevations above the flood plane such that the river probably flowed between them.

A relative depression occurred in land surface in Lower Tertiary times, causing the Ringarooma River to become dammed in places forming lakes and estuaries into which Cassiterite bearing alluvium was deposited forming the main tin leads now partially mined. This alluvium

is made up of 300 feet of gravels, grits and sands in the survey area - typical lacustrine deposits.

This period of deposition abruptly closed as Tertiary basalt lavas were extruded forming flows covering the old Ringarooma system. In all, three flows with a total thickness of 200 ft. formed at Derby. The flows are separated in time by short periods of erosion.

The Ringarooma River system re-established itself, as sea level subsequently recorded, as far down-stream as Derby but here the course was diverted to the south-eastern edge of the basalt. The river corroded a course through the granite so that it was forced past the eastern edge of the Mt. Cameron range and its new course goes to the east of Mt. Cameron and thence to the sea.

In the survey area the river follows the granite-basalt boundary and now rests for the most part on Tertiary gravels and clays.

6.1.1 Topography

The present cycle of erosion has caused the long narrow plain made up of the basalt flow to be dissected by the Ringarooma River.

In the valley of the Ringarooma River at Derby the erosion of the river through the basalt and the underlying Tertiary sediments has formed a cliff 300 feet high (see fig. 16).

The survey area topographically can be divided into a plateau region and a valley region. This can be thought of as approximately the idealised situation as shown in fig. 9 of two plains at different

levels. The necessity of using some technique such as the equivalent source technique is seen.

6.1.2 Derby Gravity Survey

The data was collected by Howland-Rose (1964) on behalf of the Australian Commonwealth Bureau of Mineral Resources. The purpose of the survey was to find from Bouguer Anomalies the actual course of the ancient Ringarooma River system. It was reasoned that the deep leads of tin such as those at the Briseis mine would continue along the river.

Measurements of the gravity field intensity at Derby were made at from 50 - 200 feet spacing on traverse lines as indicated on plate 2 to 7. In the area which was thought to be of most interest the line spacing was made much closer. This area formed a test area (fig. 24) over which the equivalent source technique could be tried.

The measurements were assumed to be corrected for drift and loop adjustments to have been made in the original data given to me by the Bureau of Mineral Resources.

6.2 Processing the Derby Gravity Data

6.2.1 Fundamental assumptions

Taking the Bouguer Anomaly in the sense of Naudy and Newmann (1965) we have to calculate the theoretical gravity of the model of the earth formulated from information at hand.

The model assumed consists of the International Ellipsoid plus a model accounting for the local geology and topography so far as it is

known. The International Ellipsoid represents the form of a self gravitating earth in hydrodynamic equilibrium. The local geology and topography plus isostatic corrections accounts for the attraction representing deviation of the earth from hydrodynamic equilibrium. Over an area as small as this survey (9 square miles), the isostatic correction will not vary significantly between stations unless one assumes the extreme case of complete local compensation - a hypothesis discounted by Vening Meinesz (Haiskanen and Vening Meinesz, 1958, p. 137). For this reason only the effects of local geology and topography need to be calculated. The geology below a certain height (the base level) should be assumed to be uniform as Vajk (1956) points out otherwise nonexisting gravity anomalies may be introduced into the results of the survey or existing gravity anomalies may be distorted. Hence it is only necessary to calculate the gravitational field intensity due to rocks above the base level as the attraction of the rock below the base level would be the same for every station in the survey if curvature of the earth is neglected. As the survey only covered a few square miles curvature of the earth was negligible.

As only relative Bouguer Anomalies were required, all corrections were made so that the corrected value at the base station (see fig. 18) was 0.

6.2.2 Free Air and Simple Bouguer Anomaly

The Free Air Anomaly and the Simple Bouguer Anomaly assuming density = 2.67 gms. per cc. was calculated from the original data using a program developed by Dr. R. Green (personal communication 1966). 2.67 was

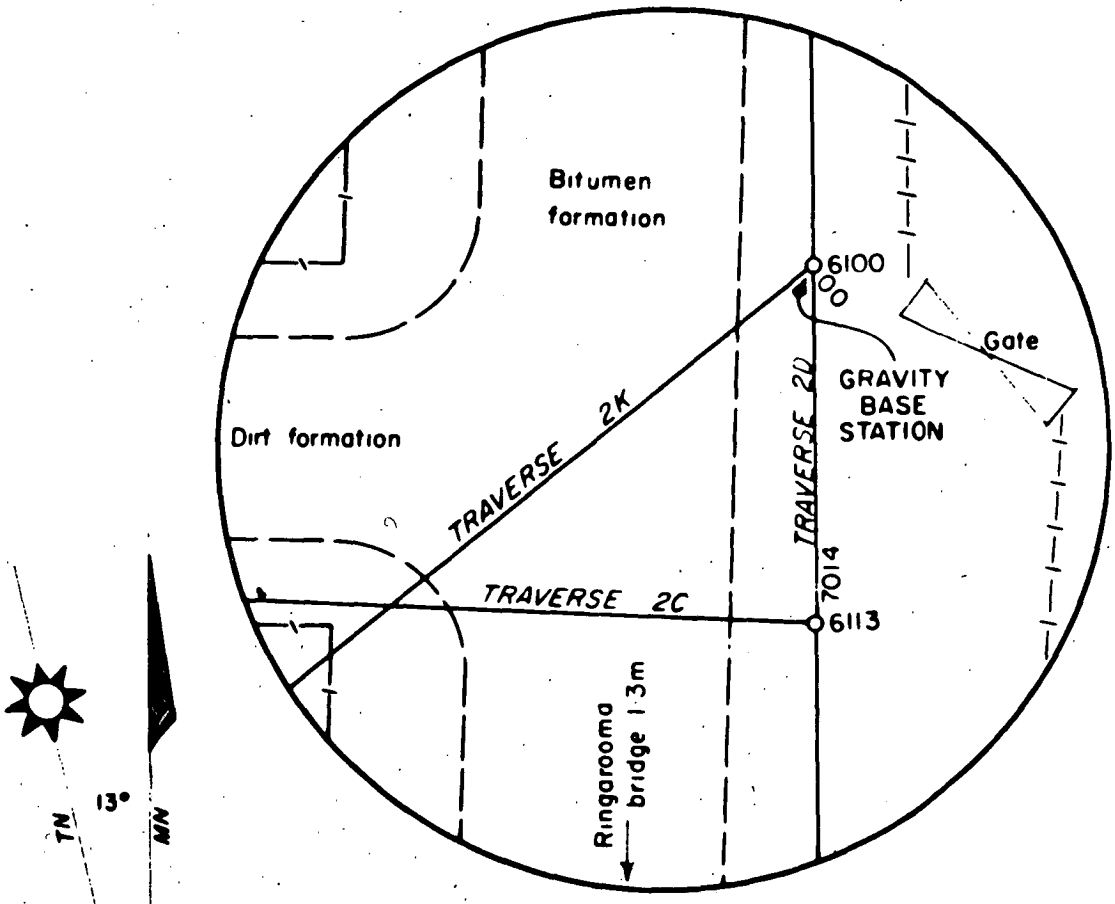

INSET

GRAVITY BASE FOR DERBY — WINNALEAH AREA

(NOT TO SCALE)

FIGURE 18

chosen as the density value because experience has indicated in the granite areas of Tasmania that 2.67 gives a representative average density. Plates 2 and 3 show the contours of the Free-Air Anomaly and the Simple Bouguer Anomaly at Derby.

It can be seen that the lack of terrain correction in plate 3 produced a steep gradient in the Simple Bouguer Anomaly map at the Briseis Mine.

6.2.3 The Extended Bouguer Anomaly

In order to calculate the Bouguer Anomaly the topography shown on plate 1 and map 1 was divided up into a number of square blocks extending from a base level to the average height of the square area they covered. Note that, although not shown, the elevation contours on map 1 were known at 10 ft. intervals. The blocks were assumed to be of uniform density equal to the density of the rock outcropping on the surface.

A diagrammatic cross-section of the model of the local geology is shown in fig. 19.

The effect of the topography was calculated over an area 9 times the area of the survey, such that the topography unaccounted for was at least a distance ℓ away from any gravity station where "ℓ" is the approximate length of the side of the area.

6.2.3.1 Rock Densities

Howland-Rose (1964) determined the densities of the rocks from samples collected in the field.

These densities were taken and given on plate 1.

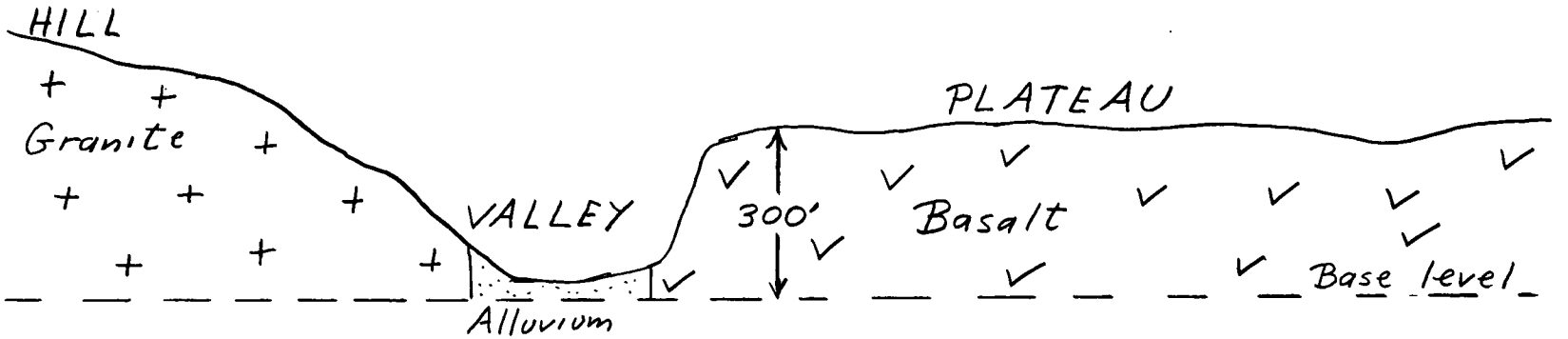

Fig. 19. Diagrammatic cross-section through Plateau and Valley. In the model all contacts shown in outcrop in plate 1 were assumed vertical down to the base level.

The density for granite sandstone and the Tertiary gravels were found to be quite typical,

As the basalt covers the majority of the area surveyed its density was critical as it was important for the contrast density of the Tertiary gravels to the basalt to be significant.

Basalt can have a density of the order of 2.00 gms/cc if it is vescicular. Some vesicles were present in the basalt but results indicate that the density was definitely not less than 2.8 gms/cc. The mineralogy (described in Appendix B) and negative correlation of the Bouguer Anomaly with topography (compare plate 1 and 4) supported this last observation (Nettleton 1942).

Methods of checking the density by generalisations of profile methods such as Grant and Elsaharty (1962) were not used.

6.2.3.2 Method of Calculation

While there are a number of methods available (Hammer, 1939; Sandberg, 1958; Beckel, 1948) to calculate terrain correction graphically, it was decided to modify Bott's (1963) method. Bott's method divides the terrain into blocks and then calculates the influence of each block at the point of measurement.

The blocks were chosen with an area of 200 yds. square as this filled the grid of Eastings and Northings conveniently. The blocks are mathematically idealised as vertical lines with a line density

$$= \rho A \qquad (6.1)$$

where A is the area of the block.

From fig. 20 it can be seen that the difference T between assuming the block to be the height of the station with density D and assuming the block to be the average height of the terrain with density d is

for $Z > z$

$$T = G D A\left[\frac{1}{\{(X-x)^2+(Y-y)^2\}^{1/2}} - \frac{1}{\{(X-x)^2+(Y-y)^2+(Z-z)^2\}^{1/2}}\right]$$
$$+ G(D-d)A\left[\frac{1}{\{(X-x)^2+(Y-y)^2+(Z-z)^2\}^{1/2}} - \frac{1}{\{(X-x)^2+(Y-y)^2+(Z-\text{base})^2\}^{1/2}}\right] \quad (6.2)$$

$Z < z$

$$T = Gd A\left[\frac{1}{\{(X-x)^2+(Y-y)^2\}^{1/2}} - \frac{1}{\{(X-x)^2+(Y-y)^2+(Z-z)^2\}^{1/2}}\right] \quad (6.3)$$
$$+ G(D-d)A\left[\frac{1}{\{(X-x)^2+(Y-y)^2\}^{1/2}} - \frac{1}{\{(X-x)^2+(Y-y)^2+(Z-\text{base})^2\}^{1/2}}\right]$$

giving for all z

$$T = D/\{(X-x)^2+(Y-y)^2\}^{1/2}$$
$$- d/\{(X-x)^2+(Y-y)^2+(Z-z)^2\}^{1/2} \quad (6.4)$$
$$(D-d)/\{(X-x)^2+(Y-y)^2+(Z-\text{base})^2\}^{1/2}$$

where G is the gravitational constant, (X, Y, Z) is the position of P the observation point, (x, y, z) is the mid-point of the top of the block and "base" is the height above mean sea level of the bottom of

STATION ABOVE TOPOGRAPHY

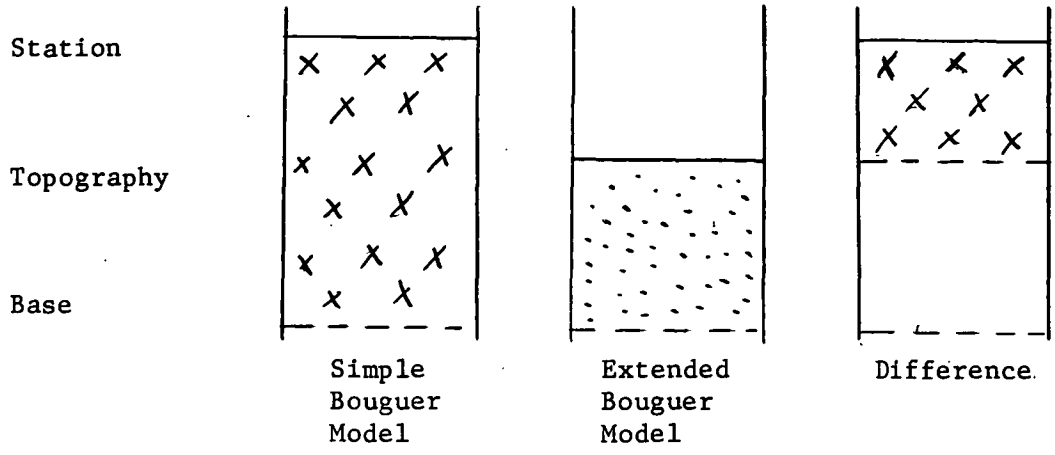

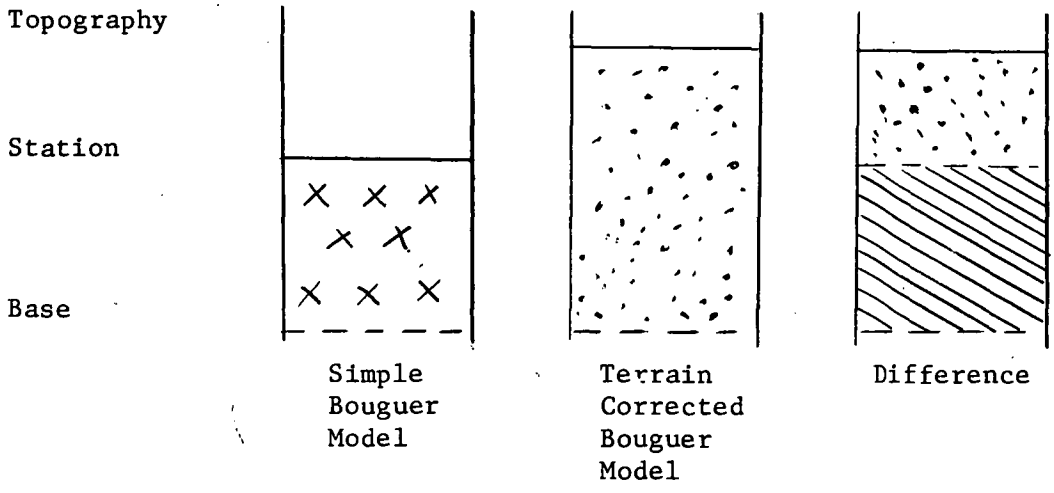

DENSITY	KEY
D	
d	
D-d	

FIGURE 20.

the block.

Using the result that the vertical component of the gravitation attraction of a mass line with line density λ gm/cm. distance ρ_1 from P to the top of the mass line and distance ρ_2 to the bottom,

$$= G\lambda\left(\frac{1}{\rho_1} - \frac{1}{\rho_2}\right) \qquad (6.5)$$

This idealisation is sufficiently accurate unless the blocks are too close to P.

Fig. 21 shows how the blocks nearest to P were divided up into first quarters then into sixteenths. The gravitational attraction of the terrain within the block containing P was worked out using Hammer's method where necessary.

Fig. 22 shows the ratio F of the gravitational attraction of a mass line distance ρ approximating a given block of side ℓ and four mass lines approximating quarters of the same block. As can be seen the ratio $F \approx 1$ if $\rho > 3\ell$. Thus these mass lines give a very good approximation. Fig. 23 shows the flow chart of the program calculating the terrain correction.

The program required 130 minutes to calculate from 1000 blocks and the Free Air Anomaly, the Bouguer Anomaly for 1200 stations.

The Bouguer Anomaly is shown in plate 4. It is seen from this map that the obvious variation of the Simple Bouguer Anomaly with terrain is not present.

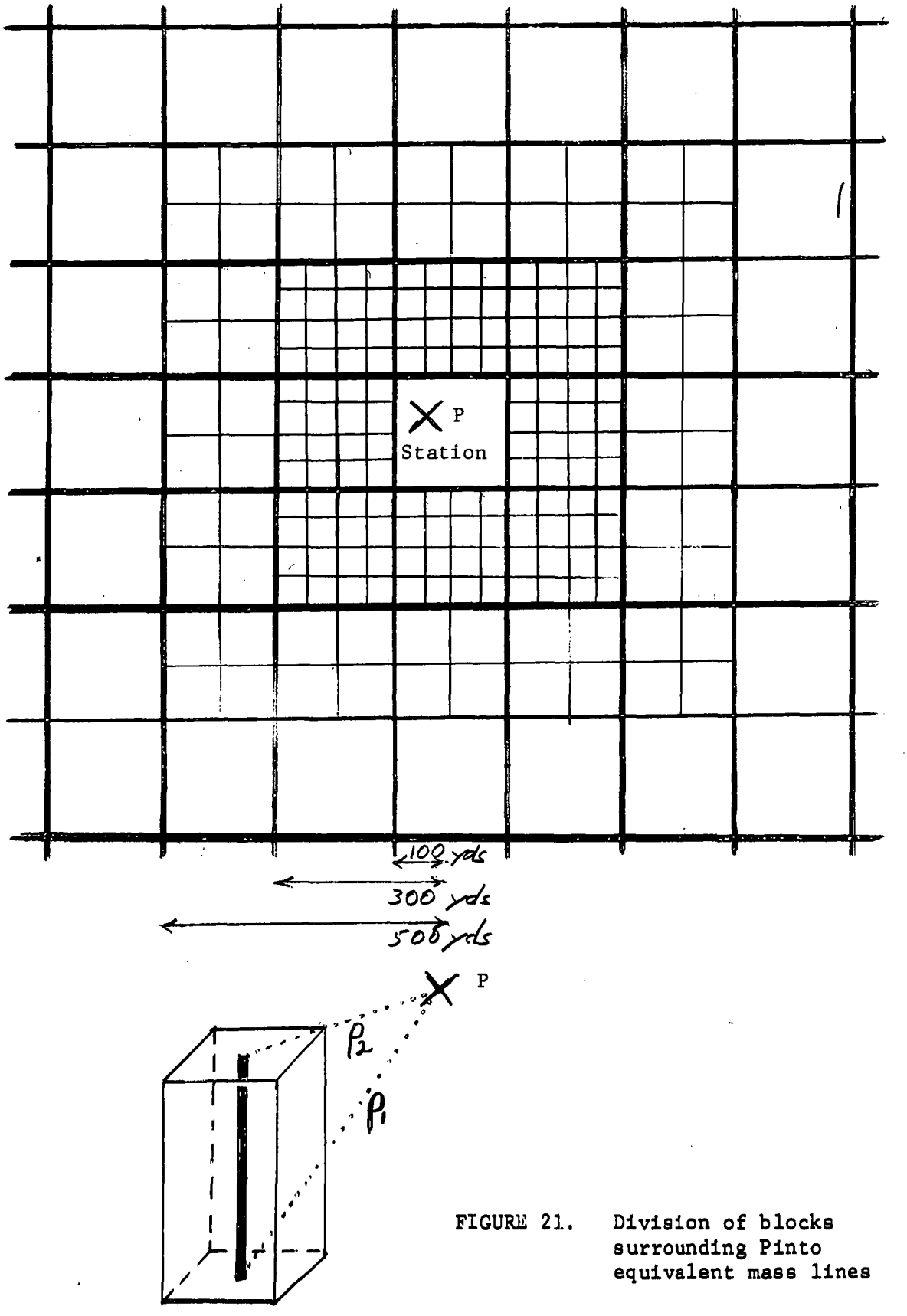

FIGURE 21. Division of blocks surrounding Pinto equivalent mass lines

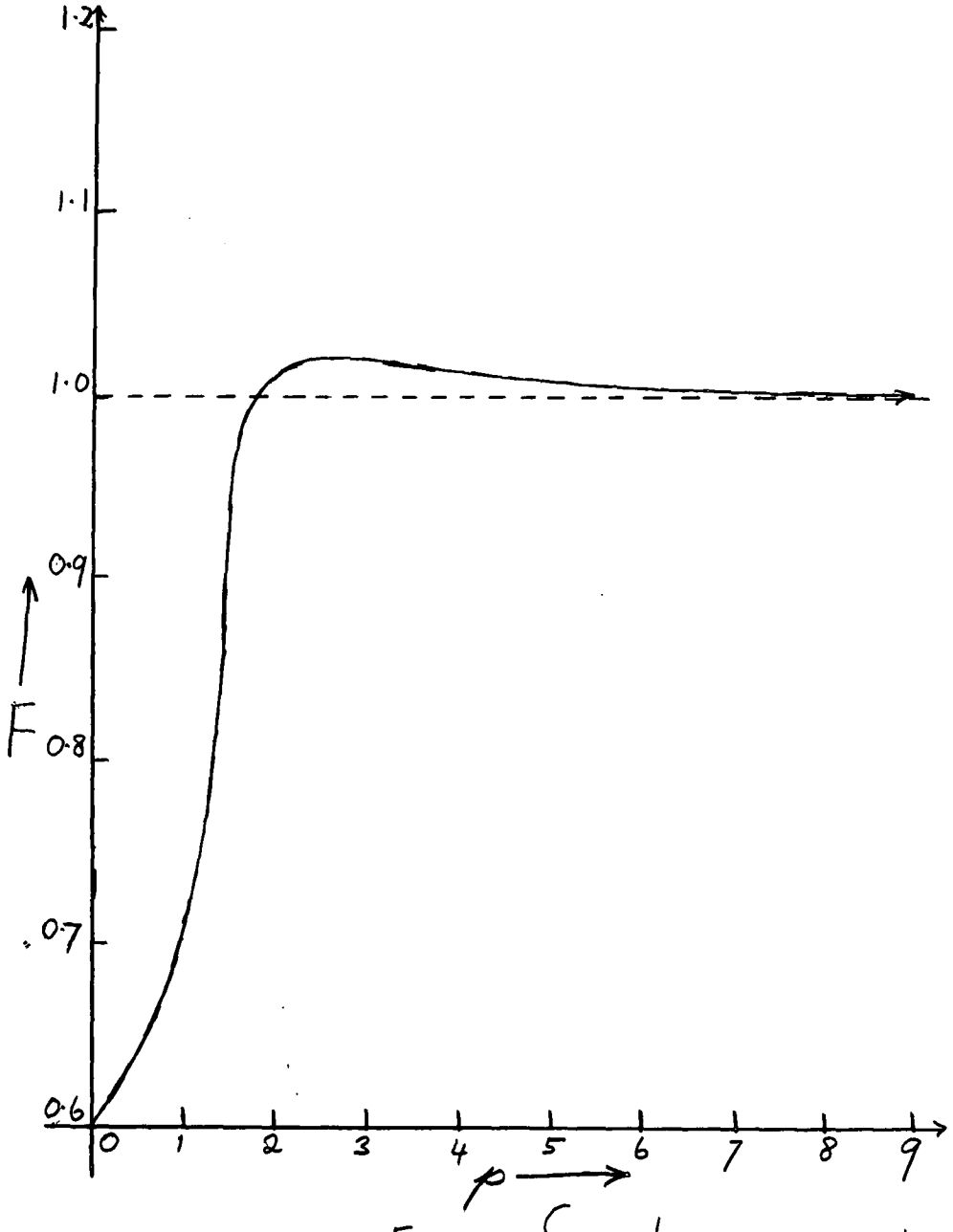

Graph of $F = \frac{p}{2}\left\{\frac{1}{((p-1)^2+1)^{1/2}} + \frac{1}{((p+1)^2+1)^{1/2}}\right\}$

FIGURE 22.

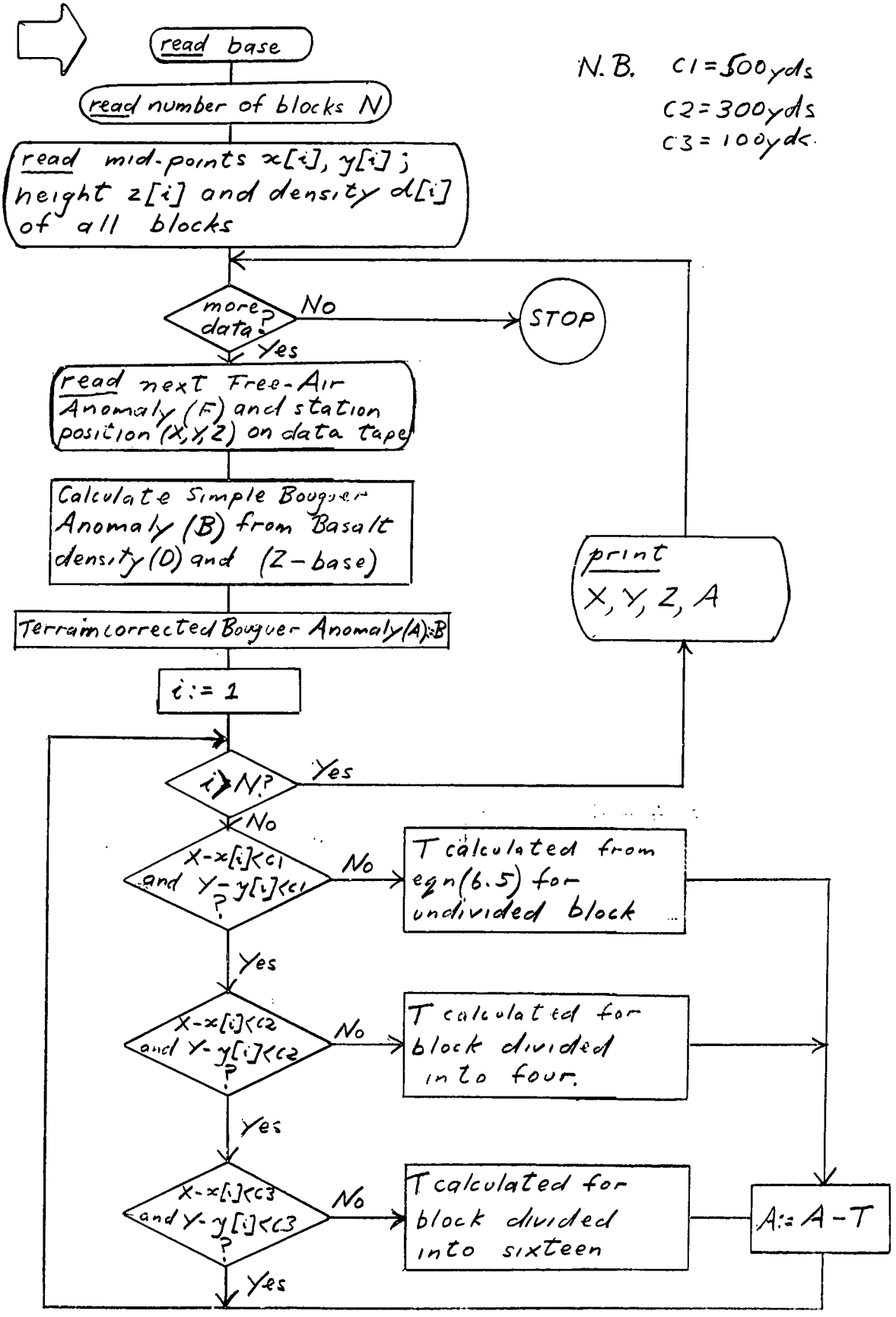

FIGURE 23. Flow chart for terrain corrected Bouguer Anomaly

This Bouguer Anomaly data was used to find the equivalent source of the area after erratic values were omitted.

6.3 Testing the Equivalent Source Technique

Part of the survey was used as a test area to test the validity of the technique in describing the gravity field. Fig. 24 shows the 1.5 mgal contour of the vertical intensity at various heights (measured in metres) above mean sea level (A.M.S.L.). The figure gives a good description of the behaviour of the gravity intensity with height.

Geological evidence (see plate 1) indicates that the source of the gravity field (the alluvium) is shallow and outcrops on the surface. This bears out the interpretation from figure 24 that the source is close to the surface as the lower contours begin to converge together. The anomaly is thus interpreted as a small sediment-filled ancient lake.

Other contours drawn of the test area gravity field not shown here, gave a good description of the type of gravity field intensity behaviour expected.

In particular, the field of the entire survey at 250 metres and 500 metres (A.M.S.L.) on plates 6 and 7 respectively show the techniques ability to carry out vertical continuation.

6.4 Derby Bouguer Anomaly Projected onto a Flat Plane

The Bouguer Anomaly at a height of 250 metres corresponding to the plateau level is shown in plate 5. Comparing this with plate 4 it can be seen that this projection elliminates some distortion in the gravitational field.

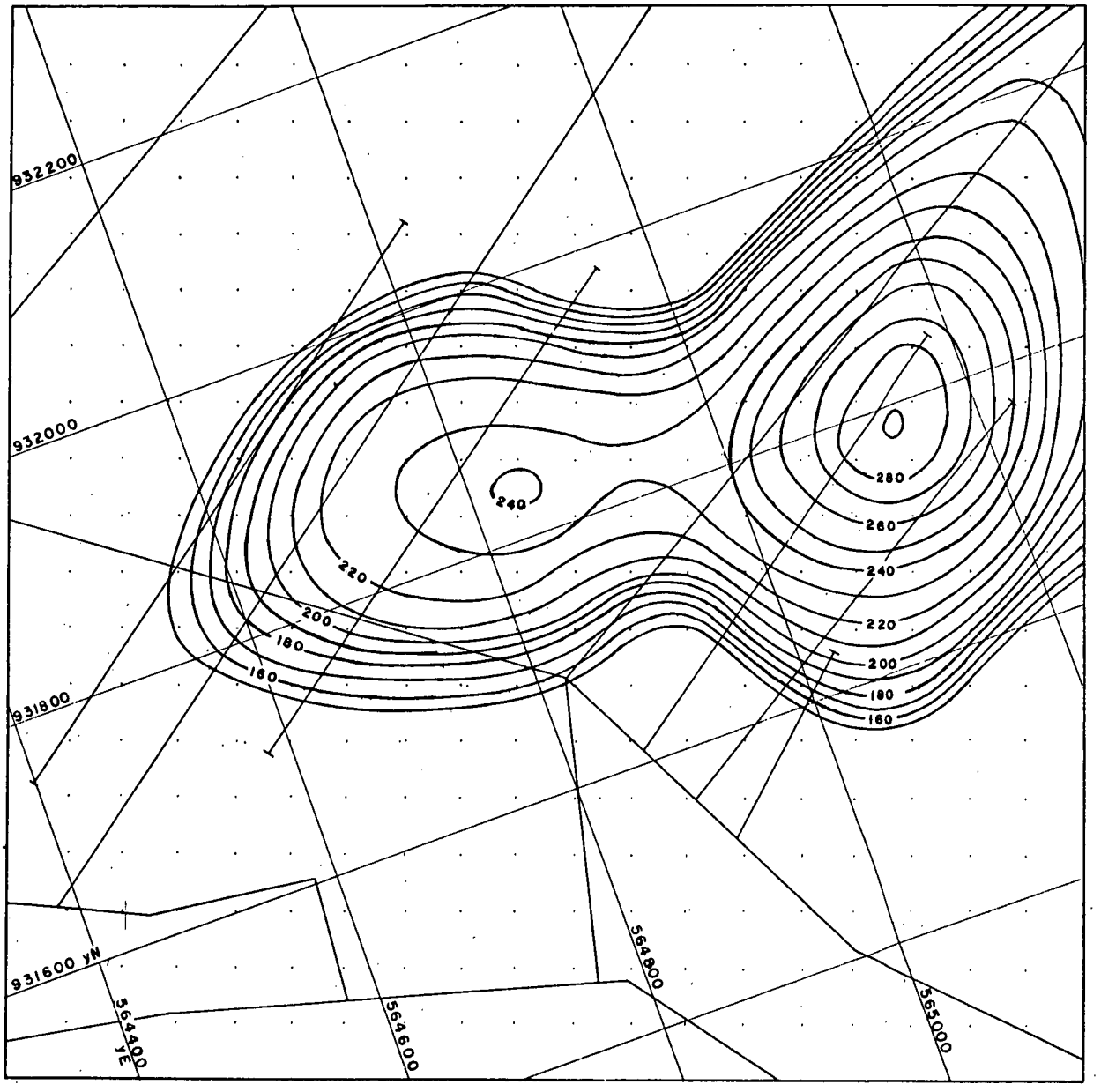

FIGURE 24. The 1.5 mgal gravity intensity anomaly at various heights indicated in metres above mean sea level - referred to the Tasmanian grid.

Continuing the field up to 500 metres from the equivalent source produces the Bouguer Anomaly contours shown on plate 6. The field at this height will be considered to represent the regional as the large scale variations only remain as the high frequencies have been highly suppressed by the upward continuation process.

The residual anomaly is thus found by subtracting the field at 250 metres from the regional here defined as above. The residual Bouguer Anomaly is shown on plate 7.

Hence the trend indicated is the ancient Ringarooma River. The trend is continuous across the area and shows clearly the river as it used to flow between the two ancient hills now represented by the Mathinna Sandstone outcrops found by Howland-Rose.

While other interpretations such as weathering in the basalt or lineament in the basement could be postulated to explain these trends it seems difficult to imagine that such effects would take the form shown.

The small relative positive anomaly over the Briseis Mine shows up an error in the model. In calculating the Bouguer Anomaly it was assumed that the 100 foot deep open-cut mine workings were empty of water. However, it has since been learnt that the Mine was actually filled with water and hence this appears as a small positive on the map.

The positive anomalies at the north-west and north-east corners of the residual Bouguer Anomaly map are interpreted as old hills on the pre-Tertiary land surface.

6.5 Future Work

Drill-holes at the points indicated on map 2 inside the back cover would confirm the interpretation of the gravity at Derby. It is suggested that the holes be drilled in the order indicated as the numbers indicate decreasing likelihood of finding the old river.

6.6 Conclusion

Thus the equivalent source technique is able in practise to find the Bouguer Anomaly on a flat plane far more accurately than has been previously possible.

The economics of the method are also reasonable. Assuming a cost of $5.00 per station, the cost of 50 cents per station in terms of computer time is quite reasonable for the equivalent source technique.

APPENDIX A

The magnetic anomalous scalar field potential $\mathcal{F}(x,y,z)$ is related to the intensity of magnetisation $\underset{\sim}{I}(\alpha,\beta,\gamma)$ at (α,β,γ) by:

$$\mathcal{F}(x,y,z) = \frac{\mu_0}{4\pi}\int_{-\infty}^{\infty}\int_{-\infty}^{\infty}\int_{-\infty}^{\infty} \underset{\sim}{I}\cdot\nabla\left(\frac{1}{r}\right)d\alpha\,d\beta\,d\gamma \qquad (1)$$

Consider $\mathcal{F}(x,y,z)$ due to a basement with upper surface described by $\gamma = f(\alpha,\beta) \leq h$ and infinite in all other directions. The components of $\underset{\sim}{I}(\alpha,\beta,\gamma)$ are supposed constant. Therefore:

$$\mathcal{F}(x,y,z)\times\frac{4\pi}{\mu_0} = I_z\int_{-\infty}^{\infty}\int_{-\infty}^{\infty}\int_{-\infty}^{f(\alpha,\beta)}\frac{(z-\gamma)\,d\alpha\,d\beta\,d\gamma}{\{(x-\alpha)^2+(y-\beta)^2+(z-\gamma)^2\}^{\frac{3}{2}}}$$

$$+ I_x\int_{-\infty}^{\infty}\int_{-\infty}^{\infty}\int_{-\infty}^{f(\alpha,\beta)}\frac{\partial}{\partial\alpha}\left(\frac{1}{r}\right)d\alpha\,d\beta\,d\gamma + I_y\int_{-\infty}^{\infty}\int_{-\infty}^{\infty}\int_{-\infty}^{f(\alpha,\beta)}\frac{\partial}{\partial\beta}\left(\frac{1}{r}\right)d\alpha\,d\beta\,d\gamma$$

The contributions of I_x and I_y are thus seen to be zero if $f(\alpha,\beta)\simeq h$ so that the integrations with respect to α, β and γ are interchangeable.

$$\therefore\ \mathcal{F}(x,y,z) = \frac{\mu_0 I_z}{4\pi}\int_{-\infty}^{\infty}\int_{-\infty}^{\infty}\left[\frac{\gamma(z-\gamma)}{\{(x-\alpha)^2+(y-\beta)^2+(z-\gamma)^2\}^{\frac{3}{2}}}\right]_{\infty}^{f(\alpha,\beta)}d\alpha\,d\beta$$

$$-\frac{\mu_0 I_z}{4\pi}\int_{-\infty}^{\infty}\int_{-\infty}^{\infty}\int_{\infty}^{f(\alpha,\beta)}\gamma\frac{\partial^2}{\partial\gamma^2}\left(\frac{1}{r}\right)d\alpha\,d\beta\,d\gamma$$

= first integral - second integral, where:

$$\text{first integral} = \frac{\mu_0 I_z}{4\pi}\int_{-\infty}^{\infty}\int_{-\infty}^{\infty}\frac{f(\alpha,\beta)\{z-f(\alpha,\beta)\}\,d\alpha\,d\beta}{\left[(x-\alpha)^2+(y-\beta)^2+\{z-f(\alpha,\beta)\}^2\right]^{\frac{3}{2}}}$$

Now as $f(\alpha,\beta) \approx h$

$$\therefore \text{ first integral} = \frac{\mu_0 I_2}{4\pi}\int_{-\infty}^{\infty}\int_{-\infty}^{\infty}\frac{f(\alpha,\beta)(z-h)\,d\alpha\,d\beta}{\{(x-\alpha)^2+(y-\beta)^2+(z-h)^2\}^{\frac{3}{2}}} \quad (2)$$

Now as $\nabla^2\left(\frac{1}{r}\right) = 0$

$$\therefore \text{ second integral} = \frac{\mu_0 I_2}{4\pi}\int_{-\infty}^{\infty}\int_{-\infty}^{\infty}\int_{-\infty}^{f(\alpha,\beta)}\gamma\left[\frac{\partial^2}{\partial\alpha^2}+\frac{\partial^2}{\partial\beta^2}\right]\left(\frac{1}{r}\right)d\alpha\,d\beta\,d\gamma$$

interchanging order of integration:

$$= \frac{I_2}{4\pi}\mu_0\int_{\infty}^{f(\alpha,\beta)}\gamma\,d\gamma\int_{-\infty}^{\infty}d\beta\int_{-\infty}^{\infty}\frac{\partial^2}{\partial\alpha^2}\left(\frac{1}{r}\right)d\alpha$$

$$+\frac{\mu_0 I_2}{4\pi}\int_{\infty}^{f(\alpha,\beta)}\gamma\,d\gamma\int_{-\infty}^{\infty}d\alpha\int_{-\infty}^{\infty}\frac{\partial^2}{\partial\beta^2}\left(\frac{1}{r}\right)d\beta$$

$$= \frac{\mu_0 I_2}{4\pi}\int_{\infty}^{f(\alpha,\beta)}\gamma\,d\gamma\int_{-\infty}^{\infty}d\beta\left[\frac{\partial}{\partial\alpha}\left(\frac{1}{r}\right)\right]_{-\infty}^{\infty}$$

$$+\frac{\mu_0 I_2}{4\pi}\int_{\infty}^{f(\alpha,\beta)}\gamma\,d\gamma\int_{-\infty}^{\infty}d\alpha\left[\frac{\partial}{\partial\beta}\left(\frac{1}{r}\right)\right]_{-\infty}^{\infty} \quad (3)$$

From Roy (1962) eq. 18 the field potential (magnetic or gravitational):

$$V(x,y,z) \text{ at } P(x,y,z) = \frac{1}{2\pi}\int_{-\infty}^{\infty}\int_{-\infty}^{\infty}\frac{1}{r}\left[\frac{\partial V(\alpha,\beta,\gamma)}{\partial\gamma}\right]_{\gamma=h}d\alpha\,d\beta \quad (4)$$

where $r = \{(x-\alpha)^2+(y-\beta)^2+(z-h)^2\}^{1/2}$. Now the field intensity:

$$\phi(\alpha,\beta,\gamma) = \frac{\partial V}{\partial\gamma}(\alpha,\beta,\gamma)$$

Thus differentiating with respect to **z** :

$$\phi(x,y,z) = \frac{1}{2\pi}\int_{-\infty}^{\infty}\int_{-\infty}^{\infty}\frac{(z-h)}{r^3}\left[\phi(\alpha,\beta,\gamma)\right]_{\gamma=h} d\alpha d\beta$$

$$= \frac{1}{2\pi}\int_{-\infty}^{\infty}\int_{-\infty}^{\infty}\frac{(z-h)\,\phi(\alpha,\beta,h)\,d\alpha d\beta}{r^3}$$

Now as ϕ satisfies $\nabla^2\phi$ this relation is a property of potential functions, so that we may replace ϕ by $\mathcal{F}$ so that we get in the magnetic field potential case:

$$\mathcal{F}(x,y,z) = \frac{1}{2\pi}\int_{-\infty}^{\infty}\int_{-\infty}^{\infty}\frac{\mathcal{F}(\alpha,\beta,h)(z-h)\,d\alpha d\beta}{\{(x-\alpha)^2+(y-\beta)^2+(z-h)^2\}^{\frac{3}{2}}}$$

$\therefore$ from eq. 2,3 and 6: $\mu_0 I_2 f(\alpha,\beta) = 2\,\mathcal{F}(\alpha,\beta,h)$

But $\alpha = x$, $\beta = y$ then

$$\mu_0 I_2 f(x,y) = \mathcal{F}(x,y,h)\times 2$$

From eq. 4:

$$\mathcal{F}(x,y,z) = \frac{1}{2\pi}\int_{-\infty}^{\infty}\int_{-\infty}^{\infty}\frac{H_\gamma(\alpha,\beta,h)\,d\alpha d\beta}{\{(x-\alpha)^2+(y-\beta)^2\}^{\frac{1}{2}}}$$

where H_γ is the vertical component of the magnetic field intensity.

Thus:

$$f(x,y) = \frac{1}{2\pi\mu_0 I_2}\int_{-\infty}^{\infty}\int_{-\infty}^{\infty}\frac{H_\gamma(\alpha,\beta,h)\,d\alpha d\beta}{\{(x-\alpha)^2+(y-\beta)^2\}^{1/2}}$$

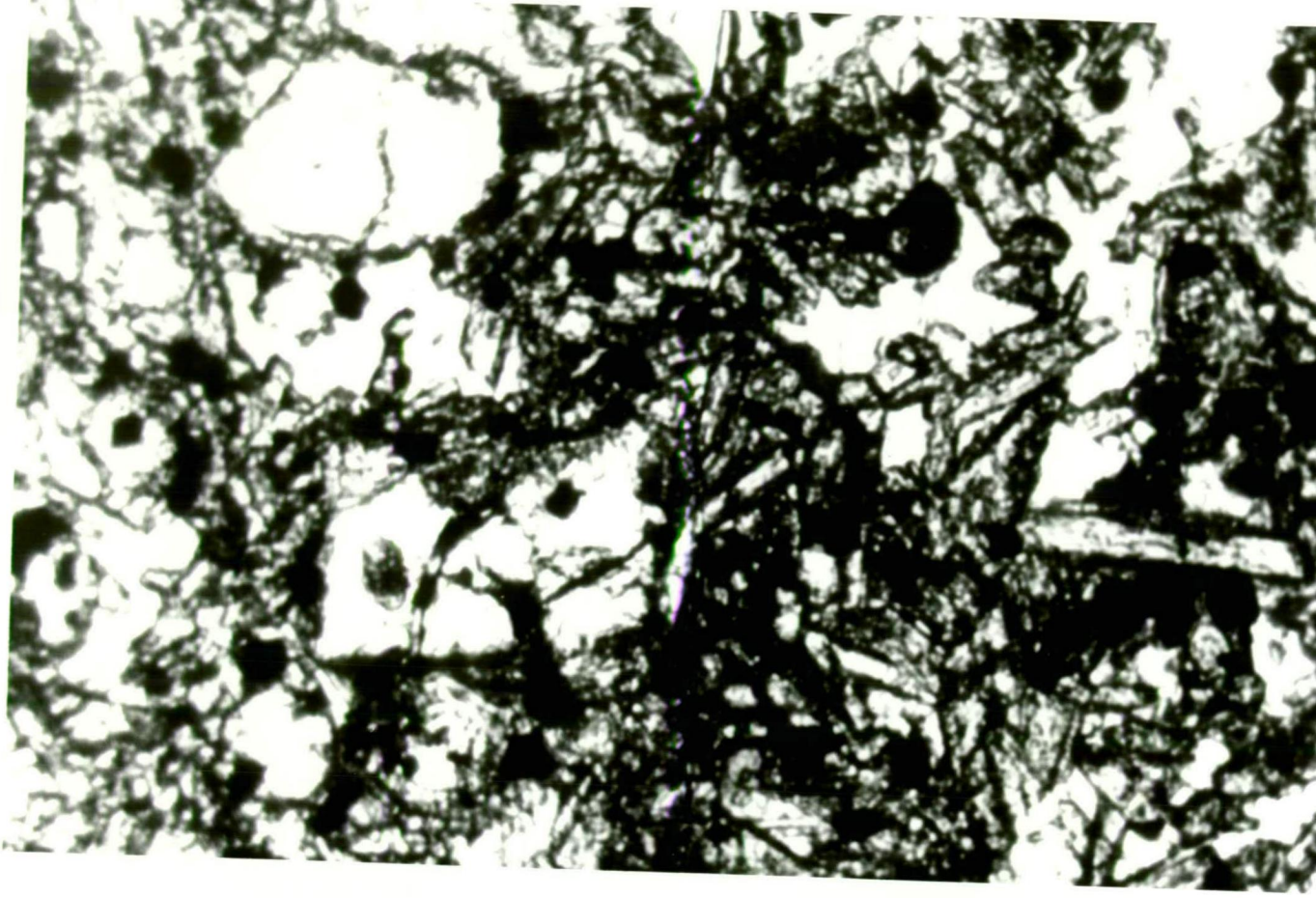

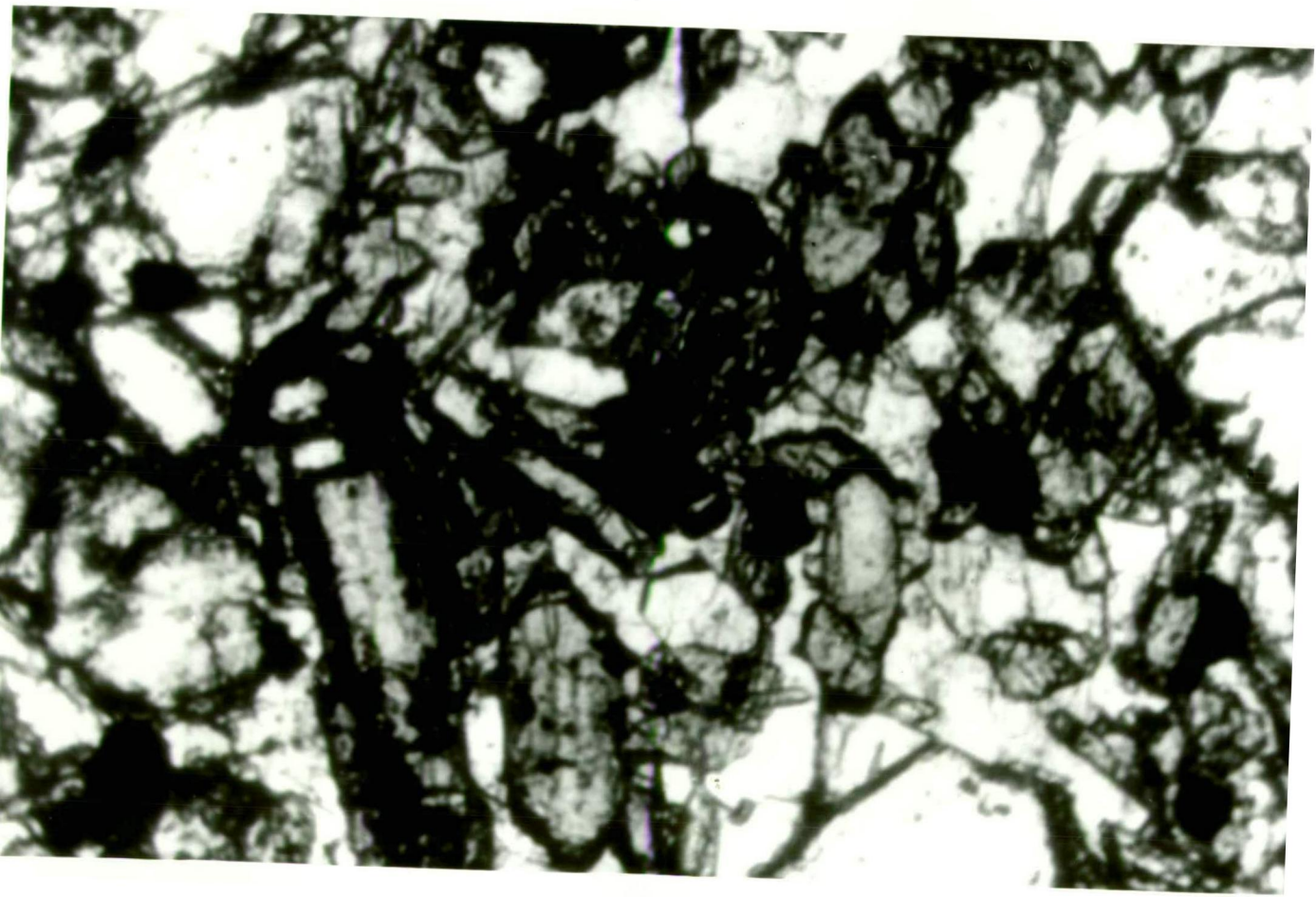

APPENDIX B

Mineralogy of Basalt (Nye, 1927)

The bottom 30' thick flow is slightly vescicular at the top and is almost completely decomposed. The few unaltered portions consist of a fine-grained olivine basalt, similar to the usual type occurring within the district. The middle flow is 40 feet thick and rests directly on the bottom one. It is almost completely decomposed in a similar manner. The unaltered kernels remaining are fine-grained, but somewhat coarser than the lower flow. Olivine occurs sparingly and the rock appears less basic and more feldspathic than the average type. The middle flow is slightly vescicular at the top and the layer of grits, from a few inches to several feet thick, separate it from the upper flow. The upper flow is a dense, fine-grained, basic type, with abundant olivine, and slightly amygdaloidal in places. It is extremely resistant to the weather at certain localities, and forms a very rocky surface.

This basalt, particularly the bottom flow, clearly belonged to the Branxholm type of Edwards (1950). It did exhibit a tendency to develop centres of crystallisation as noted by Nye (1927), and also had a large proportion of pyroxene - probably titanaugite.

The mineralogy of the basalt is seen in plate 8 opposite. The opaques are magnetite and ilmenite, which have high densities, thus making the density of 2.8 gms/cc for the basalt reasonable. The microphenocrysts are pyroxene, with a small amount of feldspar also being present.

The basalt is thus very basic - or tholeiitic, and therefore should have a higher than normal density.

The mineralogy of the slide opposite is due to Spry (personal communication 1964).

REFERENCES

Bengtsson, B.E. and Nordbeck, S., 1964. Construction of isarithms and isarithmic maps by computers: BIT, 4,87-105.

Bhattacharyya, B.K., 1965. Two-dimensional harmonic analysis as a tool for magnetic interpretation: Geophysics, 30, 829-857.

Bhattacharyya, B.K., 1966. Continuous spectrum of the total magnetic field anomaly due to a rectangular prismatic body: Geophysics, 31, 97-121.

Bickel, H.C., 1948. A note on terrain corrections: Geophysics, 13, 255-258.

Bott, M.H.P., 1961. The use of electronic digital computers for the evaluation of gravimetric terrain corrections; Geophysical Prospecting, 7 45-54

Brown, W.F., 1955. Minimum variance in gravity analysis, part I: one-dimensional: Geophysics, 20, 807-828

Brown, W.F., 1956. Minimum variance in gravity analysis, part II: two-dimensional: Geophysics, 21, 107-135

Bullard, E.C. and Cooper, R.I.B., 1948. The determination of the masses necessary to produce a given gravitational field: Proc. Roy. Soc. (London), Ser. A, 194, 332-347.

Dampney, C.N.G., 1964. The mathematical determination of geological structure: Thesis, Department of Applied Maths., Univ. of Sydney, (unpubl.)

Danes, Z.F., 1961. Structure calculations from gravity data and density logs: Mining Trans., 223, 23-29.

Danes, Z.F. and Ondrey, L.A., 1962. An analysis of some second derivative methods: Geophysics, 27, 611-615.

Dean, W.C., 1958. Frequency analysis and magnetic interpretation: Geophysics, 23, 97-127.

Ditchburn, R.W., 1963. Light, Blackie London.

Edwards, A.B., 1950. The petrology of the Cainozoic basaltic rocks of Tasmania: Proc. Roy. Soc. (Victoria), 62, 97-120.

Elkins, T.A., 1940. The reliability of geophysical anomalies on the basis of probability considerations: Geophysics, 5, 321-336.

Elkins, T.A., 1952. The effect of random errors in gravity data on second derivative values: Geophysics, 17, 70-88.

Erdelyi, A. et al., 1954. Tables of Integral Transforms, volume 1, McGraw-Hill, New York.

Fajklewisz, Z.J., 1965. Fictitious anomalies of higher vertical derivatives of gravity: Geophysics, 30, 1094-1107.

Forsythe, G.E., 1964. Editors note: Communications of the A.C.M., 7, 6, Algorithm 233.

Goldman, S., , 1955. Information Theory: Prentice-Hall Inc., New York.

Grant, F.S., 1957. A problem in the analysis of geophysical data: Geophysics, 22, 309-344.

Grant, F.S. and Elsaharty, A.F., 1962. Bouguer gravity corrections using a variable density: Geophysics, 27, 616-626.

Haiskanen, W.A. and Vening Meinesz, T.A., 1958. The earth and its gravity field. McGraw-Hill, New York

Hammer, S., 1939. Terrain corrections for gravimeter stations: Geophysics, 4, 184-194.

Hammer, S., 1963. Deep gravity interpretation by stripping: Geophysics, 28, 369-378.

Henderson, R.G., 1960. Comprehensive system of automatic computation in magnetic and gravity measurements: Geophysics, 25, 569-585.

Henderson, R.G. and Zeitz, I., 1949. The upward continuation of anomalies in total magnetic intensity fields: Geophysics, 14, 517-534.

Ho, K-C., 1955. Double interpolation formulae and partial derivatives in terms of finite differences: M.T.A.C., 9, 52-62.

Householder, A.S., 1953. Principles of Numerical Analysis, McGraw-Hill, New York.

Howland-Rose, A., 1964. The Derby-Winnaleah Gravity Survey: Bureau of Mineral Resources (Geophysics) report.

Jackson, P.L., 1965. Diffraction processing of geophysical data: App. Optics, 4, 419-427.

Jones, V.L., 1956. Extrapolation and interpolation formulae adaptable to desk and other types of digital computers: Geophysics, 19, 1047-1054.

Kempthorne, O., 1962. Design and annalysis of experiment, Wiley New York

Kunz, K.S., 1957. Numerical Analysis. McGraw-Hill, New York.

Naudy, H. and Neumann, R., 1965. Sur la definition de l'anomalie de Bouguer et ses consequences pratiques: Geophysical Prospecting, 13, 1-11.

Nettleton, L.L., 1954. Regionals, residuals and structures: Geophysics, 19, 1-22

Nye, P., 1927. The Geology of the Ringarooma Valley Area: Tas. Dept. of Mines Bull. XII.

Odegard, M.E. and Berg Jr., J.W., 1965. Gravity interpretation using the fourier integral: Geophysics, 30, 424-438.

Oldham, C.H.G. and Sutherland, D.B., 1955. Orthogonal polynomials: their use in estimating the regional effect: Geophysics, 20, 295-306.

Peters, L.J., 1949. The direct approach to magnetic interpretation and its practical application: Geophysics, 14, 290-320.

Ralston, A., 1965. A First Course in Numerical Analysis. McGraw-Hill, New York.

Romanyuk, V.A., 1959. Disturbances of the force of gravity by the atmosphere: Bull. Acad. Sci. U.S.S.R., Geophys. Ser. (English Transl.), 1959, 214-218.

Sandberg, C.H., 1958. Terrain corrections for an inclined plane in gravity computations: Geophysics, 23, 701-711.

Saltzer, H.E., 1948. Tables of coefficients for interpolating in families of two variables: J. of Math. and Phys., 26, 294-305.

Southard, T.H., 1956. Everett's formula for bivariate interpolation and throwback of fourth differences: M.T.A.C., 10, 216-223.

Stafford, J., 1965. Interpolation in a table: Communications of the A.C.M., 8, 10, Algorithm 264.

Strakhov, V.N., 1961. Methods of calculating the analytical continuation of potential fields: Bull. Acad. Sci. U.S.S.R., Geophys. Ser. (English Transl.), 1961, 137-141, 226-231, 845-856.

Strakhov, V.N., 1962a. The analytical continuation of two-dimensional potential fields, with application to the universe problem of magnetic and gravitational exploration. 1: Bull. Acad. Sci. U.S.S.R., Geophys. Ser. (English Transl.) 1962, 209-214, 227-232, 324-331.

Strakhov, V.N., 1962b. The theory of calculation of second order vertical derivatives of potential fields: Bull. Acad. Sci. U.S.S.R., Geophys. Ser. (English Transl.), 1962, 1110-1116.

Strakhov, V.N., 1963a. Some numerical methods for calculating the second-order vertical derivatives of potential fields: Bull. Acad. Sci. U.S.S.R., Geophys. Ser. (English Transl.), 1963, 65-74.

Strakhov, V.N., 1963b. The reduction of the problem of analytical continuation in a horizontal layer to that of the convolution type integral equation of the first kind with rapidly decreasing kernels: Bull. Acad. Sci. U.S.S.R., Geophys. Ser. (English Transl.), 1963, 733-739.

Strakhov, V.N., 1963c. The derivation of optimum numerical methods for the transformation of potential fields. 1: Bull. Acad. Sci. U.S.S.R., Geophys. Ser. (English Transl.), 1963, 1081-1090.

Strakhov, V.N., 1964. The problem of obtaining a best numerical transformation of potential fields: Bull. Acad. Sci. U.S.S.R., Geophys. Ser. (English Transl.), 1964, 30-35, 36-42.

Strakhov, V.N. and Devitsyn, V.M., I965. The reduction of observed values of a potential field to values at a constant level: Bull. Acad. Sci. U.S.S.R., Geophys. Ser. (English Transl.), I965, 250-255.

Strakhov, V.M. and Lapina, M.I., 1962. New methods of computing elements of the magnetic field in the upper half-space according to an assigned (on surface) distribution of vertical component: Bull. Acad. Sci. U.S.S.R., Geophys. Ser. (English Transl.), 1962, 215-226.

Strakhov, V.N. and Lapina, M.I., 1963. A new method for calculating vertical derivatives on potential fields in an upper half-space: Bull. Acad. Sci. U.S.S.R., Geophys. Ser. (English Transl.), 1963, 349-357.

Swartz, C.A., 1954. Some geometrical properties of residual maps: Geophysics. 19, 46-70.

Takeuchi, H. and Saito, H., 1964. Gravity anomalies and the corresponding crustal structure. 1. Numerical tables useful for three dimensional gravity interpretations: Bull. Earthquake Res. Inst. Tokyo, 42, 89-92.

Tarkhov, A.B. and Sidorov, A.A., 1960. The mathematical processing of geophysical data. Bull. Acad. Sci. U.S.S.R., Geophys. Ser. (English Transl.), 1960, 1189-1196.

Thyssen-Bornemisza and Stackler, W.F., 1956. Observations of the vertical gradient of gravity in the field: Geophysics, 21, 771-779.

Tsuboi, C. and Tomoda, Y., 1958. The relation between the Fourier Series method and the sin x/x method for gravity interpretation: J. Phys. Earth, 6, 1-5.

Vajk, R., 1956. Bouguer corrections with varying surface density: Geophysics, 21, 1004-1020.

Zidarov, D., 1965. Solution of some inverse problems of applied geophysics: Geophysical Prospecting, 13, 240-246.

Zilaki-Sebees, L., 1964. Regionális és maradékanomáliak meghatározása gépi számétással: Geofizikai Köztémenyek, 13, 305-313.

Geoexploration – Elsevier Publishing Company, Amsterdam – Printed in The Netherlands

THREE CRITERIA FOR THE JUDGEMENT OF VERTICAL CONTINUATION AND DERIVATIVE METHODS OF GEOPHYSICAL INTERPRETATION

C. N. G. DAMPNEY

Department of Geology, University of Tasmania, Hobart, Tasmania (Australia)

(Received November 9, 1965)

SUMMARY

Vertical continuation is shown to have some important practical applications. The practical applications of derivative methods are well known.

Various coefficient sets which compute vertical continuation and derivatives of gravity or magnetic anomaly fields are analysed on the basis of their filter response using methods from communication theory. The other important criteria in judging their data-processing methods are the effect on errors and ambiguity.

New coefficient sets are then proposed for upward and downward continuation and second derivative using these three criteria.

INTRODUCTION

Many methods are available for the interpretation of gravity and magnetic anomaly maps and most fall into one of three categories, namely: (*1*) direct qualitative interpretation of contours, (*2*) indirect interpretation in which hypothetical anomalies are fitted to the contours, and (*3*) data processing methods in which the contours are put into a more easily recognisable form.

Direct qualitative interpretation of contours is useful in working out initially the gross structures of the area. For example, areas of basins and ridges are easily picked out. However, generally speaking, without computation this first category requires considerable experience on the part of the interpreter before it can give numerical details of depth, size and shape of a probable structure producing the anomaly.

The second category is useful provided ambiguity can be removed by well supported assumptions of the body's shape, as is often done in mining geophysics. In fact, it can be proved by using Green's "Theorem of equivalent layers" (ROY, 1962) that there are an infinite number of solutions of the body causing a given anomaly. This type of method is only valid when the shape of the body is assumed.

Data-processing methods include derivative methods of various orders and vertical continuation. Derivative methods have their use in that they are able to take out the "local" component of a gravity or magnetic anomaly. As Nettleton has pointed out (NETTLETON, 1954) it is impossible to uniquely define the "local" or "regional" field. This is clearly seen in the very simple ring and point technique used to find the first derivative, or gradient, of a gravity or magnetic anomaly field intensity. For instance, what diameter do we make the ring whose average value we subtract from the centre point to get the gradient?

PRACTICAL APPLICATIONS OF VERTICAL CONTINUATION

Vertical continuation method can be very useful in interpreting gravity and magnetic anomaly maps. Basically this method works out the anomaly at some height or depth from the plane on which the anomaly is measured.

Downward continuation is able to directly calculate, at a known depth, the surface-contrast density which would produce a given anomaly, from the relationship:

$$\sigma_h(x, y) = \frac{1}{2\Pi G}\, g(x, y, h)$$

where $\sigma_h(x, y)$ is the surface contrast density at (x, y) at depth h; $g(x, y, h)$ is the anomaly at (x, y, h) and G is the gravitational constant.

The role of downward continuation in the determination of structure is seen in the magnetic anomaly case. From:

$$\Omega(x, y, z) = \iiint_{\tau} I(\alpha, \beta, \gamma) \cdot \operatorname{grad}\left(\frac{1}{r}\right) d\tau$$

where $\Omega(x, y, z)$ is the anomalous magnetic field potential at (x, y, z) due to the intensity of magnetisation $I(\alpha, \beta, \gamma)$ at (α, β, γ) over the volume τ, and:

$$r = \{(x-\alpha)^2+(y-\beta)^2+(z-\gamma)^2\}$$

can be derived (see Appendix I) the relationship that the undulating magnetic basement surface $z = f(x, y) \approx h$ of infinite depth and horizontal extent is related to $H_y(\alpha, \beta, h)$ the vertical anomalous field intensity at (α, β, h), by:

$$f(x, y) = \frac{1}{4\Pi^2 I_z} \iint_{s} \frac{H_y(\alpha, \beta, h)\, d\alpha\, d\beta}{\{(x-\alpha)^2+(y-\beta)^2\}^{\frac{1}{2}}}$$

where the surface integral is over the surface S and I_z is the vertical component of the intensity of magnetisation.

The surface integral can be approximated by a double summation, giving the structure by a direct computation from a grid:

$$f(x, y) = \frac{1}{4\Pi^2 I_z} \sum_{i=-N}^{N} \sum_{j=-N}^{N} \frac{H_z(i\Delta x, j\Delta y)}{\{(x-i\Delta x)^2+(y-j\Delta y)^2\}^{\frac{1}{2}}}$$

where Δx, Δy are unit grid lengths in the x- and y-direction and N is a value beyond which the truncation error is negligible.

Upward continuation can be used to bring ground and airborne vertical magnetic anomaly results to the same reference plane. However, as will be seen later, this process can never be perfect.

Many different systems of the vertical continuation method, using coefficient sets, have been proposed in the literature (see below). Some systems work better than others, yet all fail in some way. Criteria are therefore needed by which each system can be judged as best for the purpose at hand. This will be done, while showing why some coefficient sets so far proposed fail.

FILTER RESPONSE, ERROR CONTROL AND AMBIGUITY

As TARKHOV and SIDOROV (1960) have pointed out the regional field, random errors and other unwanted influences on the geophysical data are interference. Processing geophysical data mathematically is the elimination of interference and the ordering and collecting of the existing information. In spite of the great diversity of mathematical methods used in processing geophysical data, they are all basically filtration methods that operate like electronic filters and have the object of detecting the anomaly (the signal) in the background of more or less intense interference (the noise). In these methods the intensity is not necessarily increased, in fact, it may be decreased. However, due to a certain decrease in the unwanted information (the noise) the anomaly to interference ratio is increased.

The principles of communication theory underlie these data processing methods. Operations on geophysical data are merely various types of space filters. DEAN (1958) proved the following results:

(*1*) If h is the distance of vertical continuation, taking the positive direction as down, then the theoretical frequency response of the upward and downward vertical continuation processes is:

$$e^{h\sqrt{u^2+v^2}}$$

where u and v are frequency parameters in the x and y direction such that $u = 2\Pi f/\Delta x$, where f is the frequency of an anomaly in station spacing distance Δx. $\lambda = \Delta x/f$, where λ is the wavelength of the anomaly in the x-direction. An analogous relation can be derived for v.

Thus it can be seen that if the anomalous field intensity varies only in the

x-direction then the frequency response of the vertical continuation process is $e^{h|u|}$.

(2) The frequency response of a general coefficient set C_{mn}, where C_{mn} is the coefficient at the point $(m\Delta x, n\Delta y)$, assuming a uniform grid with station spacing in the x- and y-direction Δx and Δy respectively, is:

$$\sum_{m=-\infty}^{\infty} \sum_{n=-\infty}^{\infty} C_{m,n}\, e^{-i(um\Delta x + vn\Delta y)}$$

In practice we would run over m and n only up to N where for $|m|$ and $|n| > N$ the truncation error would be negligible.

Thus in the one dimensional case assuming $C_n = C_{-n}$ the filter response would be:

$$C_0 + 2\sum_{n=1}^{N} C_n \cos(un\Delta x)$$

This is like a fourier series which repeats itself with frequency $u\Delta x$. The period is:

$$-\frac{\Pi}{\Delta x} \leq u \leq \frac{\Pi}{\Delta x}$$

Thus the maximum frequency that the frequency response can be specified is:

$$u_{\max} = \frac{2\Pi f_{\max}}{\Delta x} = \frac{2\Pi}{\Delta x} \cdot \tfrac{1}{2} = \frac{\Pi}{\Delta x}$$

The main effect of digitalizing data is to limit the high frequency response to one half cycle per station spacing so that the frequency response of the coefficient set need only be considered up to $f = \frac{1}{2}$ or $\lambda = 2\Delta x$. This makes vertical continuation possible.

Thus, in vertical continuation coefficient sets, the coefficient sets' frequency response could be compared to the theoretical frequency response by examining the equality of:

$$e^{h|u|} = C_0 + 2\sum_{n=1}^{N} C_n \cos(un\Delta x)$$

This examination gives the *first criterion of filter response* by which coefficients sets may be judged.

However, so far no account has been made of the effect of errors.

Two sets of 100 random samples of errors having a Gaussian distribution with a probable value of 10 units were taken from a grid of numbers having that property in ELKINS' (1952) article. Their spectrum was examined using a finite fourier transform. It was found, as would be expected, that the amplitudes of the cosine term were scattered randomly through all frequencies from 0 to 0.5 using 0.01 intervals (see Fig.1). This shows that random errors (or noise) can be expected

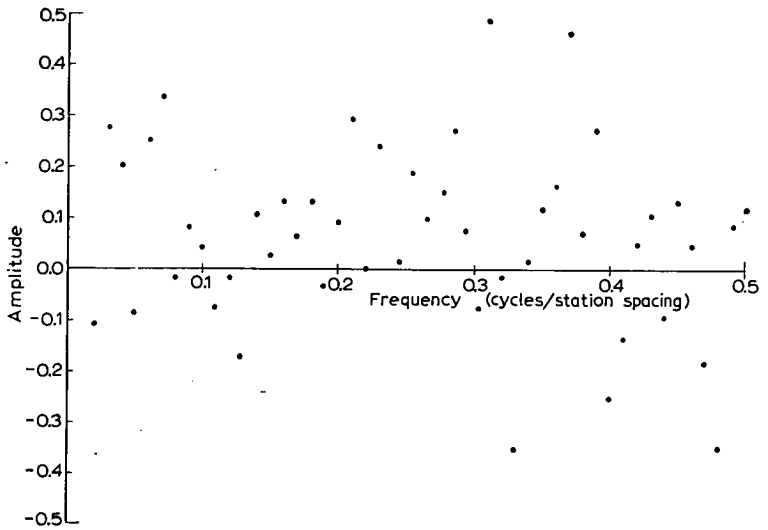

Fig.1. Amplitude of random noise spectrum.

at all frequencies with no systematic decrease in the higher or lower frequencies.

Also in the special case where, for example, a tare occurs in a gravitymeter, the resulting error could be represented by a step function and this is equivalent to the presence of all frequencies.

From its theoretical frequency response, downward vertical continuation is seen to be unstable in its high frequencies. Physically downward continuation is questionable because it appears that more detail is being squeezed out of the data than it contains.

The fallacy of using a coefficient set which has the theoretical response is seen by the effect on errors—the high frequency data would be greatly magnified in relation to the low frequency data so that high frequency noise would swamp low frequency information (or signal).

Error control is the *second criterion* by which coefficient sets should be judged. DANES and ONDREY (1962) have analysed second derivative methods and compared them, using the first criterion, to the theoretical second derivative filter response of u^2+v^2. They do not consider the effect of errors in their comparison. As it turns out (see later), there is no need to use the second criterion in analysing second derivative methods because the theoretical frequency response of second derivative methods does not increase sufficiently.

To overcome the problem of high frequency noise, distortion must be introduced into the frequency response in the high frequency part. The distortion used is smoothing.

Data-processing methods are also open to the problem of ambiguity. For example in the method of downward continuation the assumption of the depth of

continuation has to be made. While SMITH (1959a, b, 1960, 1961) and SMITH and BOTT (1958) have developed many theorems which link assumptions of density contrast, density-contrast variation and other factors to the assumption of depth, ambiguity must remain.

Thus the *third criterion* for judging data processing methods is *ambiguity*. For example, DANES (1961) in his various methods including downward continuation requires a knowledge of not only density contrast, but density-contrast variation to complete his method. His method by design, has a perfect filter response. So Danes' method in the case of a large distance of downward continuation (see Fig.5) in an area where little is known of rock density would fail for the second and third criterion, while perfectly satisfying the first criterion.

The interpreter must balance each method against these three criteria, decide how strictly he should judge the filter response, error control and ambiguity of each and then use the method most closely satisfying his needs.

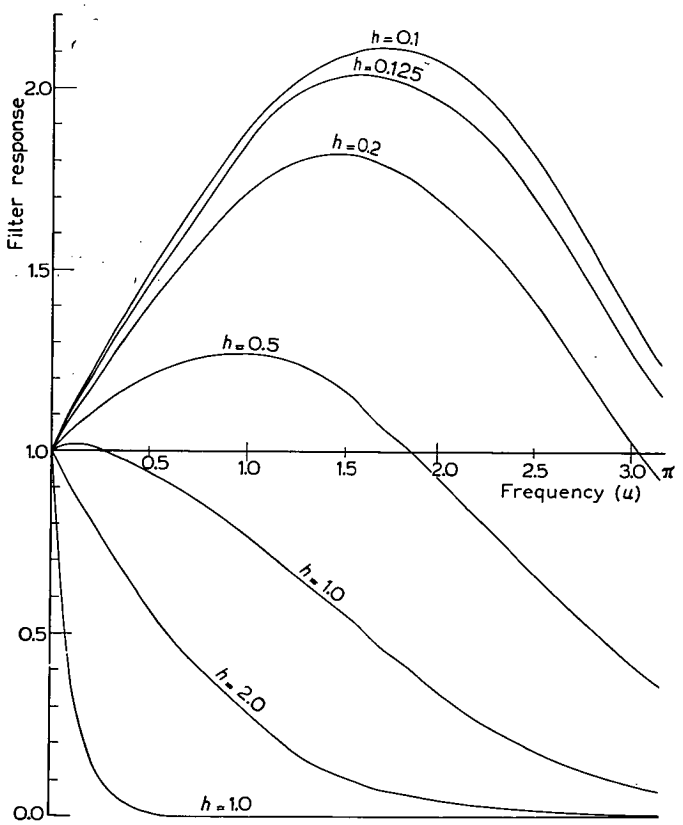

Fig.2. BULLARD AND COOPER'S (1948) downward continuation filter response.

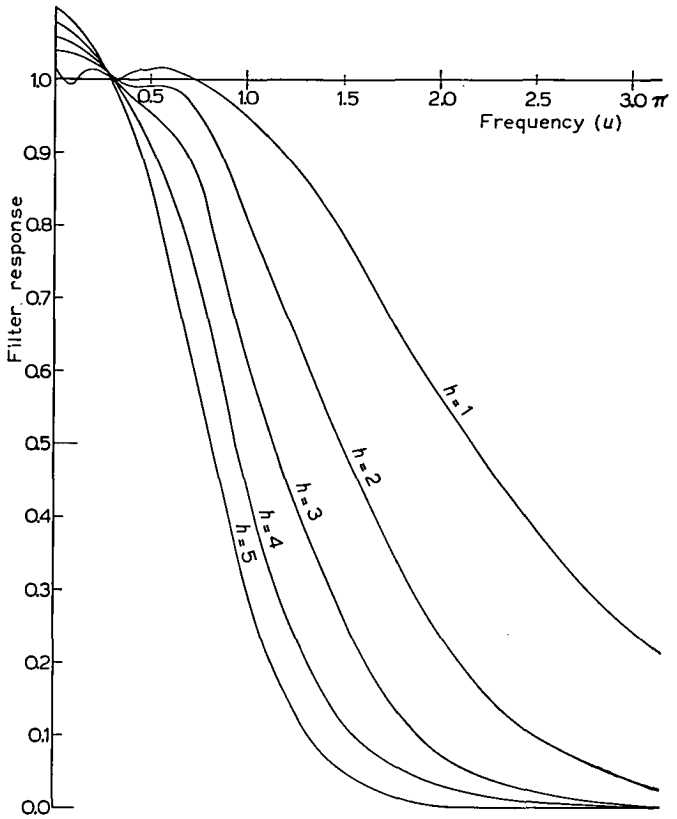

Fig.3. HENDERSON's (1960) downward continuation filter response.

SOME PREVIOUS VERTICAL CONTINUATION COEFFICIENT SETS ANALYSED

In the analysis of the downward continuation coefficient sets which follows, the anomaly is assumed, for simplicity, to vary only in one direction. For the various ring techniques the coefficients are projected onto the x-axis. In this analysis it is assumed that anomalies have already been put on a grid before interpretation begins. No account is given here of the many dangers underlying the problem of putting data on a grid, this being outside the scope of this paper. Fig.2, 3, and 4 and Table I and II show the normalised filter responses of various coefficient sets proposed in the literature.

BULLARD and COOPER's (1948) coefficient set is only one-dimensional and can, therefore only be used for interpreting profiles.

Bullard and Cooper derive the relationship between smoothed gravity $\bar{g}_z(x)$ at x on the line at depth z and $g_0(x)$ and also use smoothing related to the error function:

$$\bar{g}_z(\alpha) = \frac{1}{\Pi}\int_{-\infty}^{\infty}\int_{-\infty}^{\infty} g_0(x)e^{-p^2/4\beta}e^{pz}\cos p(\alpha-x)\,\mathrm{d}x\,\mathrm{d}p$$

$$= \int_{-\infty}^{\infty} g_0(x)\lambda(x-\alpha)\,\mathrm{d}x$$

$$= \sum_{-\infty}^{\infty} g_0(n\Delta x)\lambda(n\Delta x-\alpha)\Delta x$$

Thus:

$$C_n = \lambda(n\Delta x-\alpha)\Delta x$$

They smooth by:

$$\bar{g}_0(\xi) = \sqrt{\frac{\beta}{\Pi}}\int_{-\infty}^{\infty} g_0(x)e^{-\beta(x-\xi)^2}\,\mathrm{d}x$$

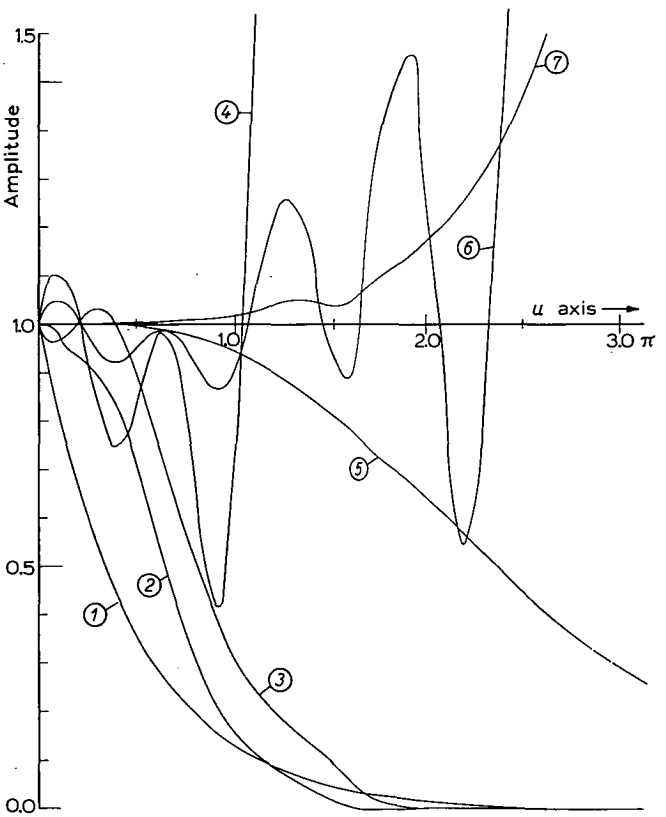

Fig.4. Filter response of indicated coefficient sets. *1* = Finite difference method, $h = 1$; *2* = PETER'S (1949) method, $h = 2$; *3* = PETER'S (1949) method, $h = 1$; *4* = PETER'S (1949) method, $h = -2$; *5* = finite difference method, $h = -1$; *6* = PETER'S (1949) method, $h = -1$; *7* = HENDERSON AND ZEITZ' (1949) method, $h = -1$.

TABLE I

BULLARD AND COOPER'S (1948) COEFFICIENT SET FILTER RESPONSE[1]

10	*2*	*1*	*0.5*	*0.2*	*0.125*	*0.1*	*radians*
1.0101	1.0101	1.0101	1.0101	1.0101	1.0101	1.0101	0.0000
0.4932	0.9245	1.0000	1.0401	1.0649	1.0711	1.0733	0.0785
0.2417	0.8491	0.9936	1.0748	1.1266	1.1400	1.1445	0.1571
0.1181	0.7778	0.9845	1.1076	1.1887	1.2099	1.2170	0.2356
0.0576	0.7106	0.9729	1.1384	1.2509	1.2807	1.2908	0.3142
0.0280	0.6471	0.9584	1.1663	1.3122	1.3514	1.3647	0.3927
0.0135	0.5872	0.9407	1.1906	1.3714	1.4207	1.4376	0.4712
0.0065	0.5308	0.9198	1.2109	1.4280	1.4881	1.5087	0.5498
0.0031	0.4782	0.8964	1.2273	1.4818	1.5533	1.5779	0.6283
0.0015	0.4295	0.8708	1.2399	1.5328	1.6163	1.6451	0.7069
0.0007	0.3844	0.8432	1.2487	1.5805	1.6764	1.7096	0.7854
0.0003	0.3430	0.8137	1.2533	1.6241	1.7328	1.7706	0.8639
0.0002	0.3049	0.7825	1.2535	1.6632	1.7850	1.8275	0.9425
0.0001	0.2702	0.7501	1.2498	1.6977	1.8328	1.8802	1.0210
0.0000	0.2387	0.7169	1.2422	1.7277	1.8762	1.9285	1.0996
0.0000	0.2103	0.6830	1.2309	1.7527	1.9147	1.9719	1.1781
0.0000	0.1846	0.6487	1.2159	1.7727	1.9479	2.0100	1.2566
0.0000	0.1616	0.6142	1.1974	1.7873	1.9756	2.0427	1.3352
0.0000	0.1411	0.5799	1.1758	1.7970	1.9980	2.0698	1.4137
0.0000	0.1228	0.5460	1.1515	1.8017	2.0151	2.0917	1.4923
0.0000	0.1066	0.5128	1.1247	1.8017	2.0270	2.1081	1.5708
0.0000	0.0923	0.4803	1.0956	1.7969	2.0336	2.1192	1.6493
0.0000	0.0797	0.4487	1.0646	1.7878	2.0351	2.1249	1.7279
0.0000	0.0687	0.4183	1.0321	1.7746	2.0320	2.1259	1.8064
0.0000	0.0591	0.3891	0.9986	1.7578	2.0248	2.1225	1.8850
0.0000	0.0507	0.3613	0.9643	1.7379	2.0136	2.1149	1.9635
0.0000	0.0434	0.3348	0.9294	1.7150	1.9989	2.1036	2.0420
0.0000	0.0372	0.3098	0.8944	1.6897	1.9810	2.0889	2.1206
0.0000	0.0317	0.2862	0.8595	1.6626	1.9607	2.0715	2.1991
0.0000	0.0271	0.2642	0.8251	1.6341	1.9385	2.0521	2.2777
0.0000	0.0231	0.2436	0.7914	1.6046	1.9148	2.0309	2.3562
0.0000	0.0197	0.2245	0.7584	1.5745	1.8899	2.0085	2.4347
0.0000	0.0167	0.2068	0.7265	1.5442	1.8645	1.9854	2.5133
0.0000	0.0143	0.1904	0.6958	1.5142	1.8391	1.9622	2.5918
0.0000	0.0121	0.1753	0.6664	1.4848	1.8140	1.9393	2.6704
0.0000	0.0103	0.1615	0.6384	1.4563	1.7897	1.9170	2.7489
0.0000	0.0088	0.1488	0.6118	1.4288	1.7663	1.8957	2.8274
0.0000	0.0075	0.1372	0.5866	1.4026	1.7442	1.8756	2.9060
0.0000	0.0064	0.1266	0.5628	1.3779	1.7235	1.8571	2.9845
0.0000	0.0055	0.1169	0.5405	1.3547	1.7046	1.8402	3.0631
0.0000	0.0047	0.1080	0.5194	1.3330	1.6872	1.8251	3.1416

[1] Each column is headed by the distance of vertical continuation in units of station spacings (Station spacing = 1.0 unit), or by "radians" which is given in units of frequency. The unit of the normalised filter response for a given distance of vertical continuation and frequency is dimensionless.

TABLE II

HENDERSON'S (1960) COEFFICIENT SET FILTER RESPONSE[1]

−5.0	*−4.0*	*−3.0*	*−2.0*	*−1.0*	*1.0*	*2.0*	*3.0*	*4.0*	*5.0*	*radians*
0.9019	0.9210	0.9404	0.9601	0.9800	1.0199	1.0398	1.0595	1.0790	1.0983	0.0000
1.0442	1.0318	1.0214	1.0128	1.0057	0.9953	0.9912	0.9874	0.9836	0.9794	0.0785
0.8704	0.9068	0.9371	0.9624	0.9832	1.0130	1.0221	1.0275	1.0291	1.0269	0.1571
0.8972	0.9256	0.9495	0.9698	0.9866	1.0098	1.0158	1.0177	1.0154	1.0085	0.2356
1.0658	1.0232	1.0027	0.9957	0.9961	1.0043	1.0067	1.0050	0.9976	0.9832	0.3142
0.9103	0.9276	0.9485	0.9685	0.9860	1.0091	1.0114	1.0040	0.9853	0.9542	0.3927
0.5527	0.7408	0.8577	0.9293	0.9732	1.0130	1.0111	0.9917	0.9538	0.8983	0.4712
−0.1267	0.4272	0.7226	0.8773	0.9581	1.0150	1.0040	0.9660	0.9027	0.8192	0.5498
−0.6403	0.2334	0.6544	0.8554	0.9528	1.0112	0.9858	0.9244	0.8333	0.7233	0.6283
1.3180	1.0650	0.9974	0.9638	0.9797	0.9971	0.9530	0.8666	0.7497	0.6193	0.7069
5.6484	2.6375	1.4962	1.1100	1.0099	0.9819	0.9161	0.8029	0.6626	0.5181	0.7854
10.5983	4.1176	1.8761	1.1840	1.0182	0.9698	0.8788	0.7376	0.5771	0.4250	0.8639
13.9335	4.7438	1.8995	1.1391	0.9997	0.9592	0.8398	0.6711	0.4955	0.3424	0.9425
3.3950	1.1110	0.7090	0.7926	0.9271	0.9518	0.8007	0.6059	0.4203	0.2717	1.021
−8.9543	−2.5160	−0.3416	0.5154	0.8750	0.9366	0.7542	0.5393	0.3510	0.2120	1.100
41.3289	9.9167	2.4477	1.0549	0.9550	0.9047	0.6968	0.4712	0.2879	0.1625	1.178
113.263	24.8208	5.1729	1.4652	1.0012	0.8756	0.6423	0.4092	0.2341	0.1232	1.257
−2.5687	−4.2193	−1.6220	0.0740	0.7978	0.8627	0.5980	9.3562	0.1898	0.0928	1.335
−284.999	−63.9689	−13.4577	−1.9886	0.5395	0.8472	0.5531	0.3075	0.1524	0.0692	1.414
−389.193	−83.6603	−16.9052	−2.4989	0.4957	0.8151	0.5023	0.2614	0.1208	0.0510	1.492
−258.901	−60.4736	−13.0092	−1.8937	0.5790	0.7762	0.4516	0.2202	0.0949	0.0373	1.571
−69.0811	−29.6844	−8.3660	−1.2556	0.6581	0.7383	0.4047	0.1846	0.0741	0.0271	1.649
247.358	16.3920	−2.2226	−0.5213	0.7382	0.7009	0.3614	0.1540	0.0575	0.0195	1.728
477.795	43.8706	0.5372	−0.2865	0.7680	0.6655	0.3219	0.1280	0.0445	0.0140	1.806
517.737	40.6837	−1.1287	−0.5800	0.7555	0.6315	0.2860	0.1095	0.0342	0.0100	1.885
1019.64	83.8747	1.6006	−0.4692	0.7764	0.5971	0.2529	0.0871	0.0261	0.0071	1.963
1272.97	82.0746	−1.6236	−0.9501	0.7604	0.5640	0.2230	0.0715	0.0199	0.0050	2.042
−38.1514	−89.1489	−20.9338	−2.6827	0.6789	0.5325	0.1963	0.0584	0.0151	0.0035	2.121
−3629.34	−450.100	−53.3778	−5.0615	0.5864	0.5017	0.1723	0.0476	0.0114	0.0025	2.199
−14042.0	−1302.00	−116.400	−8.9480	0.4498	0.4722	0.1509	0.0387	0.0086	0.0017	2.278
−20779.4	−1664.00	−128.600	−8.5916	0.5605	0.4412	0.1314	0.0313	0.0064	0.0012	2.356
16439.4	1277.12	88.8265	5.6824	1.2921	0.4070	0.1133	0.0252	0.0048	0.0008	2.435
81484.4	5697.48	369.627	21.5187	1.9954	0.3759	0.0977	0.0202	0.0036	0.0006	2.513
64480.0	4431.96	282.778	16.3556	1.8107	0.3522	0.0849	0.0162	0.0027	0.0004	2.592
−29810.7	−1150.00	−26.2928	1.2789	1.3123	0.3309	0.0737	0.0130	0.0020	0.0003	2.670
−37579.0	−1566.00	−45.6933	0.6764	1.3634	0.3078	0.0635	0.0104	0.0015	0.0002	2.749
33939.6	1819.16	106.070	6.9501	1.6295	0.2852	0.0546	0.0083	0.0011	0.0001	2.827
43212.8	1906.43	97.8603	6.4648	1.6924	0.2647	0.0469	0.0066	0.0008	0.0001	2.906
−12578.8	−807.300	−19.3035	2.3692	1.6786	0.2456	0.0403	0.0052	0.0006	0.0001	2.985
−241570	−9903.00	−349.300	−7.7623	1.5538	0.2280	0.0345	0.0041	0.0004	0.0000	3.063
−604221	−22410.0	−739.300	−17.8794	1.4840	0.2112	0.0296	0.0033	0.0003	0.0000	3.142

[1] Each column is headed by the distance of vertical continuation in units of station spacings (Station spacing = 1.0 unit), or by "radians" which is given in units of frequency. The unit of the normalised filter response for a given distance of vertical continuation and frequency is dimensionless.

where β is a smoothing parameter determining the severity of smoothing. The function is simply related to the error function by:

$$\bar{g}_0(0) = \sum_{n=-\infty}^{\infty} \sqrt{\frac{\beta}{\Pi}}\, g_0(n\Delta x) \int_{\Delta x(n-\frac{1}{2})}^{\Delta x(n+\frac{1}{2})} e^{-\beta x^2}\, dx$$

$$= \sum_{n=-\infty}^{\infty} W_n g_0(n\Delta x)$$

where:

$$W_n = \tfrac{1}{2}[\mathrm{erf}\,\{\sqrt{\beta}\Delta x(n+\tfrac{1}{2})\} - \mathrm{erf}\,\{\sqrt{\beta}\Delta x(n-\tfrac{1}{2})\}]$$

In Fig.2 their suggested set of coefficients is analysed using a station spacing of 0.125 units, over the range $0 \leq u \leq \Pi$ which is only part of the total range between 0 and cut-off where $u_{max} = 8\Pi$.

However, this range represents the most important part of the frequency response, serving as a useful part to compare with Table I which shows the computed normalised filter response for a station spacing of one unit of a complete set of coefficients, one for each grid point, worked out from Bullard and Cooper's table and approximation equation.

The normalised filter response for Bullard and Cooper's suggested coefficient set (Fig.2) was worked out for both average and middle values in each range. Only variation of the order of 5% was noted between the two responses.

The normalised filter responses in Fig.2 and Table I were calculated for various depths. Bullard and Cooper use a parameter $= \beta h^2$ in their computation, where h is the depth of continuation. As in both Fig.2 and Table I, the parameter was unity, the filter response was worked out for various depths namely for $h = 0.1$; 0.125; 0.2; 0.5; 1; 2 and 10 units corresponding to $\beta = 100$; 64; 25; 4; 1; 0.25; 0.01. Thus the severity of smoothing is increased with depth.

Fig.2 and Table I show the similarity in the variation of the filter response. In fact, the filter response was calculated for other station spacings, and showed the same similarity, so that the cut-off frequency in Bullard and Cooper's method has little influence.

Bullard and Cooper's coefficient sets show the increasing severity of smoothing with depth thus satisfying error control. However, in the smaller depths, the coefficient set filter response does not match up with the theoretical response over this important part of the range.

The normalised filter response of HENDERSON's (1960) coefficient set, is shown in Fig.3 and Table II. HENDERSON's (1960) downward continuation can be seen to have smooth error control in relation to the filter response, increasing, as required, with depth. Henderson's method is able to most often satisfy error control and filter response requirements.

Fig.4 shows the normalised filter response of PETERS' (1949), HENDERSON and ZEITZ (1949) and the finite differences (BULLARD and COOPER, 1948) coefficient sets, for the indicated values of h, with unit station spacing. The first 80 coefficients were used for the finite differences method and the first 23 coefficients in the rapidly convergent HENDERSON and ZEITZ' (1949) method. All these filter responses appear unsatisfactory, except the downward continuation finite differences coefficient set. Upward continuation coefficient sets tend to oscillate and do not, in any case, match the theoretical response, in the low-frequency range.

Upward vertical continuation is by contrast a very stable process. Gravity and magnetic data have predominantly low frequencies even near the source function. Away from the source, upward continuation introduces $e^{-h|u|}$ which again favours low frequencies. The low frequencies are essential for defining all gravity and magnetic anomalies. The higher frequencies are relatively more important for the smaller sharper anomalies and for defining sharp details.

Upward vertical continuation smooth down the higher frequencies, reducing information in this range. Low-frequency noise in a perfect response coefficient set swamps high frequency information. Generally this does not matter, so that error control is not nearly so important in this process.

The normalised filter response of HENDERSON's (1960) coefficient sets for various negative values of h with unit station spacing are shown in Table II. The mismatch in the high frequencies is at once noticeable, but the filter response decreases correctly in the important low-frequency range preserving the regional information. However, Henderson's method would allow high-frequency information to be vastly accentuated beyond their theoretical amplification, producing a derived anomaly map containing all frequencies and thus looking correct, but in actual fact not possessing the correct relationship to its original data.

The upward continuation process can therefore be only really useful as a numerical filter. As errors occurring in magnetometers and gravimeters can not be made frequency dependent, it is not yet possible to match up ground and airborne-anomaly results through all the frequencies.

Henderson's coefficient set for continuing upwards a theoretical anomaly of a particular body, which, by definition, has no error, would be highly unsatisfactory.

STRAKHOV (e.g., 1961, 1962a, b, 1963a, b, c, 1964) and STRAKHOV and LAPINA (1962 and 1963) have written many articles on potential field analysis including various methods and analysis of second-derivative and vertical continuation methods. The articles are generally intensely mathematical using many unfamiliar inequalities and equalities of harmonic analysis, though their truth is undoubted.

The reader is especially referred to his article, "The derivation of optimum numerical methods for the transformation of potential fields, I" (STRAKHOV, 1963c), as an excellent list of references, especially of many Russian authors, is included.

ELKINS (1952) showed the effect of taking the second derivative, using his own coefficient sets, of a grid of random normally distributed errors. The appearance of the anomalies he gets can be explained by the filter response unequally affecting all the frequencies in the data.

So far, the examination of various vertical continuation systems has been destructive, no better system has been proposed. Coefficient sets for vertical continuation and second derivative methods will now be derived aimed at satisfying the first and second criteria.

DERIVATION OF COEFFICIENT SETS

Downward vertical continuation

The second criterion of error control is first satisfied in this unstable process by cutting out the high-frequency data from the value of u beyond which the data errors are greater than the lowest-frequency information.

The noise to signal (information) ratio in the data, assumed to be on a grid, is taken as being the ratio: standard deviation of anomaly/standard deviation of error $= x$.

In any survey containing closed loops the error at each grid point is known. The standard deviation of these errors is taken as being the noise level. The standard deviation of the anomaly is taken as the signal level. This ratio is taken without any pretence of mathematical rigour, but the ratio is sufficiently representative for practical purposes.

Thus if the distance of downward continuation is h then the frequency above u_0 must be filtered out where:

$$e^{hu_0} = x$$

because above this value of u_0 the amplification of the errors will be greater than the amplification of the zero frequency information.

Using this fact, the maximum anomaly size that can be interpreted from downward continued data for a signal to noise ratio of 200 is shown in Fig.5.

A numerical filter is therefore required which will cut out these high frequencies. Smoothing by an erf function as used by BULLARD and COOPER (1948) would be suitable, but, for simplicity, a two-dimensional symmetrical step function is used in the frequency domain.

The coefficient set which has the required filter response is calculated. Put:

$$\sum_{m=-\infty}^{\infty} \sum_{n=-\infty}^{\infty} C_{m,n} e^{-i(um\Delta x + vn\Delta y)} = f(u, v)$$

where $f(u, v)$ is a symmetric function with respect to u and v about 0.

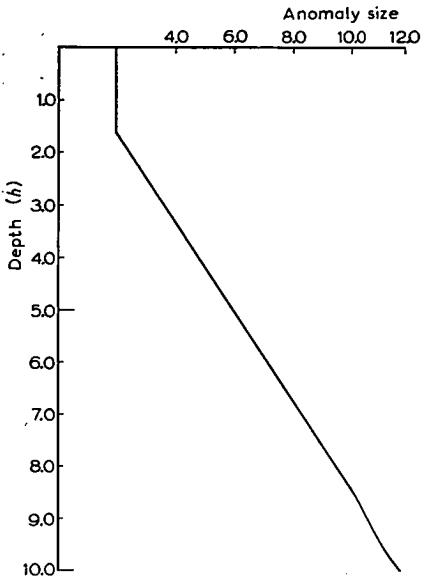

Fig.5. Minimum anomaly size detectable at depth h in units of station spacing.

Suppose $\Delta x = \Delta y = 1$, then:

$$C_{m,n} = \frac{1}{4\Pi^2} \int_{-\Pi}^{\Pi} \int_{-\Pi}^{\Pi} f(u, v) e^{-i(um+vn)} \, du \, dv$$

$$= \frac{1}{4\Pi^2} \int_{-\Pi}^{\Pi} \left(\int_{0}^{\Pi} + \int_{-\Pi}^{0} \right) f(u, v) e^{-i(um+vn)} \, du \, dv$$

In the range 0 to $-\Pi$ put $v = -v$:

$$\therefore C_{m,n} = \frac{1}{4\Pi^2} \int_{-\Pi}^{\Pi} du \, e^{-ium} \int_{0}^{\Pi} 2 \cos vm \, f(u, v) \, dv$$

as $f(u, v) = f(u, -v)$.

$$C_{m,n} = \frac{1}{\Pi^2} \int_{0}^{\Pi} \int_{0}^{\Pi} f(u, v) \cos um \cos vn \, du \, dv$$

as $f(u, v) = f(-u, v)$. Thus the coefficient set with the required filter response is found.

The two dimensional symmetric step function is given by: $f(u, v) = 1$, $-u_0 \leq u \leq u_0$, $-u_0 \leq v \leq v_0$ or $= 0$ otherwise. Therefore:

$$C_{m,n} = \frac{1}{\Pi^2} \int_{0}^{u_0} \cos um \int_{0}^{u_0} \cos vn \, du \, dv$$

$$= \frac{1}{\Pi^2} \times \frac{1}{nm} \sin u_0 m \sin u_0 n$$

Note that: $C_{m,n} = C_{m,-n} = C_{-m,n} = C_{-m,-n} = C_{n,m} = C_{n,-m} = C_{-n,m} = C_{-n,-m}$, that is $C_{m,n}$ is eight-fold symmetric.

Example: Suppose for a survey we find that $x = 112$, which means that the errors are of the order of 0.1 mgal and the variations of the anomaly of the order of 11 mgal. We wish to continue this data downwards to a distance of five units:

$$\therefore e^{hu_0} = 112$$

$$\therefore u_0 \approx 1.571 \approx \Pi/2$$

Thus:

$$C_{m,n} = \frac{1}{\Pi^2} \times \frac{1}{nm} \sin\frac{\Pi m}{2} \sin\frac{\Pi n}{2}$$

$$C_{m,0} = \frac{1}{2\Pi} \times \frac{1}{m} \sin\frac{\Pi m}{2}$$

$$C_{0,0} = \tfrac{1}{4}$$

Table III gives the right-hand quadrant of this coefficient set up to $n = 10$ and $m = 10$.

Smoothing is thus carried out on the data and then with no high frequencies present a downward continuation coefficient set is applied to the data.

A downward vertical continuation coefficient set is found, similarly to the smoothing coefficient set:

$$C_{m,n} = \frac{1}{\Pi^2} \int_0^{\Pi} \int_0^{\Pi} e^{h\sqrt{u^2+v^2}} \cos mu \cos nv \, du \, dv$$

$C_{m,n}$ was computed using a double Simpson approximation for $h = 1$ up to $n = m = 10$. The right-hand upper quadrant of this coefficient set is given in Table IV[1].

While $C_{m,n}$ appears an easy integral to work out it defied all attempts to solve it in terms of simple functions.

It is seen that the downward continuation coefficient set converges very slowly and more terms would need to be computed than are shown.

Upward vertical continuation

No error control is required for this process.

The upward continuation coefficient set was calculated exactly as the downward continuation set except that $h = -1$.

[1] It has since been pointed out that TAKEUCHI and SAITO (1964) have numerically approximated the coefficient $C_{m,n}$ for various positive values of h from $h = 0.01$ to $h = 1$. The values of $C_{m,n}$ given in Table IV are in agreement with Takeuchi and Saito's to the fourth decimal place.

TABLE III

SMOOTHING COEFFICIENT SET

n	$m = 0$	$m = 1$	$m = 2$	$m = 3$	$m = 4$	$m = 5$	$m = 6$	$m = 7$	$m = 8$	$m = 9$	$m = 10$
10	0.00000	0.00000	0.00000	0.00000	0.00000	0.00000	0.00000	0.00000	0.00000	0.00000	0.00000
9	0.01768	0.01126	0.00000	−0.00375	0.00000	0.00225	0.00000	−0.00161	0.00000	0.00125	0.00000
8	0.00000	0.00000	0.00000	0.00000	0.00000	0.00000	0.00000	0.00000	0.00000	0.00000	0.00000
7	−0.02274	−0.01447	0.00000	0.00482	0.00000	−0.00289	0.00000	0.00201	0.00000	−0.00161	0.00000
6	0.00000	0.00000	0.00000	0.00000	0.00000	0.00000	0.00000	0.00000	0.00000	0.00000	0.00000
5	0.03183	0.02026	0.00000	−0.00675	0.00000	0.00405	0.00000	−0.00289	0.00000	0.00225	0.00000
4	0.00000	0.00000	0.00000	0.00000	0.00000	0.00000	0.00000	0.00000	0.00000	0.00000	0.00000
3	−0.05305	−0.03377	0.00000	0.01126	0.00000	−0.00675	0.00000	0.00482	0.00000	−0.00375	0.00000
2	0.00000	0.00000	0.00000	0.00000	0.00000	0.00000	0.00000	0.00000	0.00000	0.00000	0.00000
1	0.15916	0.10132	0.00000	−0.03377	0.00000	0.02026	0.00000	−0.01447	0.00000	0.01126	0.00000
0	0.25000	0.15916	0.00000	−0.05305	0.00000	0.03183	0.00000	−0.02274	0.00000	0.01768	0.00000

TABLE IV

DOWNWARD CONTINUATION COEFFICIENT SET

n	$m = 0$	$m = 1$	$m = 2$	$m = 3$	$m = 4$	$m = 5$	$m = 6$	$m = 7$	$m = 8$	$m = 9$	$m = 10$
10	0.10615	−0.02190	0.00714	−0.00361	0.00188	−0.00141	0.00081	−0.00076	0.00044	−0.00047	0.00027
9	−0.13119	0.02660	−0.00918	0.00409	−0.00263	0.00146	−0.00124	0.00072	−0.00072	0.00042	−0.00047
8	0.16500	−0.03416	0.01107	−0.00565	0.00290	−0.00221	0.00126	−0.00117	0.00069	−0.00072	0.00044
7	−0.21547	0.04366	−0.01518	0.00669	−0.00436	0.00239	−0.00204	0.00120	−0.00117	0.00072	−0.00076
6	0.29011	−0.06043	0.01943	−0.01005	0.00510	−0.00389	0.00224	−0.00204	0.00126	−0.00124	0.00081
5	−0.41562	0.08427	−0.02962	0.01287	−0.00846	0.00467	−0.00389	0.00239	−0.00221	0.00146	−0.00141
4	0.63311	−0.13375	0.04254	−0.02226	0.01131	−0.00846	0.00510	−0.00436	0.00290	−0.00263	0.00188
3	−1.09070	0.22317	−0.07954	0.03454	−0.02226	0.01287	−0.01005	0.00669	−0.00565	0.00409	−0.00361
2	2.18630	−0.48546	0.15438	−0.07954	0.04254	−0.02962	0.01943	−0.01518	0.01107	−0.00918	0.00714
1	−5.84827	1.35202	−0.48546	0.22317	−0.13375	0.08427	−0.06043	0.04366	−0.03416	0.02660	−0.02190
0	15.78620	−5.84827	2.18630	−1.09070	0.63311	−0.41562	0.29011	−0.21547	0.16500	−0.13119	0.10615

TABLE V

UPWARD CONTINUATION COEFFICIENT SET

n	*m* = 0	*m* = 1	*m* = 2	*m* = 3	*m* = 4	*m* = 5	*m* = 6	*m* = 7	*m* = 8	*m* = 9	*m* = 10
10	0.00007	0.00013	0.00015	0.00014	0.00013	0.00011	0.00010	0.00009	0.00008	0.00006	0.00006
9	0.00032	0.00024	0.00020	0.00018	0.00016	0.00014	0.00012	0.00011	0.00009	0.00008	0.00006
8	0.00017	0.00026	0.00028	0.00025	0.00022	0.00019	0.00016	0.00013	0.00011	0.00009	0.00008
7	0.00062	0.00049	0.00040	0.00035	0.00030	0.00025	0.00020	0.00016	0.00013	0.00011	0.00009
6	0.00048	0.00061	0.00061	0.00051	0.00041	0.00033	0.00026	0.00020	0.00016	0.00012	0.00010
5	0.00153	0.00123	0.00097	0.00077	0.00058	0.00044	0.00033	0.00025	0.00019	0.00014	0.00011
4	0.00176	0.00193	0.00166	0.00120	0.00084	0.00058	0.00041	0.00030	0.00022	0.00016	0.00013
3	0.00590	0.00462	0.00303	0.00193	0.00120	0.00077	0.00051	0.00035	0.00025	0.00018	0.00014
2	0.01242	0.01036	0.00590	0.00303	0.00166	0.00097	0.00061	0.00040	0.00028	0.00020	0.00015
1	0.05965	0.03260	0.01036	0.00462	0.00193	0.00123	0.00061	0.00049	0.00026	0.00024	0.00013
0	0.13718	0.05965	0.01242	0.00590	0.00176	0.00153	0.00048	0.00062	0.00017	0.00032	0.00007

The same comments concerning method apply here.

However, the upward continuation coefficient set converges sufficiently quickly for practical purposes as seen in Table V.

Second derivative

As DEAN (1958) has shown the second differential theoretical filter response is u^2+v^2. The highest frequency data is therefore amplified by a factor of $2\Pi^2$. Thus as in all practical cases this value would be far below the signal to noise ratio—no account need be taken of error control, other than realising unequal amplification of errors.

Thus a coefficient set having the perfect filter response would be best for this process.

$$C_{m,n} = \frac{1}{\Pi^2}\int_0^{\Pi} dv \cos nv \int_0^{\Pi} (u^2+v^2)\cos mu\, du$$

$$= \frac{1}{\Pi^2}\int_0^{\Pi} dv \cos nv \int_0^{\Pi} u^2 \cos mu\, du$$

$$+ \frac{1}{\Pi^2}\int_0^{\Pi} dv \cos nv, v^2 \int_0^{\Pi} \cos mu\, du$$

$$= 0 \text{ (for } m \text{ and } n \neq 0)$$

$$C_{0,n} = \frac{1}{\Pi^2}\int_0^{\Pi}\int_0^{\Pi} (u^2+v^2)\cos nu\, du\, dv = \frac{2}{n^2}\cos n\Pi$$

$$C_{0,0} = 2\Pi^2/3$$

The upper quadrant of this coefficient set is found from Table VI.

TABLE VI

SECOND DERIVATIVE COEFFICIENT SET

n	$C_{0,n} = C_{n,0}$
10	0.02000
9	−0.02469
8	0.03125
7	−0.04082
6	0.05556
5	−0.08000
4	0.12500
3	−0.22222
2	0.50000
1	−2.00000
0	6.57972

CONCLUSION

The general comment on data processing methods is then made that their use must be tempered by a full appreciation of their inadequacies. There may be much to be gained by interpreting in the frequency domain, as done, for example, by ODEGARD and BERG (1965).

TUKEY (1965) has summarised much of what remains to be done in interpretation in seismology, much of which applies to gravity and magnetic interpretation.

Data-processing methods can be judged by using the three criteria of filter response, error control and ambiguity considerations.

While much remains to be done in improving the various methods of interpretation, these three criteria give a sound way of judging improvements.

ACKNOWLEDGEMENTS

The inspiration given to the author as an undergraduate by Professor K. E. Bullen is gratefully acknowledged. I wish to thank Mr. Winch, Dept. of Applied Mathematics, University of Sydney, and Dr. R. Green, Dept. of Geology, University of Tasmania, for much useful criticism and advice given in the development of this article.

REFERENCES

BULLARD, E. C. and COOPER R. I. B., 1948. The determination of the masses necessary to produce a given gravitational field. *Proc. Roy. Soc. (London), Ser. A*, 194: 332–347.

DANES, Z. F., 1961. Structure calculations from gravity data and density logs. *Mining Trans.*, 223: 23–29.

DANES, Z. F. and ONDREY, L. A., 1962. An analysis of some second derivative methods. *Geophysics*, 27: 611–615.

DEAN, W. C., 1958. Frequency analysis and magnetic interpretation. *Geophysics*, 23: 97–127.

ELKINS, T. A., 1952. The effect of random errors in gravity data on second derivative values. *Geophysics*, 17: 70–88.

GRANT, F. S. and WEST, G. F., 1965. *Interpretations Theory in Applied Geophysics*, McGraw-Hill, New York, N.Y., 583 pp.

HENDERSON, R. G., 1960. Comprehensive system of automatic computation in magnetic and gravity measurements. *Geophysics*, 25: 569–585.

HENDERSON, R. G. and ZEITZ, I., 1949. The upward continuation of anomalies in total magnetic intensity fields. *Geophysics*, 14: 517–534.

NETTLETON, L. L., 1954. Regionals, residuals and structures. *Geophysics*, 19; 1–22.

ODEGARD, M. E. and BERG JR., J. W., 1965. Gravity interpretation using the fourier integral. *Geophysics*, 30: 424–438.

PETERS, L. J., 1949. The direct approach to magnetic interpretation and its practical application. *Geophysics*, 14: 290–320.

ROY, A., 1962. Ambiguity in geophysical interpretation. *Geophysics*, 27: 90–99.

SMITH, R. A., 1959a. On the depth of bodies producing local magnetic anomalies. *Quart. J. Mech. Appl. Math.*, 12: 354–364.

SMITH, R. A., 1959b. Some depth formulae for local magnetic and gravity anomalies. *Geophys. Prospecting*, 7: 55–63.

SMITH, R. A., 1960. Some formulae for local gravity anomalies. *Geophys. Prospecting*, 8: 607–613.

SMITH, R. A., 1961. Some theorems concerning local magnetic anomalies. *Geophys. Prospecting*, 9: 399–410.

SMITH, R. A. and BOTT, M. H. P., 1958. The estimation of limiting depth of gravitating bodies. *Geophys. Prospecting*, 6: 1–10.

STRAKHOV, V. N., 1961. Methods of calculating the analytical continuation of potential fields. *Bull. Acad. Sci. U.S.S.R., Geophys. Ser. (English Transl.)*, 1961: 137–141, 226–231, 845–856.

STRAKHOV, V. N., 1962a. The analytical continuation of two-dimensional potential fields, with application to the universe problem of magnetic and gravitational exploration. 1. *Bull. Acad. Sci. U.S.S.R., Geophys. Ser. (English Transl.)* 1962: 209–214, 227–232, 324–331.

STRAKHOV, V. N., 1962b. The theory of calculation of second order vertical derivatives of potential fields. *Bull. Acad. Sci. U.S.S.R. Geophys. Ser. (English Transl.)*, 1962: 1110–1116.

STRAKHOV, V. N., 1963a. Some numerical methods for calculating the second-order vertical derivatives of potential fields. *Bull. Acad. Sci. U.S.S.R., Geophys. Ser. (English Transl.)*, 1963: 65–74.

STRAKHOV, V. N., 1963b. The reduction of the problem of analytical continuation in a horizontal layer to that of the convolution type integral equatans of the first kind with rapidly decreasing kernels. *Bull. Acad. Sci. U.S.S.R., Geophys. Ser. (English Transl.)*, 1963: 733–739.

STRAKHOV, V. N., 1963c. The derivation of optimum numerical methods for the transformation of potential fields. 1. *Bull. Acad. Sci. U.S.S.R., Geophys. Ser. (English Transl.)*, 1963: 1081–1090.

STRAKHOV, V. N., 1964. The problem for obtaining a best numerical transformation of potential fields. *Bull. Acad. Sci. U.S.S.R., Geophys. Ser. (English Transl.)*, 1964: 30–35, 36–42.

STRAKHOV, V. M. and LAPINA, M. I., 1962. New methods of computing elements of the magnetic field in the upper half-space according to an assigned (on surface) distribution of vertical component. *Z. Bull. Acad. Sci. U.S.S.R., Geophys. Ser. (English Transl.)*, 1962: 215–226.

STRAKHOV, V. N. and LAPINA, M. I., 1963. A new method for calculating vertical derivatives of potential fields in an upper half-space. *Bull. Acad. Sci. U.S.S.R., Geophys. Ser. (English Transl.)*, 1963: 349–357.

TAKEUCHI, H. and SAITO, H., 1964. Gravity anomalies and the corresponding crustal structure. 1. Numerical tables useful for three dimensional gravity interpretations. *Bull. Earthquake Res. Inst. Tokyo*, 42: 39–92.

TARKHOV, A. B. and SIDOROV, A. A., 1960. The mathematical processing of geophysical data. *Bull. Acad. Sci. U.S.S.R., Geophys. Ser. (English Transl.)*, 1960: 1189–1196.

TUKEY, J. W., 1965. Data analysis and the frontiers of geophysics. *Science*, 148: 1283–1289.

APPENDIX I

The contributions of I_x and I_y on h can be shown to be zero.

The magnetic anomalous field potential $\Omega(x, y, z)$ is related to the intensity of magnetisation $I(\alpha, \beta, \gamma)$ at (α, β, γ) by:

$$\Omega(x, y, z) = \int_{-\infty}^{\infty}\int_{-\infty}^{\infty}\int_{-\infty}^{\infty} \frac{I(\alpha, \beta, \gamma)\,(z-\gamma)\,d\alpha\,d\beta\,d\gamma}{\{(x-\alpha)^2+(y-\beta)^2+(z-\gamma)^2\}^{\frac{3}{2}}} \tag{1}$$

Consider the vertical component of $\Omega(x, y, z)$ due to a basement with upper surface described by $\gamma = f(\alpha, \beta) \approx h$ and infinite in all other directions. The vertical component of $I(\alpha, \beta, \gamma)$ is supposed constant—and denoted I_z. Therefore:

$$\Omega(x, y, z) = I_z \int_{-\infty}^{\infty}\int_{-\infty}^{\infty}\int_{\infty}^{f(\alpha,\beta)} \frac{(z-\gamma)\,d\alpha\,d\beta\,d\gamma}{\{(x-\alpha)^2+(y-\beta)^2+(z-\gamma)^2\}^{\frac{3}{2}}}$$

$$= I_z \int_{-\infty}^{\infty}\int_{-\infty}^{\infty} \left[\frac{\gamma(z-\gamma)}{\{(x-\alpha)^2+(y-\beta)^2+(z-\gamma)^2\}^{\frac{3}{2}}}\right]_{\infty}^{f(\alpha,\beta)} d\alpha\,d\beta$$

$$- I_z \int_{-\infty}^{\infty}\int_{-\infty}^{\infty}\int_{\infty}^{f(\alpha,\beta)} \gamma \frac{\partial^2}{\partial\gamma^2}\left(\frac{1}{r}\right) d\alpha\,d\beta\,d\gamma$$

= first integral − second integral, where:

$$\text{first integral} = I_z \int_{-\infty}^{\infty}\int_{-\infty}^{\infty} \frac{f(\alpha, \beta)\,\{z-f(\alpha, \beta)\}\,d\alpha\,d\beta}{[(x-\alpha)^2+(y-\beta)^2+\{z-f(\alpha, \beta)^2\}]^{\frac{3}{2}}}$$

Now as $f(\alpha, \beta) \approx h$:

$$\therefore \text{first integral} = I_z \int_{-\infty}^{\infty}\int_{-\infty}^{\infty} \frac{f(\alpha, \beta)\,(z-h)\,d\alpha\,d\beta}{\{(x-\alpha)^2+(y-\beta)^2+(z-h)^2\}^{\frac{3}{2}}} \tag{2}$$

Now as $\nabla^2\left(\frac{1}{r}\right) = 0$:

$$\therefore \text{second integral} = I_z \int_{-\infty}^{\infty}\int_{-\infty}^{\infty}\int_{-\infty}^{f(\alpha,\beta)} \gamma\left[\frac{\partial^2}{\partial\alpha^2}+\frac{\partial^2}{\partial\beta^2}\right]\left(\frac{1}{r}\right) d\alpha\,d\beta\,d\gamma$$

interchanging order of integration:

$$= I_z \int_{\infty}^{f(\alpha,\beta)} \gamma\,d\gamma \int_{-\infty}^{\infty} d\beta \int_{-\infty}^{\infty} \frac{\partial^2}{\partial\alpha^2}\left(\frac{1}{r}\right) d\alpha$$

$$+ I_z \int_{\infty}^{f(\alpha,\beta)} \gamma\,d\gamma \int_{-\infty}^{\infty} d\alpha \int_{-\infty}^{\infty} \frac{\partial^2}{\partial\beta^2}\left(\frac{1}{r}\right) d\beta$$

$$= I_z \int_{\infty}^{f(\alpha,\beta)} \gamma\,d\gamma \int_{-\infty}^{\infty} d\beta \left[\frac{\partial}{\partial\alpha}\left(\frac{1}{r}\right)\right]_{-\infty}^{\infty}$$

$$+ I_z \int_{\infty}^{f(\alpha,\beta)} \gamma \, d\gamma \int_{-\infty}^{\infty} d\alpha \left[\frac{\partial}{\partial\beta}\left(\frac{1}{r}\right)\right]_{-\infty}^{\infty} = 0 \tag{3}$$

From ROY (1962) eq. 18 the field potential (magnetic or gravitational):

$$V(x, y, z) \text{ at } P(x, y, z) = \frac{1}{2\Pi} \int_{-\infty}^{\infty}\int_{-\infty}^{\infty} \frac{1}{r}\left[\frac{\partial V}{\partial\gamma}(\alpha, \beta, \gamma)\right]_{\gamma=h} d\alpha \, d\beta \tag{4}$$

where $r = \{(x-\alpha)^2+(y-\beta)^2+(z-h)^2\}^{\frac{1}{2}}$. Now the field intensity:

$$\Phi(\alpha, \beta, \gamma) = \frac{\partial V}{\partial\gamma}(\alpha, \beta, \gamma)$$

Thus differentiating with respect to z:

$$\phi(x, y, z) = \frac{1}{2\Pi}\int_{-\infty}^{\infty}\int_{-\infty}^{\infty} \frac{(z-h)}{r^3}\left[\phi(\alpha, \beta, \gamma)\right]_{\gamma=h} d\alpha \, d\beta$$

$$= \frac{1}{2\Pi}\int_{-\infty}^{\infty}\int_{-\infty}^{\infty} \frac{(z-h)\phi(\alpha, \beta, \gamma)\, d\alpha \, d\beta}{r^3}$$

Now as ϕ satisfies $\nabla^2\phi = 0$ this relation is a property of potential functions, so that we may replace ϕ by Ω so that we get in the magnetic field potential case:

$$\Omega(x, y, z) = \frac{1}{2\Pi}\int_{-\infty}^{\infty}\int_{-\infty}^{\infty} \frac{\Omega(\alpha, \beta, h)\,(z-h)\, d\alpha \, d\beta}{\{(x-\alpha)^2+(y-\beta)^2+(z-h)^2\}^{\frac{1}{2}}}$$

$\therefore$ from eq.2,3 and 6: $I_z f(\alpha, \beta) = \Omega(\alpha, \beta, h)/2\Pi$. But $\alpha = x$, $\beta = y$ then
$I_z f(x, y) = \Omega(x, y, h)/2\Pi$.
From eq.4:

$$\Omega_z(x, y, z) = \frac{1}{2\Pi}\int_{-\infty}^{\infty}\int_{-\infty}^{\infty} \frac{H_\gamma(\alpha, \beta, h)\, d\alpha \, d\beta}{\{(x-\alpha)^2+(y-\beta)^2\}^{\frac{1}{2}}}$$

where H_γ is the vertical component of the magnetic field intensity. Thus:

$$f(x, y) = \frac{1}{4\Pi^2 I_z}\int_{-\infty}^{\infty}\int_{-\infty}^{\infty} \frac{H_\gamma(\alpha, \beta, h)\, d\alpha \, d\beta}{\{(x-\alpha)^2-(y-\beta)^2\}^{\frac{1}{2}}}$$